Characterization of Chemical and Genetic Regulators of Human Naive Pluripotent Stem Cells

by

Mükrime ALTUN

A Dissertation Submitted to the
Graduate School of Health Sciences
in Partial Fulfillment of the Requirements for
the Degree of

Master of Science

in

Cellular and Molecular Medicine

August 25, 2025

Characterization of Chemical and Genetic Regulators of Human Naive Pluripotent Stem Cells

Koç University

Graduate School of Health Sciences

This is to certify that I have examined this copy of a master's thesis by

Mükrime ALTUN

and have found that it is complete and satisfactory in all respects,

and that any and all revisions required by the final

examining committee have been made.

Committee Members:

Prof. Tamer Tevfik ÖNDER

Assoc. Prof. Tolga EMRE

Assist. Prof. Gözde KORKMAZ

Date: 25.08.2025

ABSTRACT

Characterization of Chemical and Genetic Regulators of Human Naive Pluripotent Stem Cells

Mükrime ALTUN

Master of Science in Cellular and Molecular Medicine

25 August, 2025

Pluripotent stem cells exist in two main developmental states, which are naive and primed. Naive pluripotent stem cells hold particular promise for modelling early embryonic development due to their broader developmental potential. However, the derivation and stable maintenance of human naive pluripotent stem cells remain technically challenging. This thesis aims to uncover the epigenetic mechanisms that restrict the transition from the primed to the naive state and to develop strategies that improve conversion efficiency. In particular, the effects of several chromatin modifying factors (DOT1L, P300/CBP, MENIN, and BRD9) on naive conversion were evaluated using small-molecule inhibitors. Two independent reporter systems (one based on differential enhancer usage of OCT4 and the other based on KLF17 expression) were employed to monitor naive conversion. Inhibitor treatments were conducted under a recently developed culture condition (HENSM). Conversion efficiency was assessed quantitatively using flow cytometry for fluorescent marker expression and RT-qPCR for naive-specific genes. The findings demonstrate that DOT1L inhibition using EPZ5676 and MENIN inhibition using VTP50469 significantly relieve epigenetic constraints on naive conversion. On the other hand, inhibitors targeting P300/CBP and BRD9 exhibited more limited effects. RT-qPCR results confirmed the upregulation of naive markers such as DPPA3, TFCP2L1, and KLF17, and the downregulation of primed or lineage-related genes. Collectively, these results indicate that DOT1L and MENIN function as key epigenetic barriers to naive pluripotency in human stem cells. In addition, a novel KLF17-GFP reporter line, generated in this laboratory, was functionally characterized in this thesis to validate its utility as a naive-specific marker for monitoring state transitions. In the third part of the thesis, to facilitate gene knockouts in both primed and naive iPSCs, I generated a human iPSC line carrying an inducible Cas9 gene at the AAVS1 safe harbour locus via genome editing. Overall, this study shows that inhibiting specific epigenetic regulators like DOT1L and MENIN can greatly improve the efficiency of generating human naive pluripotent stem cells. It also introduces a novel reporter system and a genome-edited iPSC line that can be suitable for dissecting the regulation of naive pluripotency and for gene knockout studies in both naive and primed conditions.

ÖZETÇE

İnsan Naif Pluripotent Kök Hücrelerinin Kimyasal ve Genetik Düzenleyicilerinin Karakterizasyonu

Mükrime ALTUN

Hücresel ve Moleküler Tıp, Yüksek Lisans

25 Ağustos 2025

Pluripotent kök hücreler, naif ve primed olmak üzere iki temel gelişimsel durumda bulunur. Naif pluripotent kök hücreler, daha geniş gelişimsel potansiyelleri nedeniyle erken embriyonik gelişimin modellenmesi açısından özel bir vaat taşımaktadır. Ancak, insan naif pluripotent kök hücrelerinin türetilmesi ve stabil olarak sürdürülmesi teknik açıdan halen zorludur. Bu tez, primed durumdan naif duruma geçişi kısıtlayan epigenetik mekanizmaları ortaya çıkarmayı ve dönüşüm verimliliğini artıracak stratejiler geliştirmeyi amaçlamaktadır. Bu kapsamda, birkaç kromatin düzenleyici faktörün (DOT1L, P300/CBP, MENIN ve BRD9) naif dönüşüm üzerindeki etkileri küçük molekül inhibitörleri kullanılarak değerlendirilmiştir. Naif dönüşümü izlemek için iki bağımsız reporter sistemi kullanılmıştır: biri OCT4'ün farklılaştırılmış enhancer kullanımına, diğeri ise KLF17 ekspresyonuna dayalıdır. İnhibitör uygulamaları, yakın zamanda geliştirilen bir kültür koşulu (HENSM) altında gerçekleştirilmiştir. Dönüşüm verimliliği, floresan marker ekspresyonu için akış sitometrisi ve naif-spesifik genler için RT-qPCR kullanılarak nicel olarak değerlendirilmiştir. Bulgular, DOT1L inhibitörü EPZ5676 ve MENIN inhibitörü VTP50469'un naif dönüşüm üzerindeki epigenetik engelleri anlamlı düzeyde azalttığını göstermektedir. Buna karşılık, P300/CBP ve BRD9'u hedefleyen inhibitörler daha sınırlı etkiler ortaya koymuştur. RT-qPCR sonuçları, DPPA3, TFCP2L1 ve KLF17 gibi naif markerların yukarı regülasyonunu ve primed ya da soy ile ilişkili genlerin aşağı regülasyonunu doğrulamıştır. Bu sonuçlar birlikte değerlendirildiğinde, DOT1L ve MENIN'in insan kök hücrelerinde naif pluripotensinin önünde önemli epigenetik bariyerler olarak işlev gördüğü anlaşılmaktadır. Ayrıca, bu laboratuvarda oluşturulan yeni bir KLF17-GFP reporter hattı fonksiyonel olarak karakterize edilmeye çalışılmış ve durum geçişlerini izlemeye yönelik naif-spesifik bir marker olarak potansiyeli değerlendirilmiştir. Tezin üçüncü bölümünde ise hem primed hem de naif iPSC'lerde gen silme çalışmalarını kolaylaştırmak amacıyla, AAVS1 güvenli bölgesine indüklenebilir Cas9 geninin entegre edildiği bir insan iPSC hattı genom düzenleme ile oluşturulmuştur. Genel olarak, bu çalışma, DOT1L ve MENIN gibi spesifik epigenetik düzenleyicilerin inhibe edilmesinin insan naif pluripotent kök hücrelerinin elde edilme verimliliğini önemli ölçüde artırabileceğini göstermektedir. Ayrıca, naif pluripotensinin düzenlenmesini incelemeye ve hem naif hem de primed koşullarda gen knockout çalışmalarına uygun yeni bir reporter sistemi ve genom düzenlenmiş bir iPSC hattı tanıtmaktadır.

ACKNOWLEDGEMENTS

First and foremost, I would like to sincerely thank my advisor, Prof. Dr. Tamer Önder, for giving me the opportunity to pursue research in the field I was most interested in and for always being available to provide scientific guidance. His discipline and encouragement have shown me that learning is a lifelong and enjoyable pursuit. Moreover, his guidance on how to question and think critically has greatly contributed to my development as a researcher.

I would like to thank the members of the Onder lab and KUTTAM who supported me and provided assistance in addressing experimental questions.

I would like to express my gratitude to the esteemed scientist Dilşad Arabacı, who showed genuine warmth and interest despite not knowing me personally.

I would like to express my gratitude to Nilya Karasürmeli, Elifsu Kartal, and Sarra El-Soussi, who became part of my life through the lab, for their patience with my academic concerns and spontaneous questions, and for always being by my side with unwavering support.

I would like to thank my dear friends Arya Akdağ, Büşra Demir, and Sena Başer, whose presence in the lab was always a source of positive energy and whose unconditional friendship and kindness I deeply appreciated.

I am deeply grateful to Eda Eraslan, who has been my greatest fortune in the lab, for her artistic personality, intellectual depth, and kind heart. I greatly value the moments we shared, the conversations we had, and the opportunity to grow together during this process.

I would like to thank my dearest friend Hilal Şimşek, who has been in my life for nine years, for her constant love and support. Even during the darkest times of demotivation and anxiety, when I felt I could not overcome the challenges, she held my hand and stood by me with unwavering support.

I would like to thank my beloved uncle, İbrahim Karahan, who has passed away. I feel very lucky that you brought art into my life and taught me what Improv Comedy means. I wish you joy wherever you are.

I am very thankful to all members of my beloved family for always supporting me and making many sacrifices. I especially thank my brother, who has always prioritized me over himself and cared about my well-being and success.

TABLE OF CONTENTS

LIST OF TABLES

LIST OF FIGURES

ABBREVIATIONS

CRISPR	Clustered Regularly Interspaced Short Palindromic Repeats
CTG	Cell Titer Glo
DE	Distal Enhancer
DNMTs	DNA methyltransferases
Dox	Doxycycline
EGCs	Embryonic Germ Cells
EpiSCs	Epiblast Stem Cells
EPI	Epiblast
ESC	Embryonic Stem Cell
ETn	Early Transposon
FACS	Fluorescence-activated Cell Sorting
FAK	Focal Adhesion Kinase
H2AK119ub	Histone H2A at Lysine 119 Ubiquitination
HDACi	Histone Deacetylase Inhibitors
hESC	Human Embryonic Stem Cell
HENSM	Human Enhanced Naive Stem Cell Medium
ICM	Inner Cell Mass
KLF17	Krüppel-like Factor 17
LIF	Leukemia Inhibitory Factor
LPA	Lysophosphatidic Acid
NHSM	Naive Human Stem Cell Medium
PE	Primitive Endoderm
ΔPE	Delta Proximal Enhancer
PGCLC	Primordial Germ Cell-like Cell
PKC	Protein Kinase C
PTMs	Post-translational Modifications
RT-qPCR	Real Time Quantitative Polymerase Chain Reaction

STAT3	Signal Transducer and Activator of Transcription 3
TALEN	Transcription Activator-like Effector Nucleases
TE	Trophoectoderm
VPA	Valproic Acid
YAP	Yes-associated Protein

Chapter 1:
INTRODUCTION

1.1 Pluripotent Origins of the Pre-implantation Embryo

Embryonic development begins when a single fertilized egg (zygote) divides repeatedly without any increase in overall volume, quickly moving from the morula to the blastocyst stage (Niakan et al., 2012). At the blastocyst stage, the first cell fate decision separates the outer trophoectoderm (TE), which will form placental tissues, from the inner cell mass (ICM) that develops into the embryo itself. A second decision within the ICM directs cells to become either epiblast (EPI) or primitive endoderm (PE), with the epiblast later giving rise to all somatic and germ-line cell types in the adult (Leung & Zernicka-Goetz, 2015). By the end of the five-day pre-implantation period, the embryo is organized as a metabolically active TE "shell" surrounding a core of pluripotent epiblast cells (Niakan et al., 2012). Although the small cell numbers and the maternal-to-zygotic transition limit traditional biochemical approaches, modern single-cell omics and high-resolution live imaging are now clarifying the molecular steps that guide the shift from totipotency through pluripotency to lineage commitment (Tadros & Lipshitz, 2009). Epiblast-derived embryonic stem cells (ESCs) retain the capacity to differentiate into all three germ layers, which are ectoderm, mesoderm, and endoderm, allowing powerful applications in disease modelling, drug discovery, and regenerative medicine (De Miguel et al., 2009; Avior, Sagi, & Benvenisty, 2016)

Obtaining human embryonic stem cells (ESCs) involves destroying 5-7-day-old blastocysts which are early embryos that many individuals regard as potential human life (Lo & Parham, 2009). In addition to ethical barriers, technical challenges in studying early human embryos, such as their limited availability, fragility, and developmental variability, have further complicated the use of ESCs (Wong et al., 2010). Because of these ethical and clinical issues, these problems have driven interest in alternatives such as induced pluripotent stem cells (iPSCs) reprogrammed from adult cells (Takahashi & Yamanaka 2006).

To understand cell fate and how iPSCs were generated, it is important to first consider Waddington's epigenetic landscape, which shows how cell potential becomes restricted and can be reversed through reprogramming.

1.2 From Waddington's Epigenetic Landscape to Cellular Reprogramming

In 1957, Conrad Waddington introduced the idea of the epigenetic landscape to explain how cells follow specific developmental paths during differentiation. According to Figure 1, in this model, a totipotent cell is represented as a marble placed at the top of a hill (Ladewig, Koch, & Brüstle, 2013; Waddington, 1957). As the marble rolls down, it moves into different valleys, which represent various cell fates that become more limited over time. Totipotent cells, found at the top, have the greatest potential because they can form both embryonic and extraembryonic tissues (Xu & Liang, 2022). As the marble continues, it passes a symbolic ridge, which marks the shift to pluripotency. Pluripotent cells still have the ability to create all three germ layers, being ectoderm, mesoderm, and endoderm, but can no longer generate extraembryonic tissues (Murry & Keller, 2008).

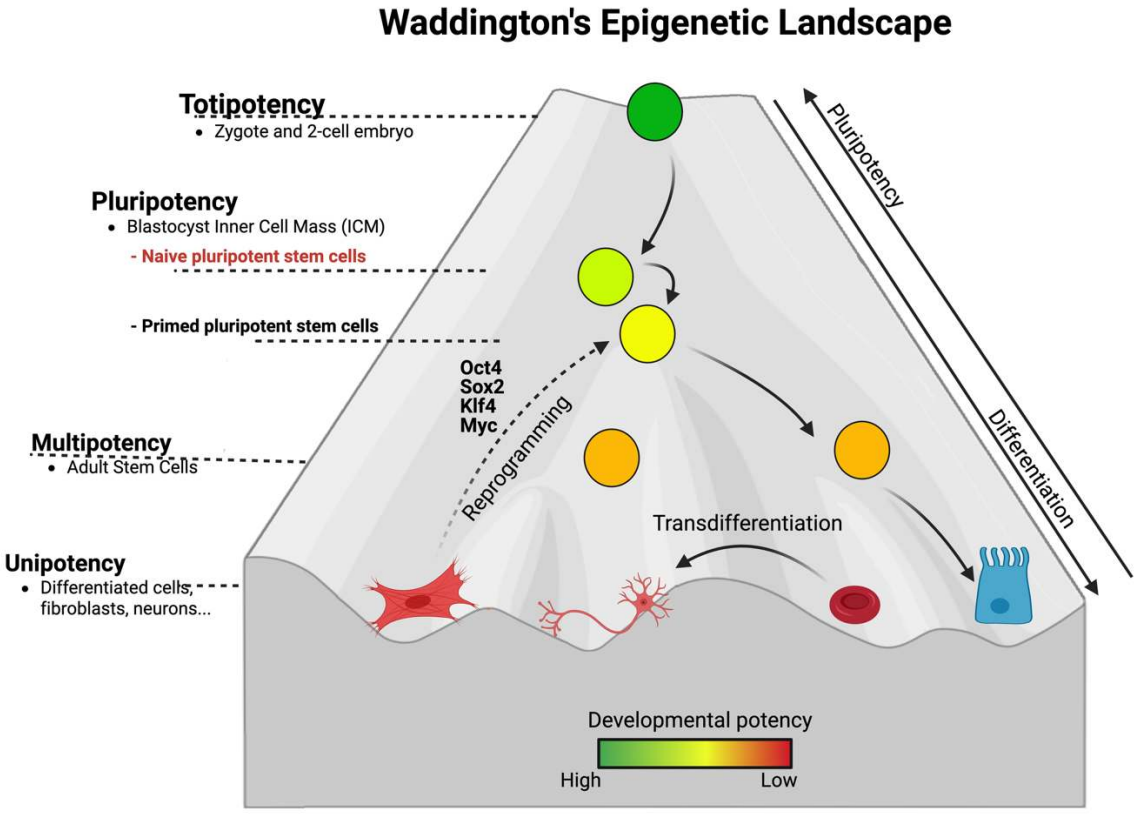

Figure 1.1. Schematic representation of a modified Waddington's epigenetic landscape model demonstrating cellular reprogramming potential (adapted from Hanna, Saha, & Jaenisch, 2010; Ladewig, Koch, & Brüstle, 2013)

Waddington originally believed this process was irreversible, meaning that once a cell committed to a certain fate, it could not return to an earlier state. However, recent discoveries have shown that cell identity can be changed (Watanabe, Yamada, & Yamanaka, 2013). Through reprogramming techniques, researchers have been able to push differentiated cells back into a pluripotent state, reversing their fate (Takahashi & Yamanaka, 2006). Takahashi et al. (2006) showed that ordinary human skin fibroblasts can be converted into induced pluripotent stem cells (iPSCs) by introducing the same four transcription factors, which are Oct3/4, Sox2, Klf4, and c-Myc, previously used in mice. The human iPSCs they produced were virtually identical to embryonic stem cells in their morphology, growth rate, surface markers, genome-wide expression patterns, epigenetic state at pluripotency genes, and telomerase activity. Functionally, the cells proved fully pluripotent: they differentiated into derivatives of all three germ layers in culture and formed teratomas containing ectodermal, mesodermal, and endodermal tissues in vivo. This study therefore confirmed that fully reprogrammed pluripotent cells can be generated from easily obtained adult fibroblasts, helping to shift the field toward iPSC-based research instead of the more ethically sensitive use of embryonic stem cells (Takahashi et al., 2007). These findings show that the developmental landscape is more flexible than Waddington had assumed. Using tools like transcription factor overexpression and epigenetic editing, scientists can now convert fully differentiated cells back into pluripotent ones, or even directly change them into another cell type, without returning to a totipotent state (Graf & Enver, 2009; Hochedlinger & Jaenisch, 2015).

1.3 Definition and Hallmarks of Pluripotency

Pluripotency refers to a temporary developmental ability found in the epiblast of the late blastocyst, where cells can both self-renew and differentiate into all somatic and germline cell types of the embryo (Wu and Belmonte, 2015). However, in contrast to totipotent cells, pluripotent cells cannot produce extraembryonic tissues like the placenta (Baker & Pera, 2018). This state can be studied in vitro using several well-known pluripotent stem cell (PSC) types, such as embryonic stem cells (ESCs), epiblast stem cells (EpiSCs), embryonic germ cells (EGCs), and induced pluripotent stem cells (iPSCs). These models offer useful systems to explore early mammalian development and disease processes under controlled conditions (Wu and Belmonte, 2015)

Pluripotency is evaluated through functional and molecular or epigenetic markers (Figure 2). Functionally, pluripotent cells are expected to show abilities such as trilineage differentiation in vitro, teratoma formation, chimera contribution, and in mouse models, germline transmission and tetraploid complementation (Du & Wu, 2024). On the molecular side, markers include the expression of core pluripotency genes like OCT4, SOX2, and NANOG, the presence of bivalent chromatin marks, levels of DNA methylation, and reliance on certain signaling pathways.

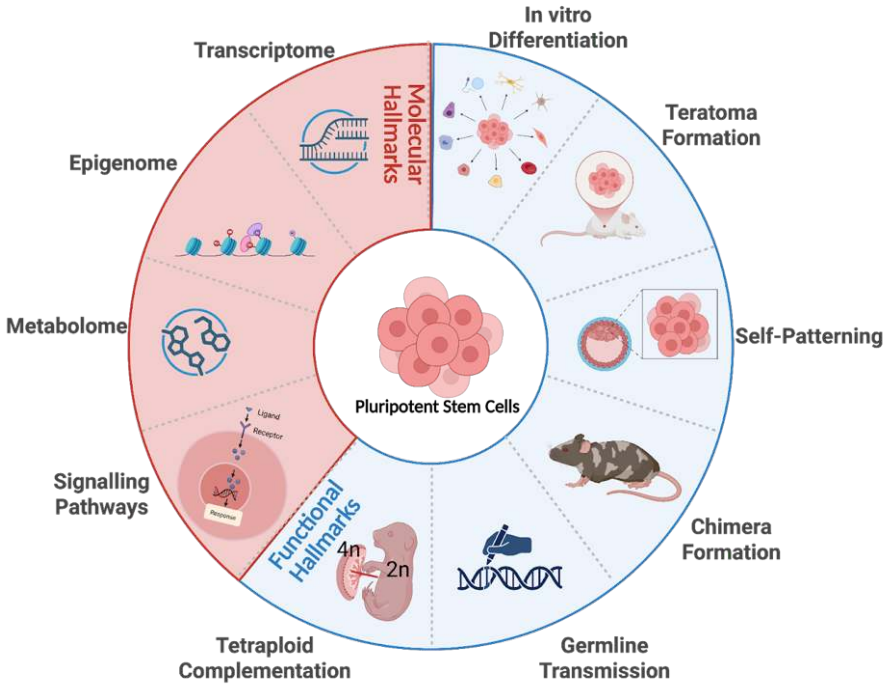

Figure 1.2. Functional and molecular hallmarks of pluripotent stem cells (adapted from Du & Wu, 2024).

Therefore, pluripotency should be viewed as a dynamic continuum rather than a singular, fixed condition, but a complex and multi-dimensional condition defined by how the cell behaves, which genes it expresses, how its chromatin is structured, what signals it responds to, and its metabolic state. With this knowledge, the concept of pluripotency has become more detailed shown in Figure 1.2. It is now known that pluripotent stem cells can exist in different forms, especially the naive and primed states (Hanna, Saha, & Jaenisch, 2010). These are not just stages in a timeline, but represent distinct molecular and epigenetic conditions, each with different signalling responses and potential to differentiate (Nichols & Smith, 2009).

1.3.1 Naive versus Primed Pluripotent States

Naive pluripotency was initially described through studies of the rodent pre-implantation epiblast within the blastocyst (Nichols & Smith, 2009). At this stage, epiblast cells are considered to be in a developmental ground state, not yet influenced by external signals and retaining broad developmental capacity. In mice, embryonic stem cells (ESCs) derived from this blastocyst-stage epiblast can be sustained in vitro under culture conditions that combine leukemia inhibitory factor (LIF) with inhibitors of the FGF/ERK and GSK3 pathways (2i) (Ying et al., 2008). Under these conditions, mouse ESCs exhibit characteristic naive features, including biallelic X-chromosome activity (XaXa) in female cells, low overall DNA methylation, elevated expression of transcription factors such as KLF4, ESRRB, and TFCP2L1, and strong clonogenic potential (Weinberger et al., 2016; An et al., 2020).

In contrast, primed pluripotent stem cells correspond to the post-implantation epiblast, which has undergone morphological reorganization into a cup-shaped epithelium (Brons et al., 2007). At this point, epiblast cells become more structured, responsive to spatial signaling, and are poised for lineage commitment. Epiblast stem cells (EpiSCs) were first isolated from this stage using culture conditions including FGF and Activin A, but excluding LIF, which distinguish them from naive ESC derivation protocols (Tesar et al., 2007). Although EpiSCs still express key pluripotency markers such as Oct4, Sox2, and Nanog, they are different from naive ESCs in several properties such as monoallelic X chromosome inactivation (XaXi) in female cells, increased DNA methylation, and their inability to contribute to chimeric blastocysts (Weinberger et al., 2016). Moreover, while naive ESCs can be converted into EpiSC-like cells by adding FGF and Activin, returning to the naive state requires reprogramming factors like KLF4, showing that the naive-to-primed shift represents a real step in development (Brons et al., 2007).

In humans, the pre-implantation blastocyst epiblast is presumed to represent a naive-like state in vivo, but standard human ESCs and iPSCs in culture more closely resemble the primed condition (Weinberger et al., 2016). Achieving a stable human naive state in vitro requires culture systems distinct from those used for rodents, reflecting species-specific differences in transcriptional regulation and signaling pathways (Theunissen et al., 2014).

These differences between naive and primed states include not only transcription and epigenetic features but also distinct signaling pathways and metabolic profiles. Naive-like human pluripotent stem cells, unlike mouse ESCs, cannot be maintained by LIF/STAT3 signaling alone (Takashima et al., 2014; Theunissen et al., 2014). Their stability requires inhibition of the ERK pathway, usually with MEK or BRAF inhibitors, together with compounds such as PKC inhibitors that help preserve naive features (Takashima et al., 2014). Moderate WNT/β-catenin activation through GSK3 inhibition can promote self-renewal, but high levels may trigger differentiation (Kim et al., 2013). In this state, cells rely more on oxidative phosphorylation, similar to the developmental "ground state" (Zhou et al., 2012).

Primed human pluripotent stem cells depend mainly on FGF2-ERK1/2 and TGF-β/Activin A-SMAD2/3 signaling (Brons et al., 2007). These pathways maintain OCT4 and NANOG expression and support the epigenetic stability of the primed state. Nodal signaling helps balance self-renewal with lineage commitment (Vallier et al., 2009), and NOTCH signaling has been linked to changes in differentiation potential (Lowell et al., 2006). Primed cells use glycolysis as their main energy source, reflecting their progression toward lineage specification (Zhou et al., 2012).

Understanding and controlling these characteristics is essential for improving reprogramming methods, directing cell fate decisions, and safely applying pluripotent stem cells in therapeutic settings.

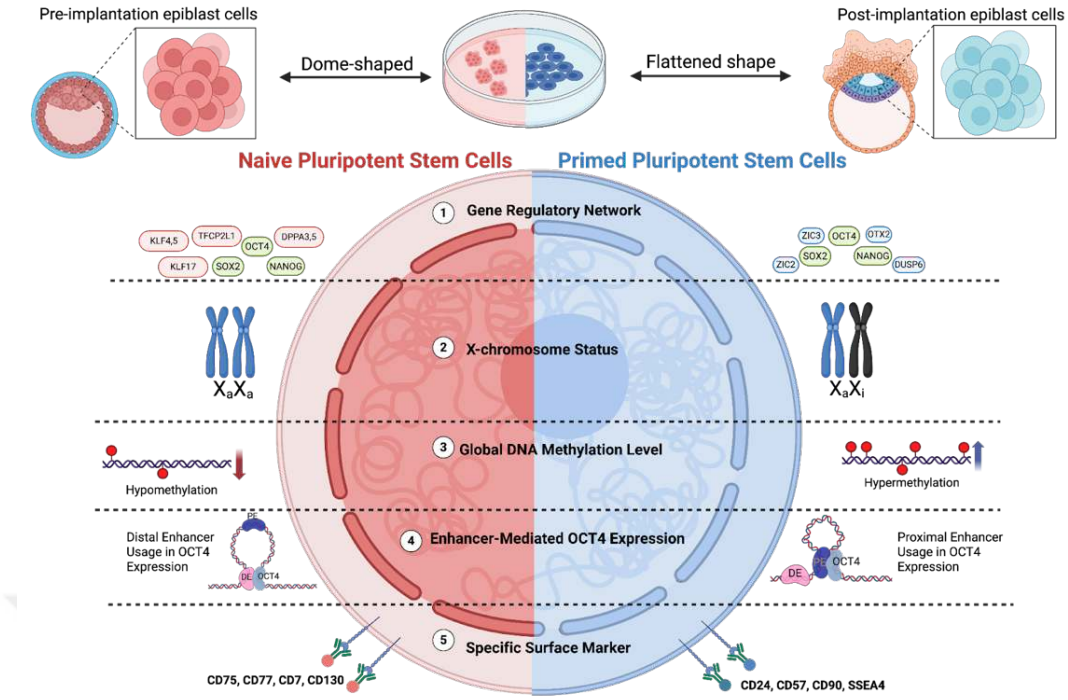

Figure 1.3. Comparison of Naive and Primed Pluripotent States (adapted from Collier and Rugg-Gunn, 2018).

1.4 Establishing Human Naive Pluripotent Stem Cells

Achieving naive pluripotency in humans has been challenging, and three main strategies have been explored that are (a) direct derivation of naive embryonic stem cells (ESCs) from embryos, (b) conversion/resetting of primed hESC/hiPSC lines to naive conditions, and (c) de novo reprogramming of somatic cells into naive hiPSCs.

1.4.1 Direct Derivation from Embryos

In this approach, human embryonic stem cell (hESC) lines are generated from the inner cell mass (ICM) of human blastocysts. Thomson et al. (1998) first obtained the derivation of several well-known lines, being H1, H7, H9, H13, and H14, with utilizing serum-containing medium and mouse embryonic fibroblast feeders. With these early derivations having established a foundation for later culture systems, the addition of FGF2 became a standard approach to support the maintenance of primed pluripotency (Amit et al., 2000; Xu et al., 2001). Building on these advances, researchers developed naive-supportive conditions to attempt the direct isolation of naive hESCs from blastocysts. For example, Theunissen et al. (2014) employed their 5i/LAF cocktail to

derive putatively naive hESC lines, while Ware et al. (2014) treated ICM outgrowths with HDAC inhibitors before transferring them into “2iF” medium containing MEK and GSK3β inhibitors along with FGF2. The resulting cells differentiated into all three germ layers, with a pronounced bias toward the endoderm lineage. More recently, Gue et. al (2021) demonstrated that embryo-derived naive hESCs can adopt TE fate. MEK/ERK inhibition enables this, NODAL/SMAD2/3 blockade increases the rate, whereas Activin signaling suppresses it.

The main advantage of this approach is that it avoids any epigenetic “memory” from a primed or somatic state. The cells start in a naive configuration and often activate the OCT4 distal enhancer without the need for a reset step (Ware et al., 2017; Bi et al., 2022). Importantly, this ability is not restricted to established cell lines, as epiblast cells isolated from E6-E7 blastocysts can also form TE/trophoblast under PD+A83, confirming that the human epiblast retains TE potential (Gue et. al, 2021). Despite this, instability remains an issue, as many early lines showed karyotypic abnormalities or spontaneous differentiation, and aneuploidy was common in lines derived using Theunissen’s 5i/LAF system (Henry et al., 2019; Theunissen et al., 2014). In addition, ethical and practical limitations, such as the limited availability of human embryos and the requirement for strict regulatory approval, further restrict the use of this method (Iltis et al., 2023).

In practical terms, these challenges contribute to highly variable outcomes from direct derivation, and the efficiency is often low. Human embryos often fail to attach or survive without exogenous FGF/Activin signals, resulting in low efficiency, so dozens of embryos may be needed for a single stable line (Desai et al., 2015). Feeder layers such as MEFs, and ROCK inhibitor can improve survival (Lai et al., 2010; Eiselleova et al., 2008), but success depends on factors such as ICM isolation and culture timing. For example, Ware et al. (2023) showed that adding a CHK1 inhibitor during the first outgrowth stage of ICM culture lowered early cell death and emphasized the importance of accurate ICM handling and culture timing for successful hESC derivation.

In summary, direct derivation has proven that human blastocysts can yield cells stably maintained in a naive state in vitro. However, the method remains labor-intensive, inefficient, and inconsistent, and its application is now less common than conversion or de novo reprogramming approaches.

1.4.2 Resetting Primed hESC/hiPSC to Naive

A major approach to achieving human naive pluripotency is the conversion, or "resetting," of established primed hESC/hiPSC lines into naive conditions. Since 2010, this has been accomplished using either transgene overexpression or chemically defined cocktails that modify signaling pathways and the epigenetic landscape (Hanna et al., 2010; Gafni et al., 2013; Theunissen et al., 2014; Takashima et al., 2014; Guo et al., 2017; Zimmerlin et al., 2016). Early studies were based on experiments in which EpiSCs from mice were reverted to the naive state (Xiao, Mai, & Xie, 2016). One of the first examples adapting this approach to human cells was reported by Hanna et al. (2010). They combined the continuous expression of OCT4, KLF4, and KLF2 with 2i/LIF conditions, producing dome-shaped colonies with naive-like characteristics. However, these cells were unstable and returned to the primed state once transgene expression was stopped. Later studies showed that transient expression of transgenes improved the stability of the naive state. For instance, Takashima et al. (2014) transiently overexpressed NANOG and KLF2 in primed hPSCs before culturing them in 2i/L with Gö6983 (PKC inhibitor), generating stable naive cells after transgene removal. Other regulators, such as Signal Transducer and Activator of Transcription 3 (STAT3) and Yes-associated protein (YAP), have also been reported to promote resetting (Chen et al., 2015; Qin et al., 2016). STAT3 acts as a main downstream component of the LIF signaling pathway and induces the expression of naive pluripotency-related genes, including KLF4 and TFCP2L1, which help to reinforce the pluripotency network (Chen et al., 2015). YAP functions as a transcriptional co-activator in the Hippo signaling pathway, where it supports cell proliferation and survival, and its activation contributes to maintaining an undifferentiated, naive-like state (Qin et al., 2016). YAP activity can also be triggered chemically by lysophosphatidic acid (LPA), offering a way to modulate this pathway without genetic modification. These studies demonstrated that the human pluripotency network can be rewired but concerns over genomic integration and a growing preference for transgene-free systems have directed research toward small-molecule protocols.

Chemical resetting related with small molecules is now the main approach. Most current protocols combine MEK and GSK3β inhibition (abbreviated as 2i) with additional inhibitors or agonists and LIF to induce naive features within 5-14 days (Gafni et al., 2013; Theunissen et al., 2014; Ware et al., 2014; Guo et al., 2017). Protocols vary in their composition, efficiency, and the stability of the naive state achieved.

One of the earliest was the Naive Human Stem Cell Medium (NHSM) described by Gafni et al. (2013), combining specific inhibitors and growth factors to promote both the induction and maintenance of the naive state. Firstly, MEK inhibition suppresses the FGF/ERK pathway, which normally drives differentiation in primed hPSCs. Secondly, GSK3β inhibition activates WNT/β-catenin signaling, resulting in the accumulation of β-catenin, relieving TCF3-mediated repression (Martello et al., 2012; Zimmerlin et al., 2016). This strengthens the pluripotency network, but excessive activation of the signalling could trigger differentiation. Thirdly, inhibitors of p38 and JNK block stress-activated MAPK pathways, reducing culture-induced stress responses, supporting proliferation and naive identity. Protein kinase C (PKC) inhibition helps limit differentiation signals linked to cytoskeletal and adhesion pathways, maintaining dome-shaped colony morphology and single-cell cloning capacity (Takashima et al., 2014; Duggal et al., 2015). When Activin A is used at controlled levels, it activates SMAD2/3 signaling to sustain pluripotency gene expression without pushing cells toward a primed phenotype (Vallier et al., 2009). Finally, low concentrations of FGF2 enhance survival and proliferation while minimizing ERK activation (Gafni et al., 2013). Together, these components create a signaling environment that facilitates the transition from primed to naive pluripotency and stabilizes the naive state under feeder-free conditions.

Around the same period, Theunissen et al. (2014) developed the 5i/LAF system, which expanded on 2i (MEK and GSK3β) by adding BRAF, SRC, and ROCK inhibitors. The inclusion of a BRAF inhibitor works together with MEK inhibition to more completely block the ERK signaling pathway, a key promoter of the primed state in human pluripotent stem cells. Targeting both BRAF and MEK ensures that the ERK pathway is suppressed at both upstream and downstream points, reducing the chance of residual activity that could drive differentiation (Bayerl et al., 2021). The SRC inhibitor limits signals from focal adhesion kinase (FAK) and integrin pathways, which are linked to cytoskeletal changes and adhesion-driven differentiation (Legate et al., 2009). Therefore, it supports the maintenance of the compact, dome-shaped morphology characteristic of naive colonies. The ROCK inhibitor helps cells survive single-cell dissociation by preventing apoptosis, being essential for efficient clonal expansion of naive cells. Subsequent experiments demonstrated that the withdrawal of FGF2 had minimal effect on the expression of naive-specific genes (Theunissen et al., 2014). As a result, the authors refined the protocol to 5i/L/A, thereby simplifying the formulation without compromising naive molecular identity.

Ware et al. (2014) introduced a simpler method by applying a short-term treatment with a mixture of histone deacetylase inhibitors (HDACi), specifically sodium butyrate and suberoylanilide hydroxamic acid (SAHA, vorinostat). HDAC inhibition increases histone acetylation, leading to a more open chromatin structure. Then, it improves access to pluripotency-related genes and supports reprogramming toward the naive state. After this priming step, cells were cultured in 2i (MEK and GSK3β inhibition) medium with FGF2. This approach generated naive-like cells with high differentiation potential, particularly toward endoderm.

Guo et al. (2017) refined this strategy to avoid the use of transgenes by combining HDAC inhibition with blocking the WNT pathway using the tankyrase inhibitor XAV939. Inhibiting WNT signaling at this stage prevents β-catenin-driven differentiation cues, thereby stabilizing the naive program. This was combined with 2i, LIF to activate STAT3 signaling, and the PKC inhibitor Gö6983. This combination, later named PXGL, was effective across multiple cell lines, reactivating the X chromosome in female cells and restoring transcriptional and epigenetic features associated with the naive state (Bredenkamp et al., 2019).

Building on earlier protocols, Bayerl et al. (2021) developed the Human Enhanced Naive Stem Cell Medium (HENSM) to more effectively induce and maintain the naive state while overcoming some limitations of previous systems. One key difference is that HENSM does not include broad HDAC inhibitors, which in PXGL can produce unwanted cell types and require multiple passages for stable naive conversion (Guo et al., 2017). Instead, it contains a defined combination of pathway-specific inhibitors that are the MEK-ERK inhibitor PD0325901, WNT inhibitor XAV939, PKC inhibitor Gö6983, SRC inhibitor CGP77675, p38-MAPK inhibitor BIRB796, and ROCK inhibitor Y27632, along with LIF and Activin A. This formulation supports feeder-free culture, reducing variability and facilitating downstream applications such as gene targeting. In practice, HENSM preserves naive characteristics over extended culture periods and shows lower genomic instability than some earlier conditions. Global DNA methylation in HENSM-cultured cells is still higher than in the in vivo preimplantation epiblast. As with other MEK inhibitor-based systems, prolonged culture can lead to loss of genomic imprinting, showing that further improvements are needed.

Advantages include using well-characterized primed lines and producing isogenic naive/primed pairs without embryos. Challenges include genomic instability from strong pathway inhibition, incomplete resetting in some conditions, and variable responses

between lines. Overall, the shift from transgene-based to chemically defined methods have improved accessibility and reproducibility, but issues such as maintaining genomic stability and fully achieving naive epigenetic features remain.

1.4.3 De Novo Reprogramming to Naive iPSCs

A third way to generate human naive pluripotent stem cells is to reprogram somatic cells, such as fibroblasts or blood cells, directly into the naive state. Standard human iPSC generation with Yamanaka factors in FGF2/KSR (serum free) medium produces primed iPSCs (Takahashi et al., 2007), but as early as 2009 researchers began combining reprogramming with naive-supportive conditions to capture the naive state in one step. Li et al. (2009) introduced OCT4, SOX2, NANOG, and LIN28 into human fibroblasts and cultured them with 2i (PD0325901 and CHIR99021), hLIF, and A83-01 that is an ALK5 inhibitor targeting the TGF-β/Activin/Nodal signaling pathway, producing colonies that looked similar to mouse ESCs. These naive-like iPSCs expressed core pluripotency genes and formed teratomas. Hanna et al. (2010) later showed that applying Yamanaka factors under 2i/LIF could push human fibroblasts toward a mouse ESC-like state, but this required continuous transgene expression. When the transgenes were switched off, the cells reverted or differentiated. This suggested that naive pluripotency may be a state that standard reprogramming cannot reach or maintain without extra support. Direct naive reprogramming often produces fewer colonies than primed iPSC generation because naive culture conditions (discussed earlier under the “resetting primed to naive” section) support early human cell growth less effectively than FGF2/KSR. As a result, many partially reprogrammed cells do not survive, and only those that fully activate the naive program remain (Wang et al., 2018). This lowers colony numbers but improves quality by removing incomplete clones, so starting cell density and timing of factor delivery are important.

Naive hiPSCs generated de novo do not carry the epigenetic memory often found in primed hiPSCs, such as residual methylation or donor-specific gene expression (Wang et al., 2018). This can also remove donor-related differentiation biases, giving more consistent potential across lines. However, they may show abnormal genomic imprinting, and also the reprogramming environment can increase the risk of mutations or chromosomal changes (Keshet & Benvenisty, 2021). Some naive-derived clones have shown segmental aneuploidies or deletions not seen in primed cells, so regular karyotype

checks are needed (Kilens et al., 2018). In addition, these protocols are more complex, often requiring sequential media and several modulators, making them technically harder than optimized primed methods.

1.5 Monitoring and Distinguishing Naive vs. Primed Pluripotent Stem Cells

1.5.1 Surface Markers

Although antibody-based methods have long been used to distinguish between different cell populations, the identification of surface markers that allow for the selective isolation of human naive pluripotent stem cells remains challenging. Systematic analyses by O'Brien et al. (2017) and Liu et al. (2017) demonstrated that no single surface antigen can reliably separate naive from primed cells. Instead, higher accuracy is achieved by combining multiple positive and negative markers.

Classical pluripotency-associated markers such as TRA-1-60, TRA-1-81, SSEA-3, and SSEA-4 are abundantly expressed in primed hPSCs, yet show variable or reduced expression in naive-like cells (Adewumi et al., 2007; O'Brien et al., 2017). In addition, CD24, highly expressed in primed hPSCs, is consistently downregulated in naive cells, making it a useful negative selection marker for identifying the naive state (Shakiba et al., 2015). Other negative markers include CD57 and CD90, both of which are more prevalent in primed populations (Trusler et al., 2018). Moreover, the expression of several surface molecules such as NLGN4X, CDH3, GPR64, and PCDH1 was consistently reduced in naive cultures, suggesting their potential as negative selection markers to help eliminate residual primed-like cells (Collier et al., 2017).

In contrast, certain positive markers, including CD75, CD130 (also known as GP130), and SUSD2, are selectively upregulated in naive-like populations. Cells co-expressing CD75 and CD130 cluster closely with transcriptional profiles of the preimplantation epiblast, supporting their classification as naive (Collier et al., 2017; Bredenkamp et al., 2019). Additional markers, including CD7 and CD77, also showed selective enrichment in naive cells, with CD7 in particular being upregulated at early stages of reprogramming.

Altogether, these findings emphasize the value of using combined surface marker strategies not only to distinguish naive and primed states, but also to identify intermediate phenotypes and reduce heterogeneity within naive-like populations (Liu et al., 2017; Karagiannis & Takashima, 2017). Using surface marker profiles provides a practical and

informative approach to isolating high-quality naive hiPSC lines and to assessing the extent of transcriptional and epigenetic resetting achieved by different reprogramming methods.

1.5.2 Reporter Systems

Naive pluripotent stem cells (PSCs) have a specific group of transcription factors and a hypomethylated genome, while primed PSCs already start showing signs of differentiation and have a different transcriptome profile (Theunissen et al., 2016). For example, transcription factors such as TFCP2L1, REX1, KLF2, KLF4, KLF17 and DPPA3 are highly expressed in naive hPSCs but are strongly reduced when cells move to the primed state (Romayor et al., 2022; Dunn et al., 2014)). On the other hand, core pluripotency genes like OCT4 (POU5F1), SOX2, and NANOG are active in both states, although their expression levels and regulation differ depending on the culture conditions. Because of these differences, researchers have created reporter systems to help visualize and separate naive and primed cells in real time (Theunissen et al., 2014; Choi et al., 2016; Gafni et al., 2013; Takashima et al., 2014; Theunissen et al., 2016). These reporter cell lines are useful for following cell state changes, selecting pure cell populations, and studying pluripotency transitions both in vitro and in vivo.

OCT4-based Reporter Systems

OCT4 (POU5F1) is a key pluripotency gene expressed in both naive and primed pluripotent stem cells. Its expression is regulated by two distinct enhancers that are the distal enhancer (DE), being active in the naive state, and the proximal enhancer (PE), functioning in the primed state (Choi et al., 2016). This differential enhancer usage has been utilized in reporter systems to distinguish between naive and primed cell states and optimize naive culture conditions. For example, Theunissen et al. (2014) developed a human embryonic stem cell (ESC) line carrying an OCT4-ΔPE-GFP reporter, in which the proximal enhancer is deleted with using TALE nucleases. In this design, GFP expression is controlled only by the distal enhancer, which makes it possible to identify naive cells. Utilizing OCT4-ΔPE-GFP line, they screened inhibitor combinations supporting naive human PSCs in 5i/L/FA conditions. Then, it is observed that under these conditions, GFP is strongly expressed, whereas in primed conditions, it is largely silenced due to the reliance on the deleted PE. Although this single-reporter system can enrich for

naive-like PSCs, it shows some “leakiness,” as primed cells may still exhibit weak GFP expression.

To increase specificity, dual-reporter strategies have been introduced. Choi et al. (2016) created a double-transgenic mouse model expressing both OCT4-ΔPE-GFP (DE-driven) and OCT4-ΔDE-tdTomato (RFP) (PE-driven). Therefore, it can be concluded that GFP is driven by the DE and RFP by the PE. In this system, GFP^{+}/RFP^{-} marks naive cells, while primed cells are GFP^{-}/RFP^{+}, allowing clear discrimination between the two states. This dual-reporter setup reduced the leakiness observed in single reporters and allowed isolation of pure cell populations by flow cytometry, as well as downstream applications such as chimera contribution assays (Sun et al., 2016). Collectively, this shows that this dual-reporter approach more accurately reflects the in vivo OCT4 enhancer activity and avoids the ambiguity seen with single reporters. Using this model, it was shown that under serum/LIF conditions, cells often exist in a mixed state expressing both reporters. On the other hand, under 2i/LIF naive conditions, cells display uniform GFP positivity and no RFP (Choi et al., 2016). In fully primed cells, analysis revealed that only RFP is active.

An established alternative OCT4-based reporter system is the EOS-GFP transgene, which has been widely used in studies aiming to “reset” human pluripotent stem cells (PSCs) to a naive state (Hotta et al., 2009). The EOS-GFP reporter is driven by a regulatory cassette that combines a mouse Early Transposon (ETn) minimal promoter with mouse Oct4 distal enhancer elements. These enhancer regions contain binding sites for key pluripotency transcription factors, including OCT4 and SOX2. Therefore, it can be ensured that GFP expression is selectively activated in cells exhibiting a naive pluripotent state. This reporter, delivered via piggyBac or lentiviral vectors, is specifically active in naive PSCs but becomes silenced in primed cells. This enabled the identification and selection of naive-like colonies based on GFP positivity within a mostly GFP-negative population.

Originally described by Hotta and Ellis (2009), the EOS system became a popular tool because it does not interfere with endogenous genes yet effectively reports the activation of the naive-specific Oct4 enhancer. One drawback of this method is that it may be susceptible to position effects or silencing over extended culture periods due to its random integration into the genome. Despite this limitation, EOS-GFP has been applied in multiple studies as a practical and reliable tool for monitoring naive pluripotency induction in human PSCs.

HERVH-Based Reporter Systems

A related method for monitoring pluripotent states makes use of the transcriptional activity of the primate-specific endogenous retrovirus HERVH (Collier & Rugg-Gunn, 2018). In these reporter systems, promoter or enhancer sequences derived from HERVH elements, known to be active in human pluripotent stem cells, are utilized to drive a fluorescent reporter gene. One of the most common configurations employs the LTR7 promoter sequence placed upstream of a GFP transgene, resulting in strong reporter activation in specific pluripotent contexts (Wang et al., 2014). Alternative versions of this reporter have been generated in which the LTR7 sequence is substituted with other regulatory elements from HERVH, or in some cases with sequences covering the entire HERVH transcript. Such differences in construct design can lead to both technical and biological heterogeneity, which may influence reporter sensitivity and complicate data interpretation.

Most HERVH-GFP reporters rely on the LTR7 promoter, a regulatory element associated with high HERVH transcription in certain pluripotent states (Wang et al., 2014). In these systems, hPSCs exhibiting high HERVH-GFP activity typically show reduced expression of primed-state markers and adopt a dome-shaped, naive-like morphology compared with HERVH-GFP-low or -negative cells (Wang et al., 2016). However, these cells do not fully match the molecular and functional characteristics of naive PSCs, and repeated fluorescence-activated cell sorting (FACS) is often required to sustain a homogeneous HERVH-GFP-high population. Moreover, endogenous HERVH transcription is also detectable in primed hPSCs, and reporter constructs are not invariably based on the LTR7 promoter. In some cases, alternative LTR subtypes or custom-engineered promoter elements are used instead (Theunissen et al., 2016). Consequently, while HERVH-GFP reporters are valuable tools for enriching naive-like cell populations, their results should be interpreted cautiously and validated in a context-specific manner.

Naive-Specific Reporter Candidate: KLF17

KLF17 is a Krüppel-like factor (KLF) family transcription factor enriched in human naive pluripotent cells (Lea et al., 2021). It encodes zinc-finger DNA-binding domains that preferentially recognize GC-rich promoters and direct gene regulation. Single cell analyses of human embryos have shown that KLF17 is co-expressed with NANOG and SOX2 in the epiblast of human blastocysts (Kagawa et al., 2022). While its expression is undetectable in primed hESCs, it is highly expressed in naive hESCs, where it has been

shown to bind the promoters of several active naive-specific genes (Bi et al., 2022). KLF17 supports naive identity and facilitates primed-to-naive transition, although its necessity appears context-dependent due to potential redundancy with other KLFs.

Functional studies support a role for KLF17 in the naive state. In primed hESCs, ectopic KLF17 can induce a naive-like transcriptome and facilitate resetting under naive-permissive conditions (Bi et al., 2022; Lea et al., 2021). In one study, CRISPR knockout of KLF17 led to a collapse of naive pluripotency and differentiation under HENSM/HENSM-ACT conditions (Bayerl et al., 2021), whereas another study found that KLF17 loss did not prevent establishing naive hESCs (Lea et al., 2021).

Taken together, current evidence supports KLF17 as a strong naive marker (Okubo et al., 2023; Bi et al., 2022). Therefore, a KLF17 promoter-driven fluorescent reporter can be used to identify naive cells. Endogenous KLF17-GFP knock-in lines have already been used for this purpose (Wu et al., 2025). During primed-to-naive resetting, KLF17 rises after the earliest changes. Upregulation is clear around day 7-8, consistent with a marker that reports the later phase of the transition rather than the very onset (Bi et al., 2022).

1.6 Epigenetic Regulation of Pluripotent States

Epigenetic and chromatin regulators are essential for defining and maintaining cell identity (Biswas & Rao, 2018). They control changes in chromatin structure and gene expression, mainly by adding or removing chemical modifications on DNA and histone proteins. Based on their function, these regulators are grouped into three main types that are readers, writers, and erasers. Reader proteins detect specific histone post-translational modifications (PTMs) and attract other protein complexes that can activate or repress genes (Musselman et. al, 2012). To exemplify, bromodomain-containing proteins such as BRD4 and BRD9 bind to acetylated lysines and help maintain active enhancer activity.

Writers are enzymes that introduce new epigenetic marks, influencing chromatin structure and gene activity (Biswas & Rao, 2018). DNA methyltransferases (DNMTs) catalyze cytosine methylation. Histone methyltransferases include DOT1L, which methylates H3K79, and MLL1/KMT2A, which methylates H3K4. Histone acetyltransferases such as CBP and p300 acetylate lysine residues on histones and non-histone proteins. On the other hand, erasers remove these marks, often leading to chromatin condensation or transcriptional resetting. This group includes TET1-3

enzymes, which mediate the iterative oxidation of 5-methylcytosine in DNA demethylation pathways, and histone deacetylases (HDACs), which remove acetyl groups from histones, typically resulting in transcriptional repression.

The coordinated activity of these regulators is particularly important during transitions between pluripotent states, as they remove lineage-specific epigenetic memory and create a chromatin environment that supports pluripotency (Pastor et al., 2016). As noted earlier, human naive pluripotent stem cells resembling the pre-implantation epiblast are characterized by open chromatin, reduced DNA methylation, and low levels of repressive histone marks. In contrast, human primed pluripotent stem cells reflecting the post-implantation epiblast exhibit higher heterochromatin content, increased DNA methylation, and activation of genes related to early lineage commitment (Nichols & Smith, 2009; Pastor et al., 2016). Moving cells into the naive state, either by reprogramming somatic cells or resetting primed human ESCs, is challenging due to several epigenetic barriers. These include repressive histone modifications, active somatic enhancers, and chromatin remodelers, which block the activation of the naive transcriptional program.

1.6.1 Mechanism and Role of DOT1L

DOT1L is a histone methyltransferase that adds methyl groups to lysine 79 of histone H3 (H3K79) within gene bodies (Allis & Jenuwein, 2016). In differentiated and primed pluripotent cells, this mark is enriched on many actively transcribed genes and supports transcription elongation, helping to maintain lineage-specific gene expression (Steger et al., 2008). This function makes DOT1L an epigenetic barrier during cell fate reprogramming (Onder et al., 2012). Inhibition of DOT1L improves reprogramming efficiency, increases the number of iPSC colonies. When combined with other epigenetic inhibitors, can even replace some Yamanaka factors (KLF4 and c-MYC), allowing iPSC generation using only OCT4 and SOX2 because DOT1L inhibitors (like SGC0946 or EPZ-5676) relaxes chromatin and may thereby increase the accessibility of pluripotency factors to their target enhancers.

Inhibition of DOT1L promotes primed-to-naive conversion in part by reducing H3K79me2 at developmental regulators such as *Gata3 and Gata6*, with evidence for a primordial germ cell-like (PGCLC) intermediate in the mouse BiPNT (BMP4 induced mouse primed to naive transition) system (Yu et al., 2022). Although H3K79 methylation

is linked to active transcription, its removal does not cause immediate global gene silencing but instead shifts chromatin toward a more permissive, ESC-like state (Wille & Sridharan, 2022). This change facilitates repression of persistent barrier genes such as Nfix, supports mesenchymal-to-epithelial transition (MET), reduces accessibility at trophoblast and endoderm-associated loci, and enriches naive-specific chromatin features (Li et al., 2010). By contrast, a DOT1L-specific global decrease in accessibility at trophoblast or endoderm loci is not firmly established; restriction of trophoblast programmes during naive induction is more clearly associated with PRC2/H3K27me3 (Kumar et al., 2022).

The overall effect results from a broad reorganization of chromatin rather than changes in single target genes (Wille & Sridharan, 2022). As a result, DOT1L inhibition promotes the shutdown of somatic and primed gene programs and the activation of key naive pluripotency factors. In both mouse and human cells, DOT1L inhibitors have been used in naive induction protocols and show the greatest effect during intermediate stages of reprogramming, after epithelialization but before full activation of pluripotency genes. By removing H3K79me-dependent transcriptional memory, DOT1L inhibition helps overcome a major epigenetic barrier and supports the establishment of a stable naive state (Wood, Tellier, & Murphy, 2018).

1.6.2 Mechanism and Role of MENIN

MENIN, encoded by MEN1, is a core scaffold of the MLL1/KMT2A histone methyltransferase complex (Koen, Timmers, & Brown, 2018). It anchors MLL1 to specific promoters, including developmental regulators such as HOX. In this way, MENIN ensures stable H3K4me3 deposition, maintains lineage-associated transcriptional programs, and reinforces cell identity (Agarwal & Jothi, 2012). In pluripotent cells, this maintenance of differentiation-associated genes can oppose acquisition of the naive state. Small-molecule disruption of the MENIN-MLL1 interface like VTP-50469 releases MLL1 from chromatin, reduces H3K4me3 at target loci, and dampens lineage gene expression (Krivtsov et al., 2019). Originally developed for MLL-rearranged leukemia, where it downregulates HOX/MEIS1 and induces differentiation, MENIN inhibition has a parallel utility in reprogramming: it acts as a barrier remover rather than a direct activator, increasing the efficiency and often the kinetics of iPSC generation and favoring transitions toward naive-like pluripotency under permissive

conditions. Overall, MENIN-MLL1 sustains lineage transcriptional memory, and its pharmacological inhibition attenuates this memory, creating a chromatin context more permissive for establishment of the naive transcriptional network (Wang & Helin, 2025).

1.6.3 Mechanism and Role of P300/CBP Inhibitors

P300 and CBP, encoded by KAT3A and KAT3B, are histone acetyltransferases that act as transcriptional coactivators (Martire et al., 2020). They deposit acetyl groups on histones, most notably H3K27 at enhancers, and recruit transcriptional machinery to active loci. Each contains a catalytic HAT domain, which supports new gene activation, and a bromodomain that recognizes acetylated lysines to anchor the complex to chromatin. In differentiated cells, P300/CBP are enriched at super-enhancers, where they maintain the expression of cell identity genes (Witte et al., 2015). While this activity is essential for development, it can restrict reprogramming by preserving the active enhancer architecture of the somatic state.

Selective inhibition of the CBP/p300 bromodomain such as I-CBP112 and SGC-CBP30 disrupts chromatin binding-dependent maintenance of somatic enhancers and facilitates their silencing, yet leaves HAT catalytic activity intact, consistent with the observation that broad HAT inhibition (A-485), impairs reprogramming (Ebrahimi et al., 2019). In human OSKM reprogramming, bromodomain inhibition acts early, accelerates colony formation, promotes the mesenchymal-to-epithelial transition, and aids activation of pluripotency genes.

According to Ebrahimi et al. (2019), used together with DOT1L inhibition, CBP/EP300 bromodomain inhibitors accelerate human reprogramming and allow iPSC derivation using only OCT4 and SOX2. In practice, OS colonies were obtained when a DOT1L inhibitor was combined with forskolin, VPA, and DZNep; adding CBP30 further increased efficiency, consistent with removal of complementary epigenetic barriers. By contrast, catalytic inhibition of the CBP/p300 HAT domain with A-485 broadly depletes H3K27ac, blocks induction of core pluripotency genes, and prevents iPSC formation. Genomic profiling indicates that bromodomain inhibition lowers H3K27ac and chromatin accessibility at enhancers of somatic regulators such as PRRX1. This shift promotes their silencing without compromising activation of pluripotency networks.

In the context of naive conversion, P300/CBP activity supports primed-state and differentiation-associated transcription, which can hinder reversion to the ground state.

Bromodomain inhibition erases acetylation at these enhancers, allowing naive-specific regulatory elements to emerge (Ebrahimi et al., 2019). Together with DOT1L inhibition and naive-inducing signaling inhibitors, this strategy drives a shift toward the chromatin-accessibility and DNA-methylation features of naive pluripotency. Targeting the bromodomain but not the HAT domain detaches enhancer anchoring of the old program while retaining the acetyltransferase function required for naive gene activation.

1.6.4 Mechanism and Role of BRD9 Inhibitors

BRD9 is the bromodomain-containing subunit of the non-canonical BAF (ncBAF/GBAF) complex, which also includes GLTSCR1/GLTSCR1L (Mashtalir et al., 2018). BRD9 uses its bromodomain to recognize acetyl-lysines. This interaction helps recruit ncBAF to target loci, where the BRG1/SMARCA4 ATPase remodels chromatin.

In embryonic stem cells, BRD9/ncBAF co-localizes with core naive regulators such as KLF4 and Sp5 and supports naive gene expression. Pharmacological inhibition with I-BRD9 rapidly removes BRD9 from thousands of genomic sites and shifts transcription to a primed-like state (Gatchalian et al., 2018). In line with this state dependence, BRD9 is not required for maintaining primed human iPSCs but is essential under naive conditions (Sevinç et al., 2022). During somatic-cell reprogramming, BRD9 acts as a barrier. Genetic or chemical inhibition enhances OSKM activity, reduces accessibility at fibroblast enhancers, and downregulates somatic regulators. In human fibroblasts, BRD9 loss mainly decreases accessibility at enhancers of extracellular-matrix and adhesion genes, which accelerates silencing of the somatic program. BRD9 inhibition shows an additive effect with DOT1L inhibition, suggesting that they act as complementary chromatin barriers. Taken together, these findings support a timing principle: BRD9 targeting is most effective when applied transiently early in reprogramming to erase somatic identity, whereas sustained inhibition in established naive ESCs destabilizes naive enhancers and networks (Gatchalian et al., 2018; Sevinç et al., 2022).

1.6.5 Epigenetic Modifiers Identified by Genome-wide CRISPR

Screening experiments in molecular biology provide high-throughput and unbiased approaches to identify genes or factors that shape a given biological process (Bock et al., 2022). One widely applied method is the pooled CRISPR-Cas9 screen, in which a library of single-guide RNAs (sgRNAs) targeting thousands of genes is delivered to cells at a

low multiplicity, so that the majority of cells incorporate only a single sgRNA (Shalem et al., 2013). After subjecting the cells to a specific selection or assay like utilizing a pluripotency induction protocol, next-generation sequencing of sgRNA barcodes indicates which knockouts are enriched or depleted. This analysis enables the generation of ranked gene lists that highlight genes either promoting or constraining the phenotype of interest.

Collier et al. (2022) showed through a genome-wide CRISPR screen that HDACs, LSD1 (KDM1A), and PCGF3 may function as regulators of naive pluripotent stem cell (PSC) reprogramming. HDACs and LSD1 are chromatin-modifying enzymes. They usually act as repressors. HDACs remove acetyl groups from histone tails, which makes chromatin more compact. When HDAC activity is lost (by HDAC2 deletion) primed PSCs convert more easily to the naive state (Kondo et al., 2014). This fits with earlier findings that broad HDAC inhibition, such as valproic acid treatment, increases histone acetylation and promotes naive gene activation. LSD1 removes methyl groups from histone H3 lysine 4 (H3K4), deleting an activating mark. It often works with HDAC1/2 in the CoREST complex (Martinez-Gamero et al., 2021). Together, they silence enhancers by deacetylation and demethylation. Loss of LSD1 has the opposite effect. Enhancers stay methylated and also gain acetylation. This activates naive genes but disrupts normal differentiation. Pharmacological inhibition of LSD1 has also been shown to speed up iPSC induction. PCGF3 is different. It is part of the PRC1.3 Polycomb complex. This complex monoubiquitylates histone H2A at lysine 119 (H2AK119ub) and compacts chromatin (Collier et al., 2022). As a result, developmental genes stay repressed. Without PCGF3, PRC1.3 becomes unstable. Primed PSCs can still survive, but they fail to form naive colonies or express naive markers. Instead, differentiation genes remain active, and cells become partially differentiated.

The overall aim of this thesis was to investigate epigenetic and genetic regulators of naive pluripotency in human induced pluripotent stem cells (hiPSCs) through complementary pharmacological and genetic approaches. Specifically, this work pursued three main objectives:

1. To determine the role of key chromatin-modifying enzymes in primed-to-naive transition, by evaluating the effects of selective inhibition of DOT1L, MENIN, P300/CBP, and BRD9 using small-molecule inhibitors, in combination with OCT4 distal enhancer-driven GFP and KLF17-GFP reporter assays as well as gene expression analyses.

2. To functionally characterize a novel KLF17-GFP reporter line generated in this laboratory, in order to validate its utility as a naive-specific marker for monitoring state transitions.
3. To establish and apply a genome-edited iPSC line carrying an inducible Cas9 at the AAVS1 safe harbor locus, enabling systematic knockout of both core pluripotency genes (TGFBR2, TP53, RPL3, OCT4) and candidate naive regulators (HDAC2, LSD1, PCGF3).

By integrating pharmacological inhibition, reporter-based monitoring, and CRISPR-mediated perturbation, this thesis aimed to identify major epigenetic barriers that restrict naive pluripotency, to validate a new reporter system for naive state tracking, and to provide genetic tools for dissecting the regulation of human naive.

Chapter 2:
MATERIALS AND METHODS

2.1 Obtaining from Primed Stem Cells to Naive Stem Cells under HENSM Conditions

Naive pluripotent conversion was performed using the HENSM-ACT protocol with human pluripotent stem cell (PSC) lines, including WIBR3 ΔPE OCT4-GFP, NO #2 Wild type and KI KLF17 cell lines. Primed PSCs were initially 50,000 cells per well seeded onto 1% or 2% Geltrex-coated 12-well plates in E8 or mTeSR medium. After cell attachment, the culture medium was replaced with HENSM-ACT medium, composed of a 1:1 mixture of DMEM/F12 (Gibco) and Neurobasal (Gibco), supplemented with 1% Penicillin-Streptomycin (Biowest), 1% GlutaMAX (Gibco), 1% Non-Essential Amino Acids (NEAA), 1 mM Sodium Pyruvate, 1% N2 supplement, 2% B27 supplement, 50 μg/mL L-ascorbic acid, 2-phosphate magnesium salt, 0.2% Geltrex added to the medium after filtering, 20 ng/mL recombinant human LIF, 2 μM XAV939, 2 μM Gö6983, 1.2 μM PD0325901, 1.2 μM CGP77675, 1.2 μM Y-27632, 0.8 μM BIRB796, and 10 ng/mL Activin A. Cells were maintained in these conditions for conversion. Naive identity, as evidenced by dome-shaped colony morphology, is generally observed by passage 2. In our experiments, cells were generally maintained up to passage 5 to obtain consistent and reliable data reflective of the naive state. For passaging, cultures were washed once with phosphate-buffered saline (PBS) and incubated with 0.8× TrypLE Express (Gibco) or 1× Accutase (StemCell Technology) for 3 minutes at 37°C. After enzymatic treatment, the enzyme was aspirated. The loosely adherent colonies were then gently resuspended in HENSM-ACT medium supplemented with 10 μM freshly added Y-27632 and replated at a 1:3 to 1:4 ratio depending on the confluency. Cells were passagged every 3 or 4 days.

2.2 Maintenance of iPSCs

Induced pluripotent stem cells (iPSCs) were maintained on Geltrex-coated plates (Gibco, A1413302) using an in-house formulation of mTeSR medium, prepared according to published protocols (Ludwig & A. Thomson, 2007). Cultures were fed daily with fresh medium and passaged every 3-4 days depending on their confluency, once colony confluency approached ~65-70%. For passaging, cells were rinsed with PBS and incubated with 0.5 mM EDTA in PBS at 37 °C for 4 minutes to loosen cell-cell contacts.

The EDTA solution was removed, and colonies were gently dissociated by pipetting. Appropriate numbers of colony fragments were replated onto new Geltrex-coated dishes in mTeSR supplemented with 10 μM Y-27632 (ROCK inhibitor) to enhance post-passaging survival. Medium was replaced the following day with mTeSR lacking Y-27632, and cultures were maintained under standard conditions (37 °C, 5% CO_2, 5% O_2).

2.3 Synthesis complementary DNA

Total RNA was extracted from cells using the NucleoSpin RNA Kit (Macherey-Nagel), following the kit's protocol. For reverse transcription, 500 or 1000 ng of purified RNA was used as input. RNA samples were combined with 2.5 μL of 2 mM dNTP mix (Thermo Scientific) and 2 μL of random hexamer primers (Invitrogen). The volume was adjusted to 16.5 μL with nuclease-free water, and the mixture was incubated at 65°C for 5 minutes, then immediately cooled on ice.

The reverse transcription (RT) reaction mix was prepared separately, containing 5 μL of 5X First Strand Buffer (Invitrogen), 2 μL of 0.1 M DTT (Invitrogen), and 0.5 μL of RNasin Plus RNase inhibitor (Promega). This RT mix was added to the RNA-primer mixture and incubated at room temperature for 10 minutes. Subsequently, 1 μL of M-MLV reverse transcriptase (Invitrogen) was added, and the reaction was carried out at 37°C for 1 hour. The enzyme was inactivated by heating the reaction to 70°C for 15 minutes. The resulting cDNA was diluted with nuclease-free water. 75 μL of the water was used and stored at -20°C until further use.

2.4 RT-qPCR

For quantitative PCR, reactions were assembled using 10 μL of 2X SYBR Green Master Mix (Qiagen). Each 20 μL reaction contained 2 μL of 2.5 μM forward and reverse primer mix, 6 μL of nuclease-free water, and 2 μL of diluted cDNA. Amplification was performed using a Roche LightCycler instrument. A protocol of 40 cycles of 30 seconds at 95 °C, 30 s at 60 °C and 30 s at 72 °C is generally preferred. First, Ct values were determined utilizing the second derivative maximum method. Then ΔCt was calculated. The relative expression levels were obtained using the 2^-ΔCt formula, normalized to the control group to calculate fold change, and finally the error margins (maximum and minimum) were included. Gene expression levels were normalized to the housekeeping gene, which is GAPDH for our experiments.

Table 2.1: The table of primers utilized in RT-qPCR

GAPDH Forward	GCCAGCCGAGCCACAT
GAPDH Reverse	CTTTACCAGAGTTAAAAGCAGCCC
hNLRP7 Forward	AGGACGGACAGGTGCAAGAAATA
hNLRP7 Reverse	CCCTGGGTAACATCTTCCTCT
KLF17 Forward	AGCAAGAGATGACGATTTTC
KLF17 Reverse	GTGGGACATTATTGGGATTC
SUSD2 Forward	CCTGGCATGTCAAGTCGCT
SUSD2 Reverse	CCTGTGAGTAGGGCATTCCTG
DNMT3L Forward	CAGTGCCTGCTCCTTATGGCT
DNMT3L Reverse	TGAACAAGGAAGACCTGGACG
hTFCP2L1 Forward	CTCAGGTGCTGACTTGCTGA
hTFCP2L1 Reverse	ATGGCGTGGTACACAGACAG
NANOG Forward	TGATTTGTGGGCCTGAAGAAA
NANOG Reverse	TGGTGGTAGGAAGAGTAAAG
endo_OCT4 Forward	CCTCACTTCACTGCACTGTA
endo_OCT4 Reverse	CAGGTTTTCTTTCCCTAGCT
hCD24 Forward	ACCCACGCAGATTTATTCCA
hCD24 Reverse	ACCACGAAGAGACTGGCTGT
hNLRP2 Forward	ATAACACGGAAAGAACGACCA
hNLRP2 Reverse	TAGAACAGGGCAGTGAGAAAC
SOX17 Forward	GTGGACCGCACGGAATTTG
SOX17 Reverse	GGAGATTCACACCGGAGTCA
ARGFX Forward	CCGGAGTCAACAGTAAAGGTTTG
ARGFX Reverse	GGTGGGCACATTCTTCTTGGA
DPPA3 Forward	TTAATCCAACCTACATCCCAGGG
DPPA3 Reverse	AGGGGAAACAGATTCGCTACTA

2.5 Preparation of Concentrated Virus

To initiate viral production, HEK293T cells were maintained in D10 medium consisting of DMEM High Glucose supplemented with 10% FBS and 1% Pen/Strep and seeded onto 10-cm dishes at a density of 2.5 × 10^6 cells per dish. On the following day, cells were transfected with three plasmids, namely 250 ng of the envelope plasmid VSV-G (Addgene #8454), 2250 ng of the packaging plasmid psPAX2 for lentiviral constructs (Addgene #12260), and 2500 ng of the plasmid of interest. Transfections were performed using PEI as the transfection reagent. To improve its efficiency, frozen PEI was pre-incubated at 70 °C for 10 minutes before first use. For complex formation, plasmids (5 µg) and PEI (20 µL) were separately diluted in 250 µL of basal DMEM in individual tubes. The combined mixture was incubated for 30 minutes and subsequently added dropwise to HEK293T cells in freshly changed medium. Cells were incubated for a minimum of 16 hours to allow transfection. After 16 hours, the old medium was replaced with fresh medium. Viral supernatants were harvested at 48 and 72 hours post-transfection. The collected supernatants were pooled into a Falcon tube and centrifuged at 2000 rpm for 5 minutes to remove dead cells. Without disturbing the pellet, the clarified supernatants were filtered through 0.45-µm membranes to eliminate cellular debris. PEG8000 (50%) was added to the filtered medium at a 1:4 ratio and incubated for 48 hours at 4 °C. Samples were then centrifuged at 2000 rpm for 20 minutes. After the centrifugation, the supernatant was discarded, and the resulting pellets were resuspended in 160 µL of cold PBS to achieve a 100× concentration. The resuspended virus was aliquoted into 20-µL portions and stored at −80 °C as concentrated viral stocks.

2.6 iPSC Transfection Protocol

For transfection experiments, iPSCs were cultured in 6-well plates and seeded the day before in E8 medium supplemented with 10 µM Y-27632 (ROCK inhibitor) to reach ~65% confluency at the time of transfection. On the day of transfection, the plasmid DNA was first diluted in 125 µL of only DMEM together with 10 µL of P3000 reagent (Invitrogen, L3000001) and incubated for 5 minutes at room temperature. In parallel, 3.75 µL of Lipofectamine 3000 (Invitrogen, L3000001) was diluted in 125 µL of only DMEM and also incubated for 5 minutes. The two solutions were then combined and incubated for an additional 15 minutes to allow formation of DNA-lipid complexes. This mixture was added dropwise onto the iPSCs, which were left in contact with the complexes for

16 hours. Following this incubation period, the transfection medium was replaced with fresh standard iPSC culture medium.

2.6.1 Integration of the TRE-Cas9-NeoR Cassette into the AAVS1 Locus

To integrate the TRE-Cas9-NeoR cassette into the AAVS1 genomic locus, Lipofectamine™ 3000 (Thermo Fisher Scientific) was used according to the manufacturer's protocol. A total of 1.5 µg AAVS1-TALEN-L, 1.5 µg AAVS1-TALEN-R (Gonzalez et al., 2014), and 3 µg AAVS1-TRE-Cas9-NeoR plasmid were combined with the transfection reagent and applied to 6×10^5 iPSCs. After 48 hours, cells were subjected to selection in medium supplemented with 60 µg/mL neomycin for one week. Surviving colonies were subsequently plated into 96-well plates at a density of three cells per well to promote the derivation of single-cell clones. Genomic DNA was isolated from expanded clones, and PCRs were performed using specific primers to confirm targeted integration. PCR analysis identified both mono-allelic and bi-allelic integration events of the Cas9 cassette at the AAVS1 locus.

2.7 Plasmid Cloning and Transformation

Single-guide RNA (sgRNA) target sites were chosen as 20-nt sequences immediately upstream of an NGG PAM (the PAM was not included in the oligonucleotides). For each target, two complementary oligos bearing BsmBI -compatible overhangs were designed, ordered at standard desalt grade, and resuspended to 100 µM. The lentiGuide-Puro vector (5 µg) was digested with BsmBI at 37 °C for 30 min and dephosphorylated in the same reaction using alkaline phosphatase (with fresh DTT). Digests were resolved on agarose; the backbone band (leaving the ~2 kb filler behind) was excised and purified. For oligo annealing, 1 µL of each 100 µM oligo, 1 µL 10× T4 ligation buffer (ATP-containing), and 0.5 µL T4 PNK were combined and brought to 10 µL with water, incubated 37 °C 30 min and 95 °C 5 min, then slow-cooled to 25 °C (≈5 °C/min); the duplex was diluted 1:200. Ligation was performed by mixing 50 ng BsmBI-cut vector with 1 µL annealed duplex in Quick Ligase buffer for 10 min at room temperature; a no-insert ligation served as a negative control. Ligation products were transformed into recombination-deficient E. coli and plated on antibiotic-selective LB agar (typically ampicillin) overnight at 37 °C. Two to four colonies were picked for miniprep, and inserts were verified by colony PCR and/or Sanger sequencing across the U6/sgRNA region.

Table 2.2. Sequences of guide RNAs (gRNAs) employed for lentiGuide-Puro cloning (5′-3′).

TGFBR2 gRNA 1 Top	CACCGAAAGCGACCTTTCCCCACCA
TGFBR2 gRNA 1 Bottom	CTGGTGGGGAAAGGTCGCTTTCAAA
TGFBR2 gRNA 2 Top	CACCGGTCCACAGGACGATGTGCAG
TGFBR2 gRNA 2 Bottom	CCTGCACATCGTCCTGTGGACCAAA
TP53 gRNA 1 Top	CACCGGAGCGCTGCTCAGATAGCGA
TP53 gRNA 1 Bottom	CTCGCTATCTGAGCAGCGCTCCAAA
TP53 gRNA 2 Top	CACCGGCAGTCACAGCACATGACGG
TP53 gRNA 2 Bottom	CCCGTCATGTGCTGTGACTGCCAAA
RPL31 gRNA 1 Top	CACCGAGAGGGATACTCACACTCCA
RPL31 gRNA 1 Bottom	CTGGAGTGTGAGTATCCCTCTCAAA
RPL31 gRNA 2 Top	CACCGGCTTCAAGAAGCGTGCACCT
RPL31 gRNA 2 Bottom	CAGGTGCACGCTTCTTGAAGCCAAA
POU5F1 gRNA 1 Top	CACCGGCGTACTGTGGGCCCCAGGT
POU5F1 gRNA 1 Bottom	CACCTGGGGCCCACAGTACGCCAAA
POU5F1 gRNA 2 Top	CACCGCCCACAGAACTCATACGGCG
POU5F1 gRNA 2 Bottom	CACCGCCCACAGAACTCATACGGCG
HDAC2_v3_6-3_gRNA Top	CACCGATGGCTGTTAATTGGGCTGG
HDAC2_v3_6-3_gRNA Bottom	AAACCCAGCCCAATTAACAGCCATC
HDAC2_v3_6-5_gRNA Top	CACCGATGGCTGTTAATTGGGCTGG
HDAC2_v3_6-5_gRNA Bottom	AAACCCAGCCCAATTAACAGCCATC
LSD1_Guide2 Top	CACCGTGCAGCGGCAGCAACCGGGA
LSD1_Guide2 Bottom	AAACTCCCGGTTGCTGCCGCTGCAC
LSD1_Guide1 Top	CACCGAAGAAGGCGGCAGCCGCGG
LSD1_Guide1 Bottom	AAACCCGCGGCTGCCGCCTTCTTC
LSD1_Guide3 Top	CACCGCCGCAAGAAAGAGCCTCCGC
LSD1_Guide3 Bottom	AAACGCGGAGGCTCTTTCTTGCGGC
PCGF3_v3_6-2_gRNA Top	CACCGGATCACAATCCTGCAGGTG
PCGF3_v3_6-2_gRNA Bottom	AAACCACCTGCAGGATTGTGATCC
PCGF3_v3_6-4_gRNA Top	CACCGACTCACCCGATGTACTGCAG
PCGF3_v3_6-4_gRNA Bottom	AAACCTGCAGTACATCGGGTGAGTC

2.8 PCR

PCR was performed to amplify a defined DNA fragment by thermal cycling. Genomic DNA was extracted and purified from sample NM 740952.50S. Target-specific forward and reverse primers were utilized in Table 2.3. During the annealing step, primers hybridized to complementary template strands and initiated synthesis. Each cycle comprised denaturation at 95 °C, 3min, annealing at 55-72 °C (adjusted to the primer pair's Tm), and extension with a thermostable DNA polymerase (NEB E0553S) to copy the target region. This cycle was repeated 30-40 times to obtain exponential amplification. Reactions ended with a final extension at 72 °C, 5min and were held at 4 °C. Temperatures and extension times were optimized for each primer pair as summarized in Table 2.4.

Table 2.3. Primer sequences listed in the 5' to 3' direction.

PCR Type	Sequence
AVVS1 3′ BB	TTCTTCCTCCCCGATGCCCAGATA
AVVS1 5′INT_Neomycin	CAGTCTTTCGACCCAAGCGGCT
AVVS1 Locus PCR_ Genome 5′	CTGTTTCCCCTTCCCAGGCAGG
AVVS1 Locus PCR_ Genome 3′	GGGAACGGGGCTCAGTCTGA
TRE_CAS9_BSRGI_Frw	GATCTGTACACCACTTTGGCCGCGAATCG
TRE_CAS9_BSRGI_Rvs	GATCTGTACACTTACTTTTTCTTTTTTGCC TGGCCG

Table 2.4 PCR reaction and cycling conditions for Primer Pairs

PCR Type	Denaturation / Annealing / Extension	Cycles
5′ INT PCR	95°C, 30s/ 70°C, 30s/ 72°C,1min	35
3′ INT PCR	95°C, 30s/67°C, 30s/ 72°C,1min	35
3′ BB PCR	95°C, 30s/60°C, 30s/ 72°C,1min	34
Locus PCR	95°C, 30s/70°C, 30s/ 72°C,1min	35
Control PCR	95°C, 30s/62°C, 30s/ 72°C,1min	35

2.9 Plasmid DNA Isolation

Single colonies were picked from LB-agar and grown in 100- 200mL LB with the appropriate antibiotic (typcially ampicillin 100 µg/mL) for overnight at 37 °C, 220-250 rpm. Cells were harvested by centrifugation (4 °C, 4,000-6,000 × g, 15-20 min). Supernatants were discarded and plasmid DNA was isolated from the pellets using the Macherey-Nagel NucleoBond Xtra Midi kit, following the manufacturer's instructions. DNA was eluted in the supplied buffer (or nuclease-free water), quantified by NanoDrop and quality was assessed by A260/280 ≈ 1.8-2.0. Plasmids were stored at -20 °C. Insert identity was confirmed by restriction analysis and/or Sanger sequencing of the sgRNA region.

2.10 Western Blotting

Boiled lysates (30 µg per lane) and a prestained protein ladder (Abcam, ab116028) were run on precast SDS-PAGE gels (Bio-Rad, 456-1084). Proteins were transferred to PVDF membranes (Bio-Rad, 1620177) using the Trans-Blot Turbo system. Membranes were blocked in 5% blotting-grade blocker (Bio-Rad, 1706404) in TBS-T for 1 h at room temperature. Primary antibodies were applied overnight at 4 °C: anti-Cas9 (7A9-3A3, CST #14697, 1:1000) and anti-β-actin (Sigma-Aldrich A5441, 1:1000). The next day, membranes were washed in TBS-T (3×, 15 min each) and incubated with HRP-conjugated secondary antibody (Abcam, ab31430, 1:10,000) for 1 h at room temperature. After three additional TBS-T washes, signals were developed with ECL substrate and imaged on an Odyssey system (LI-COR).

2.11 Immunofluorescence-Based Detection and Imaging

iPSCs grown in tissue culture plates were fixed with freshly prepared 4% paraformaldehyde (PFA) in PBS (pH 7.4) for 15 min at room temperature. Cells were then washed three times with PBS (5 min each). Fixed samples could be stored in PBS at 4 °C until further use. Permeabilization was performed with 0.1% Triton X-100 in PBS for 10 min at room temperature, followed by three PBS washes. Blocking was carried out for 30 min at room temperature using a buffer of 1% BSA, 22.52 mg/mL glycine, and 0.1% Tween-20 in PBS. Primary antibodies were diluted in a staining buffer containing 1% BSA and 0.1% Tween-20 in PBS and applied overnight at 4 °C. The following were used: anti-KLF17 (rabbit polyclonal, Atlas; 1:250), anti-OCT4 (mouse monoclonal,

Abcam; 1:1000), and anti-Tra-1-60 (mouse monoclonal, Abcam; 1:250). After primary incubation, cells were washed three times with PBS. Secondary antibodies were diluted in 1% BSA/PBS and incubated for 1 h at room temperature in the dark. This included goat anti-rabbit Alexa Fluor 594 (1:1000, for KLF17) and avidin-FITC (1:1000, for Tra-1-60). Samples were again washed three times with PBS. Nuclei were counterstained with DAPI (1 µg/mL in PBS) for 5 min at room temperature, followed by a final PBS wash. Imaging was performed using a Cytation 5 fluorescence microscope (BioTek). Each well was filled with enough solution to fully cover the cell.

2.12 TRA-1-60 Colony Staining

Staining buffer (47 mL PBS used for tissue culture, 1.5 mL freshly thawed FBS, and 1.5 mL 10% Triton X-100 prepared from stock), DAB aliquots (−20 °C, bench-side freezer), Ni aliquots (stored in the same freezer as DAB), 0.35% H_2O_2 (diluted 1:100 from stock hydrogen peroxide), 1 M NaOH (laboratory stock solution), and 4% paraformaldehyde (PFA; freshly prepared, stored at +4 °C for up to one month). Antibodies included biotin-conjugated anti-TRA-1-60 (primary antibody; stored at +4 °C in antibody box 2) and HRP-conjugated streptavidin (secondary antibody; stored in the same box). Cooking cream was used to enhance colony contrast during visualization. Cells were fixed with 4% PFA (300 µL per well for 12-well plates, 100 µL per well for 48-well plates) for 15-30 min at room temperature on an orbital shaker. After fixation, wells were washed once with PBS. The primary antibody solution was prepared by diluting biotin-conjugated TRA-1-60 at 1:250 in staining buffer (e.g., 4 µL antibody in 1 mL buffer). Plates were incubated overnight at 4 °C on an orbital shaker. The next day, wells were washed three times with PBS. Secondary antibody (HRP-streptavidin) was diluted 1:500 in staining buffer and applied for 1 h at room temperature with orbital shaking. Following incubation, plates were washed five times with PBS. The chromogenic developing solution was prepared freshly using 5 mL PBS, 250 µL Ni, 250 µL DAB, and 250 µL 0.35% H_2O_2. The pH was adjusted to 7.4 with 1 M NaOH before immediate application. The solution was added to each well to cover the colonies and incubated for 30 min. After discarding the developing solution, wells were rinsed with PBS to remove residual stain. Plates were maintained in PBS overnight at room temperature and could be stored for up to three days before non-specific background

staining occurred. For visualization, PBS was removed and replaced with cream to enhance colony contrast and enable accurate quantification.

2.13 CellTiter-Glo (CTG) luminescence-based assay

Cells were seeded in 96-well plates and cultured with or without Dox for 7 days. At the endpoint, old medium was removed, and a working solution was prepared by mixing CellTiter-Glo reagent with fresh medium at a 1:10 ratio (e.g., 4 mL medium with 400 µL reagent for 100 wells). A total of 40 µL of this solution was added per well, followed by 10 minutes of incubation at room temperature. Luminescence signals were then measured using a microplate reader.

2.14 Statistical Analysis

Statistical analyses were performed using GraphPad Prism-10 (t-tests and one-way ANOVA) and Microsoft Excel.

Chapter 3:
RESULTS

3.1 Comparative Effects of Epigenetic Inhibitors on Naive Conversion across NO WT #2, WIBR3 ΔPE OCT4-GFP and Knockin-KLF17-GFP Reporter Lines

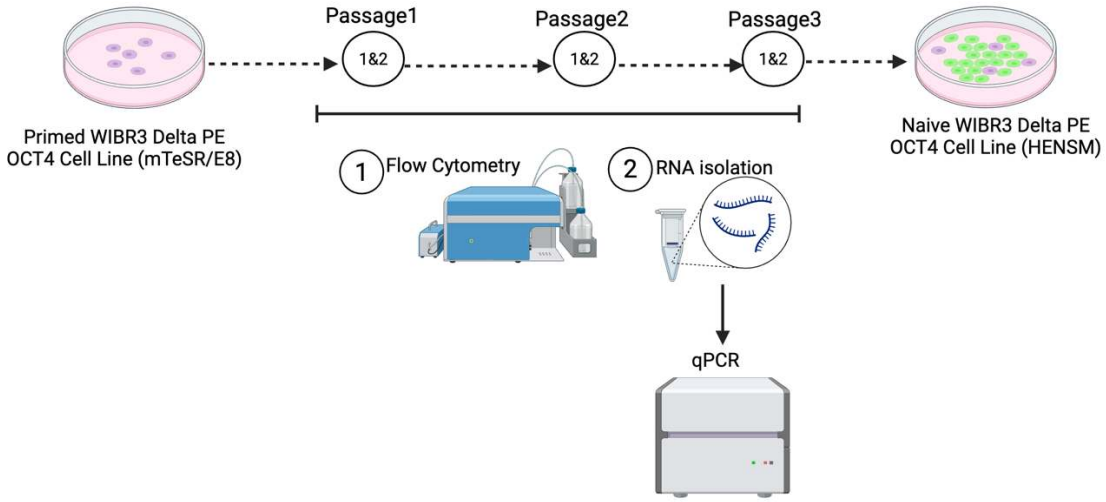

Figure 3.1 Experimental Setup for Monitoring the Effect of Epigenetic Inhibitors on Naive Conversion.

WIBR3 ΔPE OCT4-GFP cells, which lack the proximal enhancer region of the OCT4 gene, were used in this experiment to evaluate the effects of selected epigenetic inhibitors on naive conversion. These cells were initially maintained in E8 medium and seeded onto 12-well plates at a density of 50,000 cells per well.

As previously explained, the ΔPE OCT4-GFP reporter line exhibits GFP expression upon the acquisition of naive pluripotency characteristics. Therefore, GFP fluorescence intensity is used to assess the efficiency of the naive state.

After seeding, primed medium was removed and replaced with HENSM to initiate the conversion process. The first three days in HENSM were designated as passage 0 (P0). Subsequent passages were performed every three days.

To monitor the efficiency of conversion, flow cytometry was performed prior to each passage, particularly focusing on GFP expression levels. If an inhibitor enhances naive conversion, an increased GFP-positive population is expected by passage 4 (P4).

In addition, to support the flow cytometry findings, RT-qPCR was also performed at passages 1-3 to assess the expression levels of important primed and naive markers.

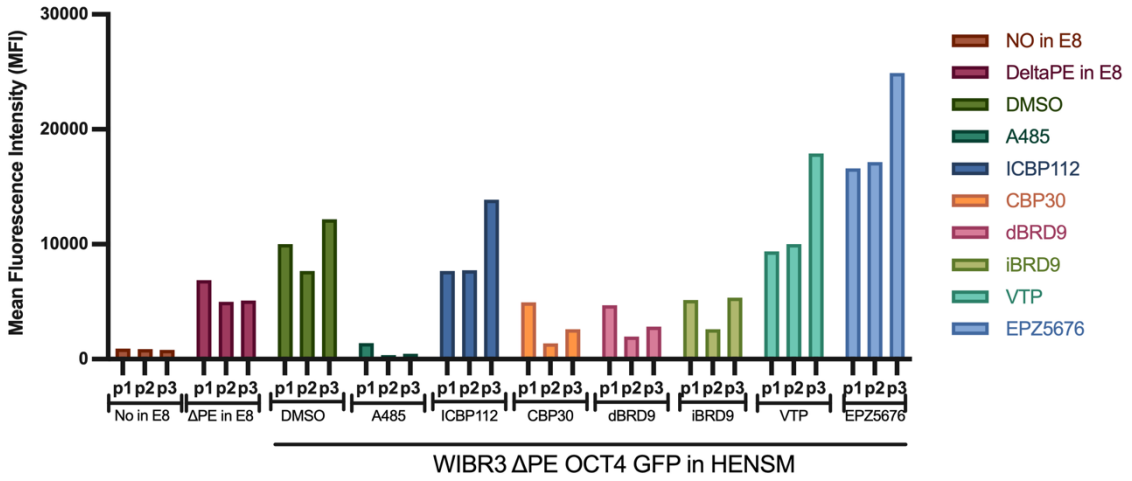

Figure 3.2. Mean fluorescence intensity (MFI) of WIBR3 ΔPE OCT4-GFP reporter iPSC line cultured in HENSM medium under different inhibitor treatments (A485, iCBP112, CBP30, dBRD9, iBRD9, VTP50469 and EPZ5676) compared to control conditions (NO #2 WT cell line in E8 (primed), ΔPE OCT4-GFP cell line in E8 (primed) and in DMSO) across passage 1-3.

To examine the role of chromatin-associated factors in naive conversion, we applied a set of inhibitors that had previously been used in our laboratory to improve reprogramming efficiency. These compounds targeted different epigenetic regulators that had been identified through a CRISPR-Cas9 loss-of-function screen, including CBP/p300 (A485, iCBP112, CBP30), the non-canonical BAF complex (dBRD9, iBRD9), the MENIN-MLL1 complex (VTP-50469), and DOT1L (EPZ5676). The WIBR3 ΔPE OCT4-GFP reporter cells were cultured in HENSM medium under these treatments, and GFP mean fluorescence intensity (MFI) was measured across three passages. Control groups included the NO wild-type iPSC line in E8 and the ΔPE OCT4-GFP reporter line in E8, while DMSO treatment was applied only to the ΔPE OCT4-GFP line as the solvent control. The use of two different cell lines as controls was important to separate background fluorescence from true reporter activation. The NO line, which lacks a reporter cassette, served as a true negative reference, whereas the ΔPE line maintained under primed conditions showed a low level of leaky GFP activity. Including both controls allowed a more precise gating strategy during flow cytometry, ensuring that basal fluorescence was accurately distinguished from genuine increases in GFP signal under naive conversion conditions. Among the tested compounds, EPZ5676 consistently

produced the strongest increase in GFP reporter activity, while VTP-50469 induced a moderate effect in Figure 3.2. In contrast, BRD9 and CBP/p300 inhibition-maintained fluorescence levels close to, or below, the DMSO control. Taken together, these results show that DOT1L and MENIN inhibition most effectively enhance reporter activation during naive conversion. Based on these results, VTP50469 and EPZ5676 were selected for use in the subsequent experiments.

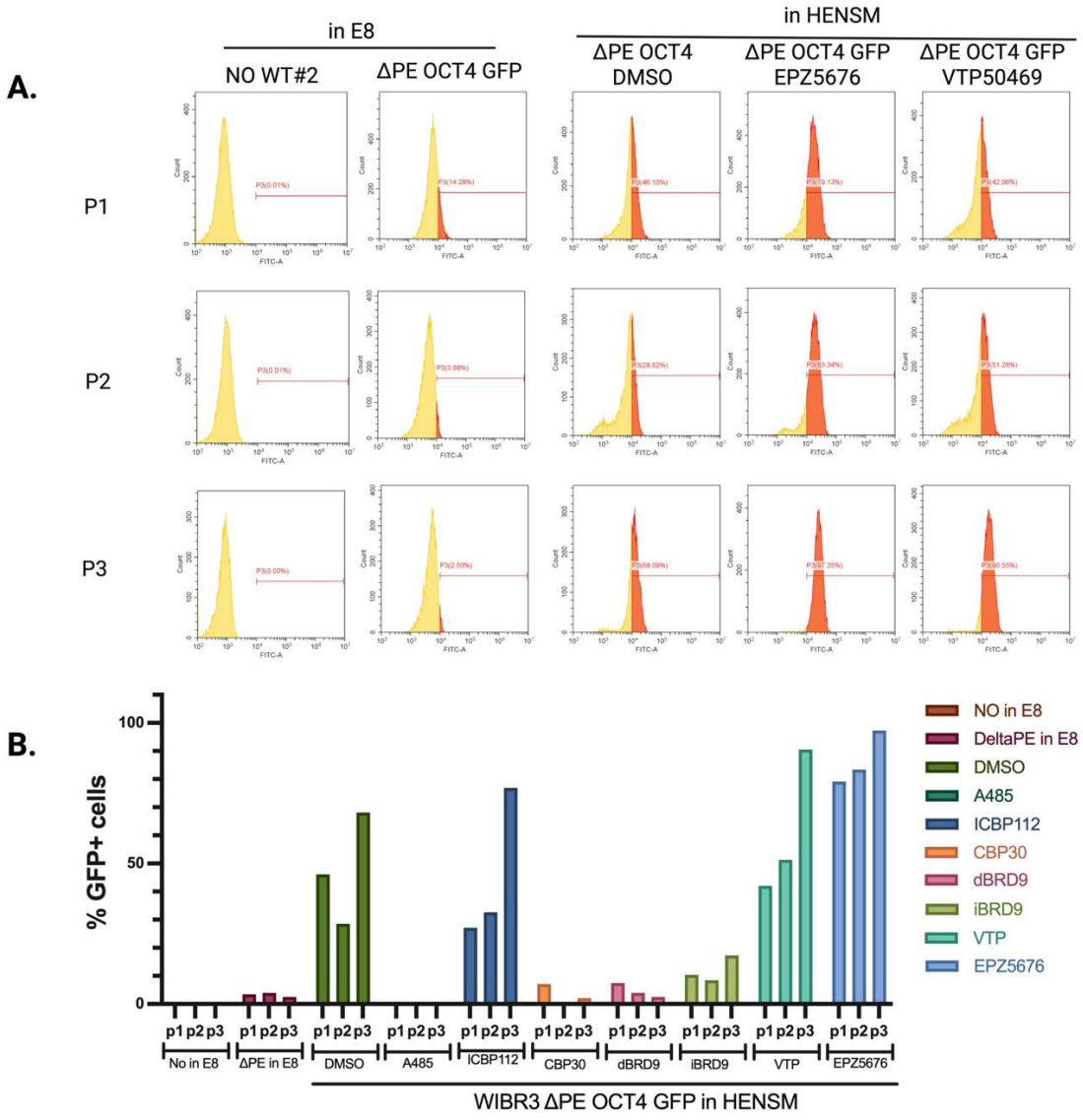

Figure 3.3. Percentage of GFP⁺ cells in the WIBR3 ΔPE OCT4-GFP reporter iPSC line cultured in HENSM with small-molecule inhibitors (A485, iCBP112, CBP30, dBRD9, iBRD9, VTP50469, EPZ5676). Controls: NO WT iPSCs in E8 (primed), ΔPE OCT4-GFP in E8 (primed), and ΔPE OCT4-GFP treated with DMSO in HENSM (solvent control). (A) Flow-cytometry histograms for P1-P3; the GFP gate was set using NO WT (B) Bar plots show % GFP⁺ cells across passages P1-P3.

To further assess the impact of these inhibitors on naive conversion, they were added to WIBR3 ΔPE OCT4-GFP cells cultured in HENSM, and the effect on GFP expression was evaluated by flow cytometry. Shifts in the GFP fluorescence channel were used to monitor changes in naive pluripotency acquisition (Figure 3.3). Examining the FITC-A shift across passages 1-3, we observed a progressive increase, particularly at passages 3. For EPZ5676, the percentage increases from around 79% at passage 1 to around 97% at passage 3 (Figure 3.3, panel A). On the other hand, for VTP50469, the percentage increases from around 42% at passage 1 to around 91% at passage 3. In the DMSO control, it rises from around 46% at passage 1 to around 68% at passage 3. It can be concluded that DOT1L and MENIN inhibition most effectively enhance reporter activation during naive conversion.

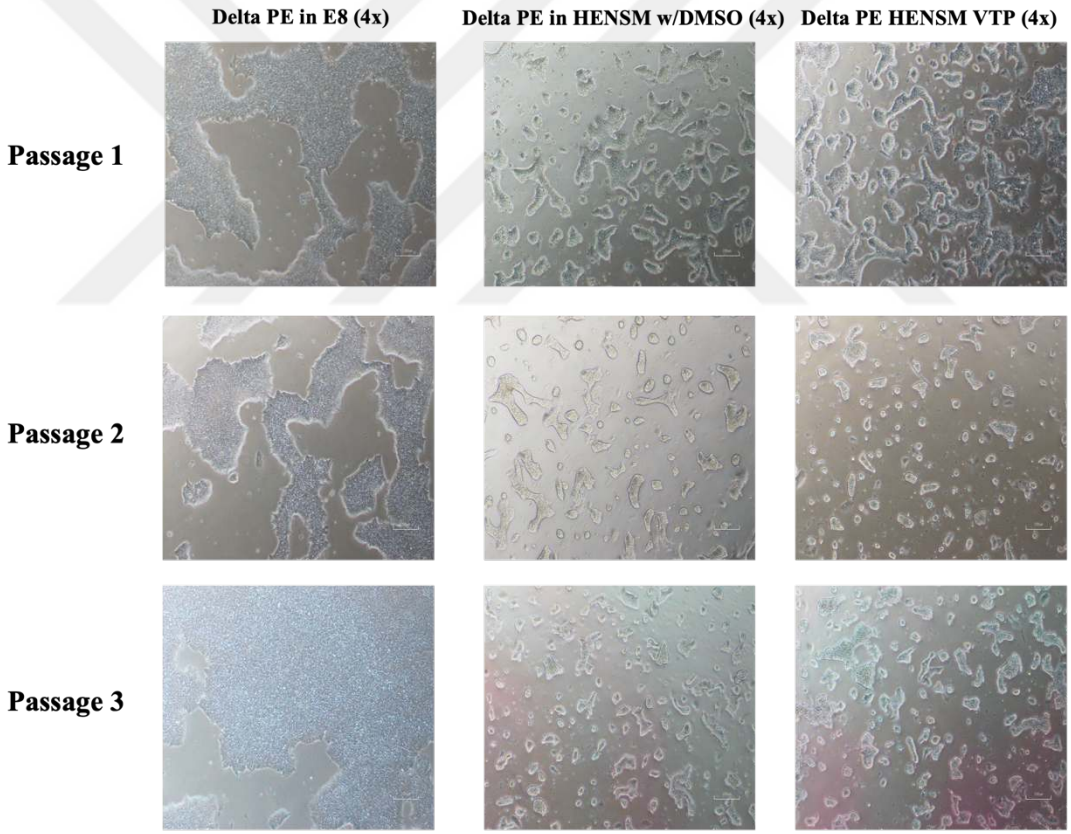

Figure 3.4. WIBR ΔPE OCT4 GFP cell morphology during naive conversion in HENSM, passages 1-3. (4× bright-field; DMSO vs VTP50469) (Delta PE in E8 used as the control group).

Figure 3.4 shows 4× bright-field images of the ΔPE line during naive conversion in HENSM. Cells were treated with DMSO (solvent control) and VTP50469 across passages 1-3. VTP50469 treatment gave colonies with a more naive-like shape, which were

compact, phase-bright, and domed with sharp borders and limited spreading. In contrast, Delta PE cells in primed culture were flat and irregular, with wider spaces between cells and broken edges. At later passages, these differences were clearer. The control cultures looked sparse and disrupted, while VTP50469 cultures stayed cohesive and well defined. Overall, the morphological trend supports a treatment-dependent enhancement of naive features in the ΔPE background, consistent with the expression analyses presented elsewhere (Figure 3.3-3.4)

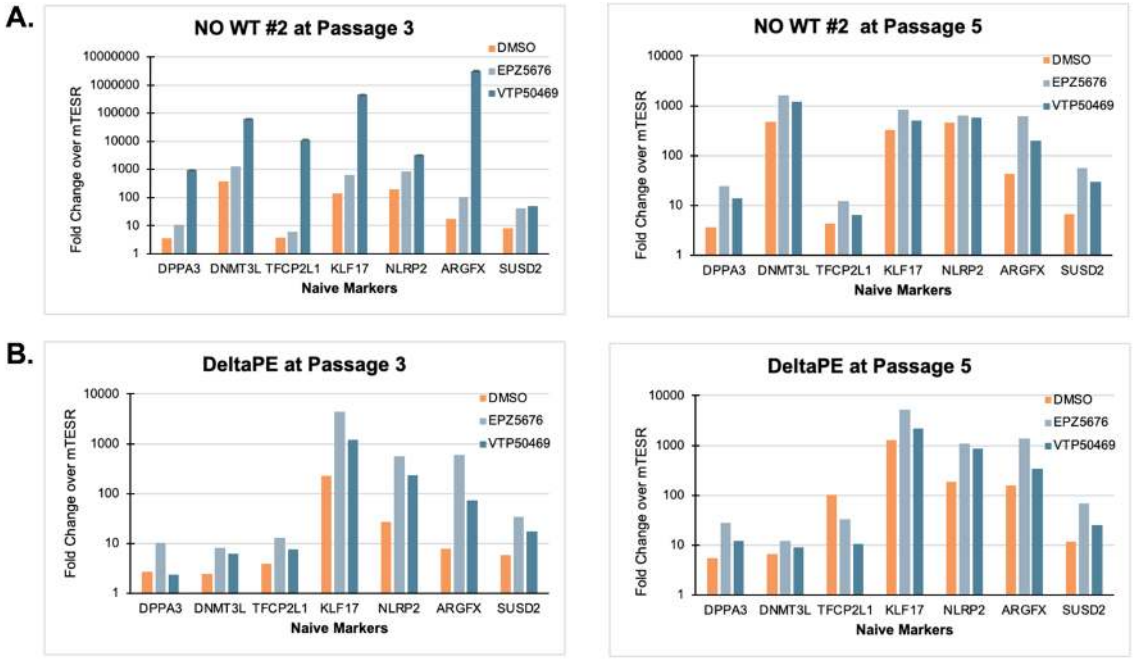

Figure 3.5. Comparison of naive pluripotency marker expression at passages 3 and 5 in different cell lines after conversion with HENSM containing EPZ5676 or VTP50469. (A) Wild-type cell line (NO WT #2). (B) Control cell line (WIBR ΔPE OCT4-GFP).

All experiments were performed in HENSM. We profiled two related hiPSC lines that are NO WT #2, a parental wild-type clone without reporter integration (baseline control) and ΔPE OCT4-GFP (WIBR3 ΔPE), which reports activation of the distal OCT4 enhancer upon naive entry. For each line, cells were analyzed at passage 3 and passage 5 under the indicated treatments. Relative mRNA expression levels were normalized to the corresponding primed counterparts of each line cultured in mTeSR, but the y-axis is displayed on a log10 scale for readability. DMSO served as the control, while EPZ-5676 (DOT1L inhibitor) and VTP-50469 (MENIN inhibitor) were used as treatment groups.

In NO WT cells, RT-qPCR revealed that naive-associated markers (DPPA3, DNMT3L, TFCP2L1, KLF17, NLRP2, ARGFX and SUSD2) were significantly higher

in both EPZ-5676 and VTP50469-treated samples compared with DMSO (Figure 3.5, panel A). The two inhibitors acted in the same direction; except for NO WT passage 3 in panel A, EPZ consistently produced the larger effect across genes and passages. In the ΔPE line, EPZ5676 and VTP50469 also increased the expression of naive markers especially KLF17, NLRP2 and SUSD2 (Figure 3.5, panel B-C), but the magnitude of induction was generally smaller than in NO WT. Across passages, the treatment effects observed at passage 3 in the WIBR ΔPE OCT4-GFP line was largely maintained, and for naive genes strengthened, at passage 5. In contrast, the NO WT line showed a progressively weaker response as passaging continued, indicating genotype-specific stability differences under prolonged culture.

3.2 Characterization of KLF17 hiPSC Reporter Line during Naive Conversion

Here, we aimed to characterize a KLF17-T2A-EGFP knock-in hiPSC reporter line previously generated in our laboratory (Karasürmeli, 2023). The KLF17 reporter cell line was generated because endogenous KLF17 is enriched in the naive state. Unlike the ΔPE reporter, it is expected to overcome the problem of leaky activity. The reporter yields GFP fluorescence upon naive conversion and remains low in primed conditions. Therefore, this line can serve as a more reliable tool to study the transition during naive conversion.

To evaluate reporter performance across states, we measured KLF17 and state-specific markers in primed and naive cultures using flow cytometry, RT-qPCR and immunofluorescence. Initially, all experiments were conducted with the validated clone 2E1-c10, confirmed by junction PCRs and Cre-mediated excision of the PGK-Puro cassette (Karasürmeli, 2023).

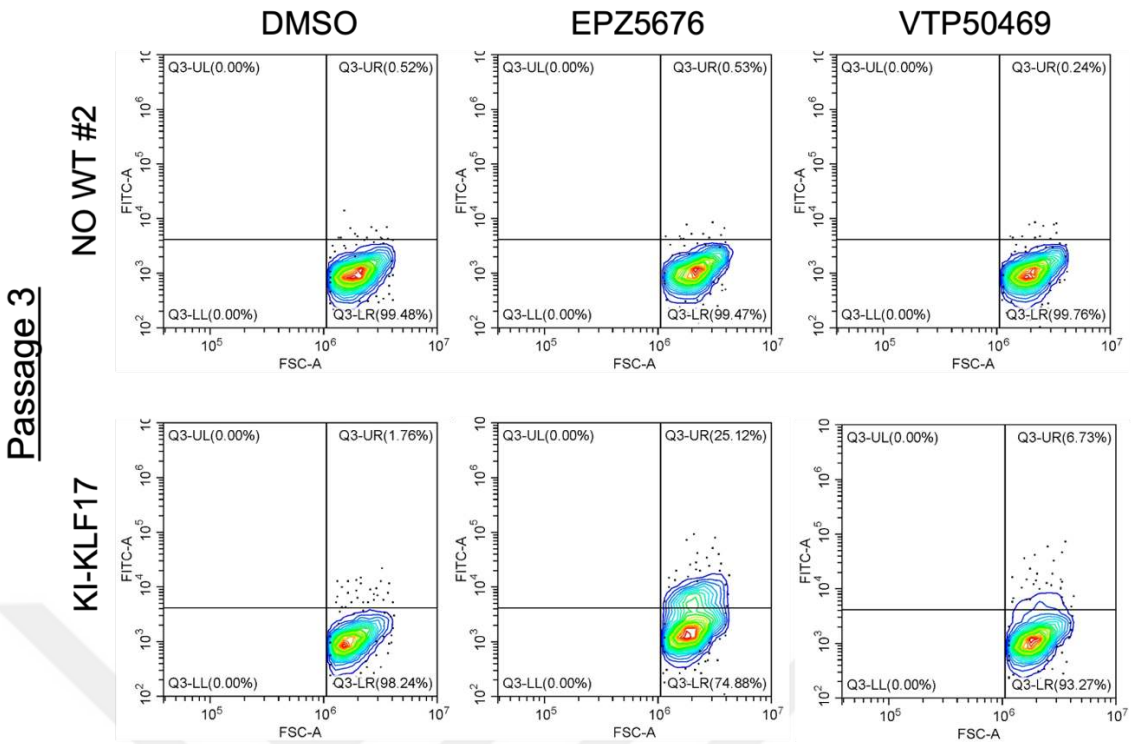

Figure 3.6. Flow cytometry analysis of GFP-positive iPSC populations following naive conversion with EPZ5676 and VTP50469 inhibitors at passage 3.

To improve the naive conversion efficiency of the KI KLF17 c10 line, and to enable the detection of GFP-positive naive cells by flow cytometry, we tested the inhibitors VTP50469 and EPZ5676 separately in combination with HENSM. At passage 3, flow cytometry showed that only a small proportion of GFP-positive cells was present in the DMSO control, reflecting minimal conversion. Cells treated with VTP50469 displayed similarly low percentages, suggesting that MENIN inhibition did not enhance conversion efficiency at this stage. In contrast, EPZ5676 treatment already produced a clear increase

in GFP-positive populations compared to both control and VTP50469 groups, indicating that DOT1L inhibition can promote naive marker expression early in conversion.

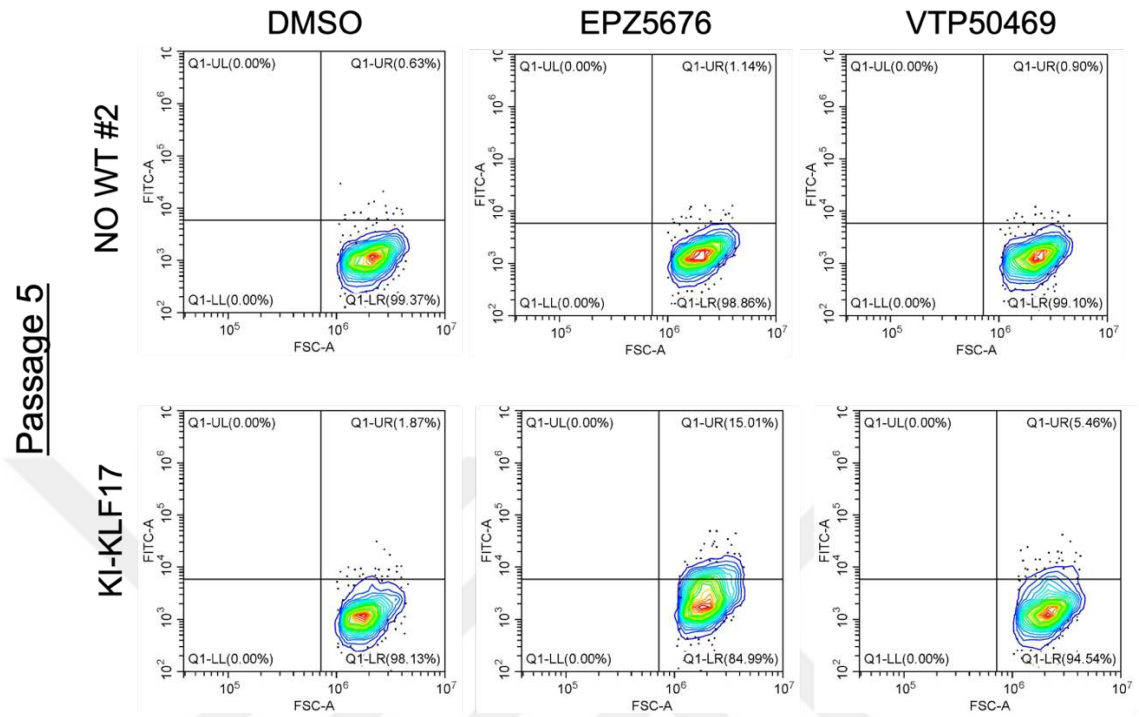

Figure 3.7. Flow cytometry analysis of GFP-positive iPSC populations following naive conversion with EPZ5676 and VTP50469 inhibitors at passage 5.

At passage 3, EPZ5676 treatment led to a substantial increase in GFP-positive iPSC populations (~25%), whereas DMSO control and VTP50469-treated groups showed only background levels in Figure 3.6. However, by passage 5 the proportion of GFP-positive cells in the EPZ5676 group declined to ~15% in Figure 3.7. VTP50469 treatment did not enhance GFP expression at either passage compared to the control. These results demonstrate that, under HENSM conditions, EPZ5676 enhances GFP shift at later passages, while VTP50469 does not produce a comparable effect.

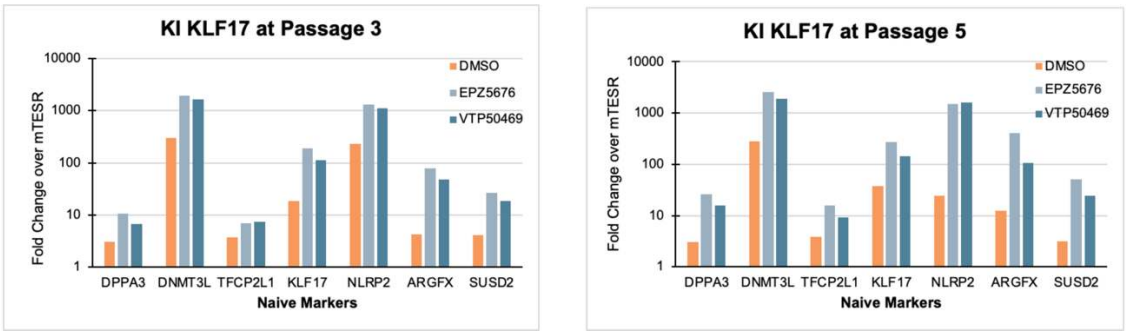

Figure 3.8. Comparison of naive pluripotency marker expression at passages 3 and 5 in different cell lines after conversion with HENSM containing EPZ5676 or VTP50469 for KLF17-GFP knock-in cell line (KI KLF17)

In Figure 3.8, qPCR analysis was shown at passage 3 and passage 5 under the indicated treatments. Relative mRNA expression levels were normalized to the corresponding primed counterparts of each line cultured in mTeSR, but the y-axis is displayed on a log10 scale for readability. DMSO served as the control, while EPZ-5676 (DOT1L inhibitor) and VTP-50469 (MENIN inhibitor) were used as treatment groups. RT-qPCR revealed that naive-associated markers (DPPA3, DNMT3L, TFCP2L1, KLF17, NLRP2, ARGFX and SUSD2) were significantly higher in both EPZ-5676 and VTP50469-treated samples compared with DMSO. EPZ consistently produced a bit larger effect across genes and passages. In the KLF17-KI line, EPZ5676 and VTP50469 also increased the expression of naive markers especially KLF17, DNMT3L and NLRP2 (Figure 3.8). In the KLF17-T2A-EGFP knock-in line, both inhibitors robustly elevated KLF17 transcript levels together with other naive markers relative to DMSO.

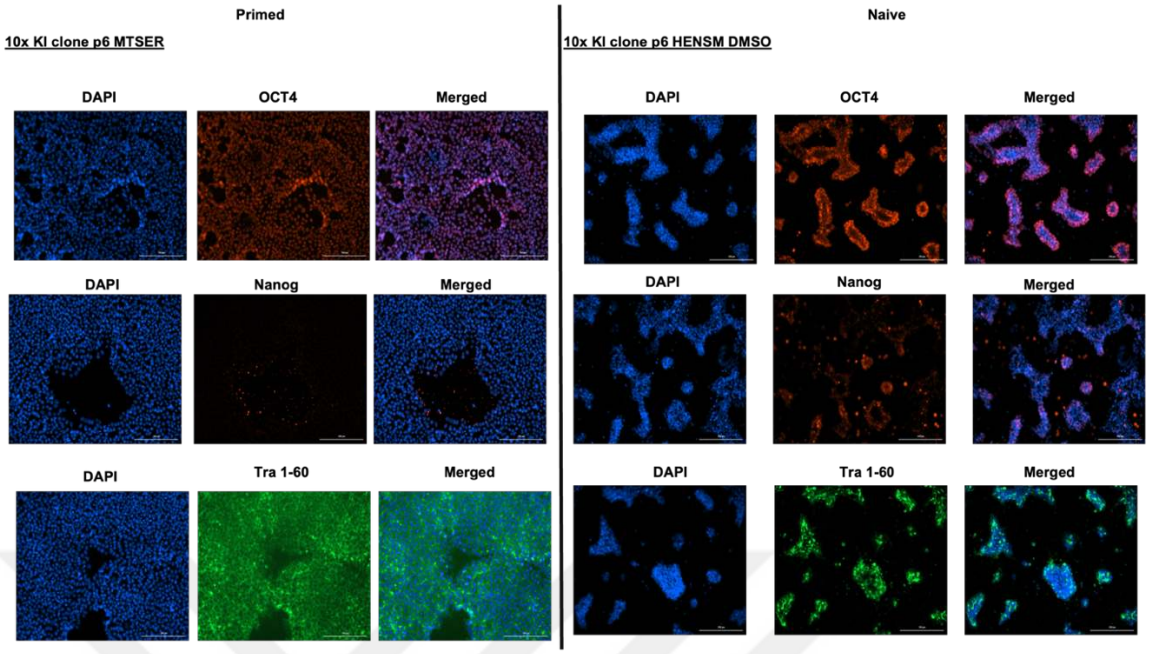

Figure 3.9. Representative immunofluorescence images of KI-KLF17 clone 10 (c10). OCT4 (red, upper panel), NANOG (red, lower panel), and TRA-1-60 (green) staining is shown under mTeSR (left) and HENSM (right) conditions at passage 6, acquired with the Cytation cell imaging system. Nuclei were counterstained with DAPI (blue).

Here, we aimed to test whether our KLF17 knock-in reporter line is functional. KLF17 is a naive-specific marker, so it should be active only in the naive state and not in the primed state. Therefore, we expected to see GFP signal in naive cells but not in primed cells. To confirm this, we performed immunofluorescence staining.

In this Figure 3.9, we show OCT4, NANOG, and TRA-1-60 expression in both primed (mTeSR) as a control and naive (HENSM) conditions, which are pluripotency-associated markers (O'Brien et al., 2017). All three markers showed positive fluorescence signals in both states, confirming maintenance of pluripotency.

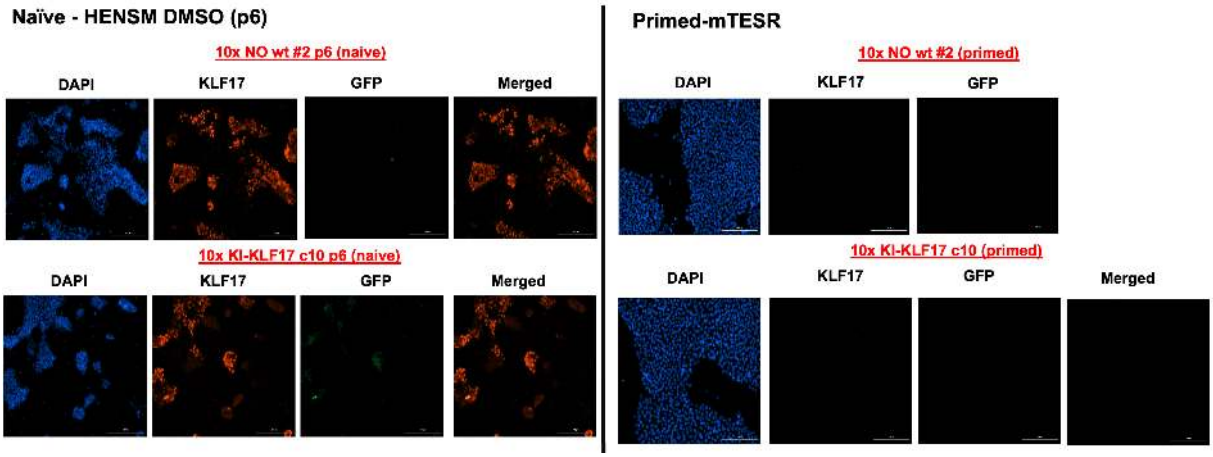

Figure 3.10. Representative immunofluorescence images of NO WT #2 and KI KLF17 c10. KLF17 staining (red) is shown after naive conversion with HENSM at passage 6 (left) and in as primed state with mTSER (right), acquired with the Cytation cell imaging reader at 10× magnification. Nuclei were counterstained with DAPI (blue).

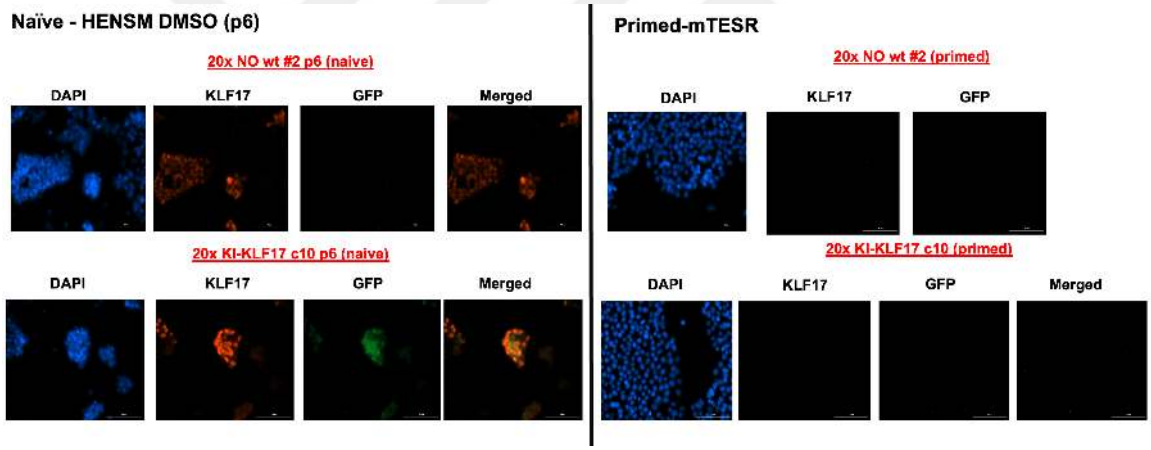

Figure 3.11. Representative immunofluorescence images of NO WT #2 and KI KLF17 c10. KLF17 staining (red) is shown after naive conversion with HENSM at passage 6 (left) and in primed state with mTSER (right), acquired with the Cytation cell imaging reader at 20× magnification. Nuclei were counterstained with DAPI (blue).

Figure 3.10 and 3.11 show immunofluorescence results for NO WT and KI KLF17 c10 cell lines after naive conversion at passage 6. Staining with the KLF17 antibody (red) confirmed expression of the KLF17 protein, consistent with its role as a naive-specific marker, since in the primed state no cells were stained with the KLF17 antibody. In this reporter line, GFP expression is expected if the knock-in was successful. At higher magnification (20×) in Figure 3.11, GFP fluorescence overlapped with KLF17 staining,

indicating correct reporter activity (Appendix A.1). The right side of both figures shows the same cell line under primed culture conditions (mTeSR), where KLF17 expression was absent, as expected since KLF17 is specific to the naive state.

These results validate that the KI KLF17 c10 line faithfully reports naive-specific expression. Using the NO wild-type line provides an additional control, in which no KLF17 signal was detected under primed conditions and also no GFP signal under naive conditions, further confirming the specificity of the antibody and the reporter system.

3.3 Generation of an Inducible-Cas9 iPSC Line for CRISPR Knockout Analysis of Naive-State Acquisition

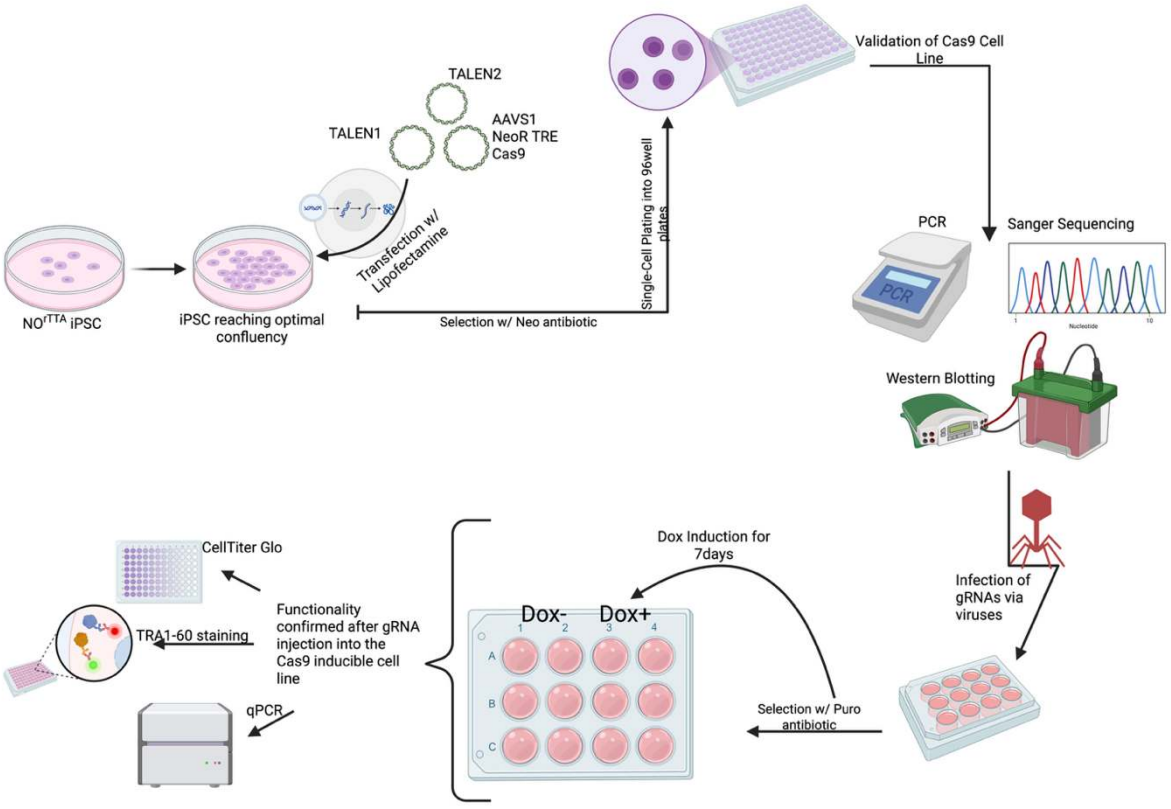

Figure 3.12. Workflow for generating, validating, and functionally testing a doxycycline-inducible Cas9 iPSC line.

Following the workflow depicted in Figure 3.12, we established a human iPSC line in which TRE-Cas9 cassette is inserted at the safe harbour *AAVS1* locus. We need this line because we plan a large, unbiased CRISPR screen to identify genetic regulators of naive state acquisition. This Cas9 allele can be activated by rtTA present in this iPSC line at the hROSA26 locus upon doxycycline addition. Correctly targeted clones were identified by junction PCRs, verified by Sanger sequencing and showed Cas9 protein by

Western blot. Functionally, gRNA delivery produced the expected effects only under Dox+ conditions, whereas Dox− controls remained unchanged after puromycin selection. Together, these data demonstrate a robust, doxycycline-inducible Cas9 platform for subsequent CRISPR studies.

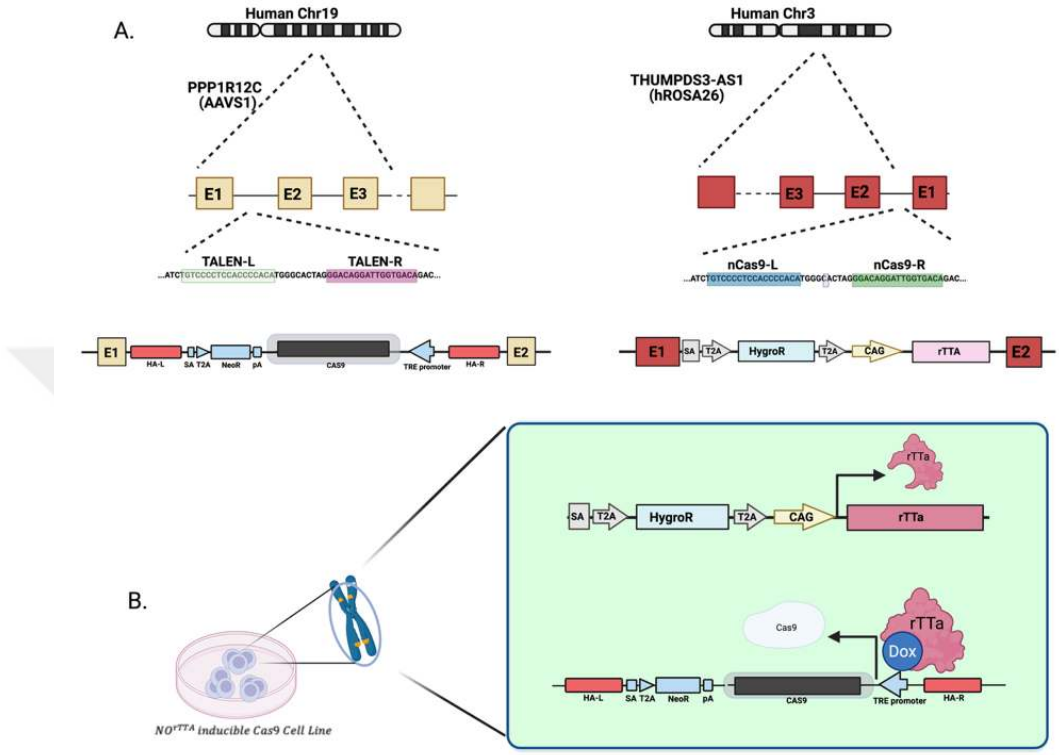

Figure 3.13. Targeted integration strategy and inducible-expression design. (A) Genomic schematics of the PPP1R12C (AAVS1; chr19) and ROSA26 (chr3) loci. (B) Mechanism of doxycycline inducibility.

The parental human iPSC line, which already carries rtTA at ROSA26, was transfected with an AAVS1 donor plasmid encoding TRE-Cas9 and PGK-Neo, flanked by left and right homology arms (LHA/RHA), together with AAVS1-specific TALENs to achieve targeted integration (Figure 3.13, panel A). After neomycin selection, single-cell clones were isolated and expanded. In the absence of doxycycline (Dox−), the TRE promoter remains inactive and Cas9 is not expressed. On the other hand, with doxycycline addition (Dox+), rtTA binds TRE and activates Cas9 transcription from the AAVS1 locus. The lower-left icon denotes the validated Cas9 iPSC clone used in downstream experiments (Figure 3.13, panel B).

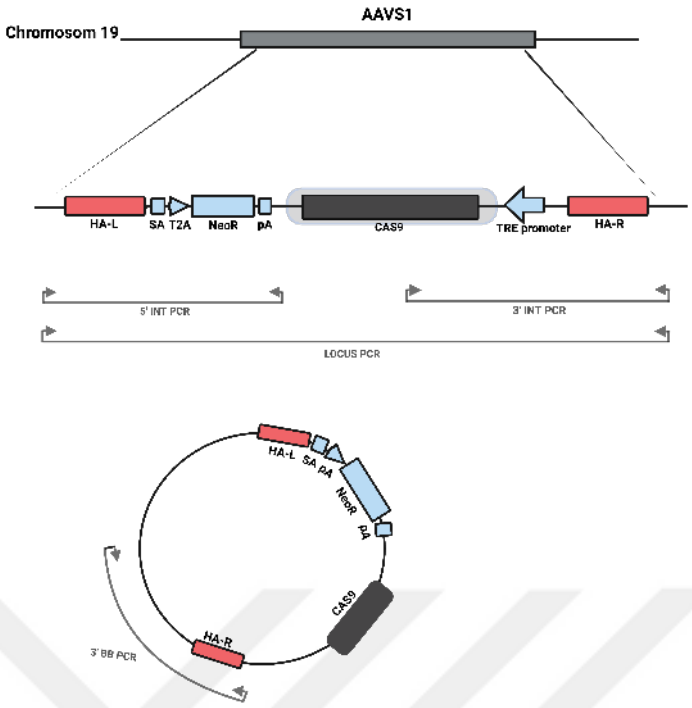

Figure 3.14. PCR Analysis Regions for Verifying the AAVS1-Integrated Cas9 Cassette

To confirm site-specific integration of the Cas9 cassette, five PCR assays were performed that are 5′-internal (5′-INT), 3′-internal (3′-INT), Locus PCR, Backbone (BB) and Control PCR (Figure 3.14-3.16). The 5′-INT and 3′-INT assays use one primer in the cassette and one in the genomic locus and therefore yield a product only if the cassette is integrated. The Locus PCR amplifies the unedited locus and is expected to give a band only when integration has not occurred (integration makes the amplicon too long to amplify efficiently). The BB PCR tests for random plasmid integration outside the homology arms. A control PCR targeting a housekeeping locus yielded a band in all genomic DNA samples, confirming DNA integrity and reaction performance.

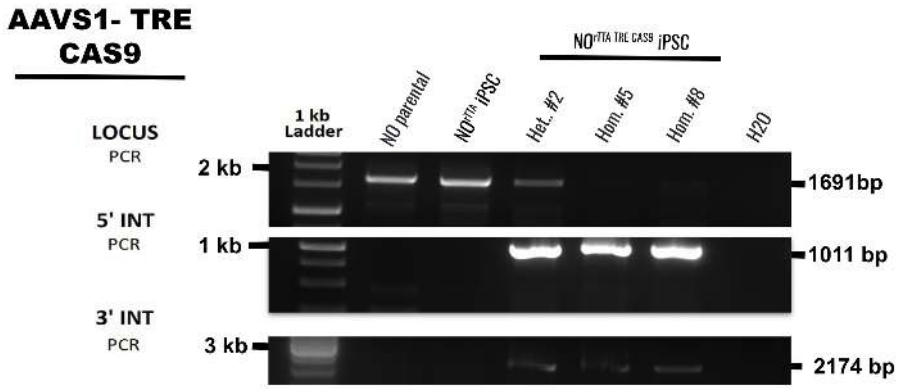

Figure 3.15. Validation of Cas9 Cassette Integration at the AAVS1 Locus in Homozygous and Heterozygous Clones and WT Cells Using Locus PCR; positive only in the unedited allele; lost when the cassette is inserted, 5′-INT and 3′-INT PCR; positive only upon correct integration.

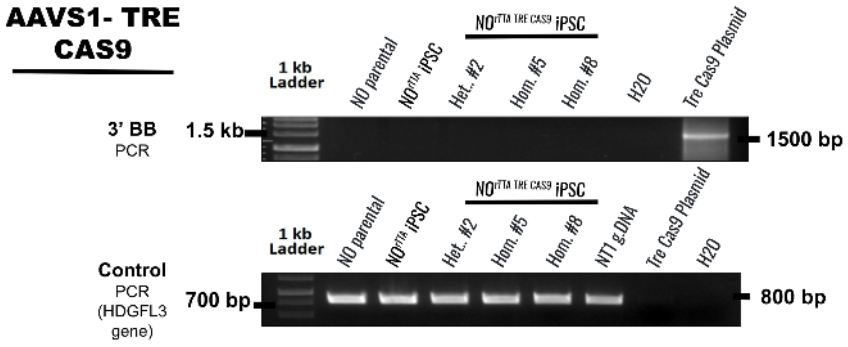

Figure 3.16. Validation of Cas9 Cassette Integration at the AAVS1 Locus in Homozygous and Heterozygous Clones and WT Cells Using 3'-BB, and Control PCR Assays.

In the Locus PCR, the parental and rtTA lines produced the expected band and served as positive controls (Figure 3.15). Among the single-cell clones, one showed a faint Locus PCR band, consistent with heterozygous integration, while two showed no band, consistent with homozygous knock-in. Although the full locus PCR was expected to produce a ~10 kb amplicon, such long-range products are often difficult to amplify efficiently. Instead, a 1691 bp junction PCR band was consistently obtained and used to confirm the correct genomic integration, which was considered sufficient for validation. As expected, both 5′-INT and 3′-INT PCRs yielded products in the edited clones but not in the parental/rtTA controls. For junction PCR validation, the expected amplicon sizes

were 1011 bp for the 5′ integration site and 2174 bp for the 3′ integration site. Compared with the 5′-INT PCR results, the 3′-INT bands were weaker.

The BB PCR was negative in all samples, indicating the absence of random integration. In the case of random integration, a 1500 bp band corresponding to the plasmid backbone would be expected. Lastly, the Control PCR was positive, confirming assay performance (Figure 3.16). As an internal control, the HDGFL3 locus was chosen because it is a single-copy, non-targeted genomic region that yields a stable 800 bp product, thereby confirming DNA integrity and PCR efficiency. Together, based on the locus PCR results, the presence of a band indicated heterozygosity for colony 2, while colonies 5 and 8 were determined to be homozygous. However, given its homozygous integration, Cas9 clone 5 (Cas9 #5) was selected for subsequent assays.

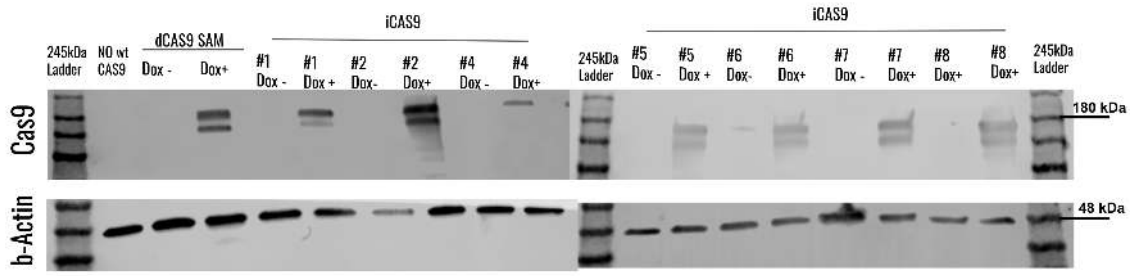

Figure 3.17. Western blot showing Cas9 protein levels in iCas9 clones ± Dox; controls include a dCas9 parental line and NO-WT + lentiCas9-Blast.

Whole-cell lysates from iCas9 clones cultured ± doxycycline (1 μg/mL Dox) for 2 days were probed with an anti-Cas9 antibody. In the inducible clones, Cas9 was absent or very low in Dox- and robustly detected in Dox+, appearing at the expected ~160-kDa size. The TRE-dCas9 parental line showed a Cas9-sized band only in the presence of Dox, while NO-WT cells transduced with lentiCas9-Blast served as a positive control, although in our blot no specific band was detected. β-actin (42 kDa) was used to confirm equal loading. While band intensity varied among clones, the overall pattern demonstrates doxycycline-dependent induction of Cas9 protein in the iCas9 background.

3.4 Functional Validation of an Inducible-Cas9 (iCas9) iPSC Line for CRISPR Knockout Analysis of Naive-State Acquisition

To test the functionality of the iCas9 cell line, selected gRNAs targeting NT1, RPL3, TP53, TGFbR2 and POU5F1 were cloned into the lentiGuide-Puro backbone and delivered into the cells via lentiviral transduction. Our internal controls were included to

anchor the pluripotency and viability readouts. The gRNA designs were derived from Ihry et al. (2019). TP53, which governs cell-cycle arrest, DNA repair, and apoptosis, served as the survival-positive control. RPL3, a ribosomal subunit required for protein synthesis and growth, utilized as the viability-negative control. We treated TGFBR2, a receptor in the TGF-β pathway linked to hPSC self-renewal, as the depletion positive control. Similarly, POU5F1/OCT4, a core regulator of pluripotency and self-renewal, was used as another control.

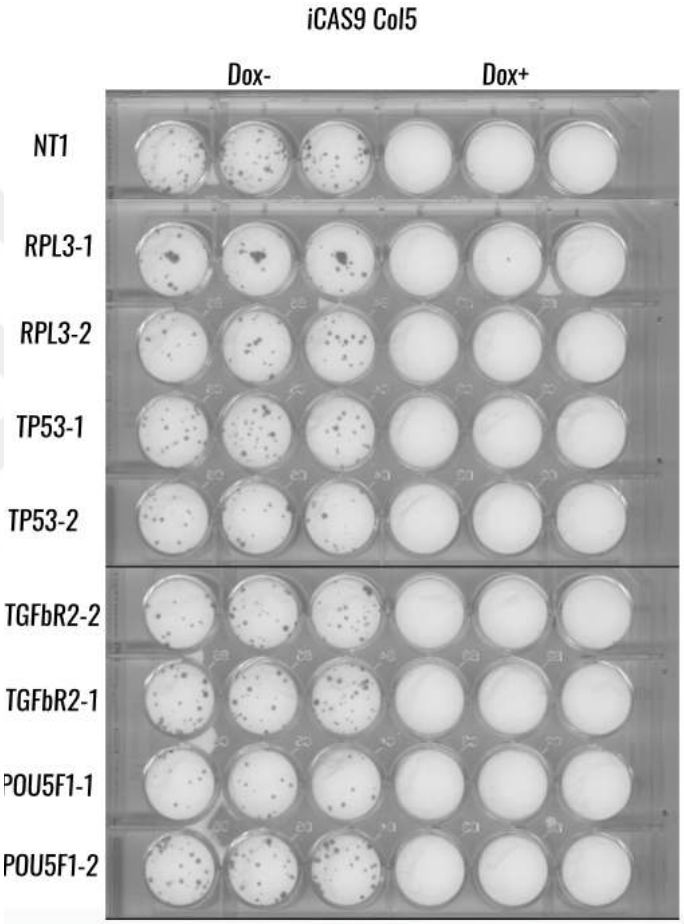

Figure 3.18. Assessment of doxycycline (Dox)-induced activity in Cas9 clone 5 cells by TRA-1-60 staining, following targeting of RPL3, TP53, TGFBR2, and POU5F1 (Dox−, left; Dox+, right).

As shown in Figures 3.18, iCas9 cells carrying gRNAs of the RPL3, TP53, TGFBR2, and POU5F1 were cultured for 7 days with or without doxycycline (Dox). Following this treatment, pluripotency features were assessed by TRA-1-60 staining. Since some of these genes are key pluripotency markers, the aim was to observe whether their knockout upon Dox induction would lead to loss of pluripotent features, thereby functionally

validating the activity of the iCas9 cell line. However, Dox-treatment on its own affected cell viability. In this context, NT1 was used as the control. As it does not target any essential pluripotency gene, no cell death was anticipated, however, cell loss was also evident in its wells. During Dox induction, we defined the expected phenotypes for each control target. For RPL3, a ribosomal gene, knockout was expected to impair cell survival. For TP53, a key regulator of apoptosis, knockout was anticipated to increase proliferation and potentially promote differentiation. Deletion of TGFBR2 was not expected to affect pluripotency under our conditions. In contrast, loss of POU5F1 (OCT4) was expected to abolish the pluripotent state.

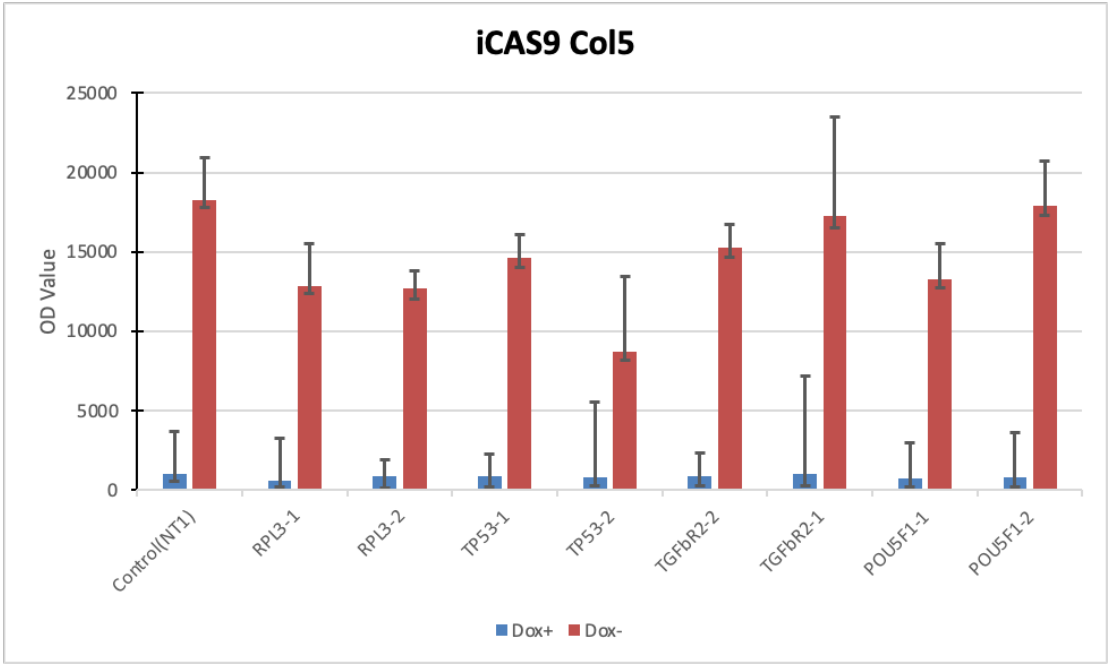

Figure 3.19. Assessment of Doxycycline (Dox)-induced Activity in Cas9 Clone 5 Cells by CellTiter-Glo Assay.

In addition, cell viability in a separate experimental group was evaluated using the CellTiter-Glo Luminescent Cell Viability Assay, which was chosen to measure cellular metabolism and indirectly assess cell viability in Figure 3.19. The results observed here are consistent with those in Figure 3.18, as no OD signal was detected in Dox-treated cells, indicating a loss of viability.

Figure 3.20. Morphological comparison of Cas9#5 NT1 control, TP53 knockout, and POU5F1 knockout hiPSC colonies under phase-contrast microscopy.

When 1,000 cells were seeded per well in 12-well plates, all cells died after DOX induction. To understand this issue, we used 6-well plates and seeded 1×10^5 cells per well, and DOX was given for more than 4 days. Under these conditions, NT1 (control) and TP53 knockout cells continued to grow. In contrast, POU5F1 knockout cells lost their pluripotent morphology, and cells died, which can be seen as floating dead cells in the right picture in Figure 3.20. These results were expected that TP53 knockout allows continuous growth, while POU5F1 knockout leads to loss of pluripotency and cell death.

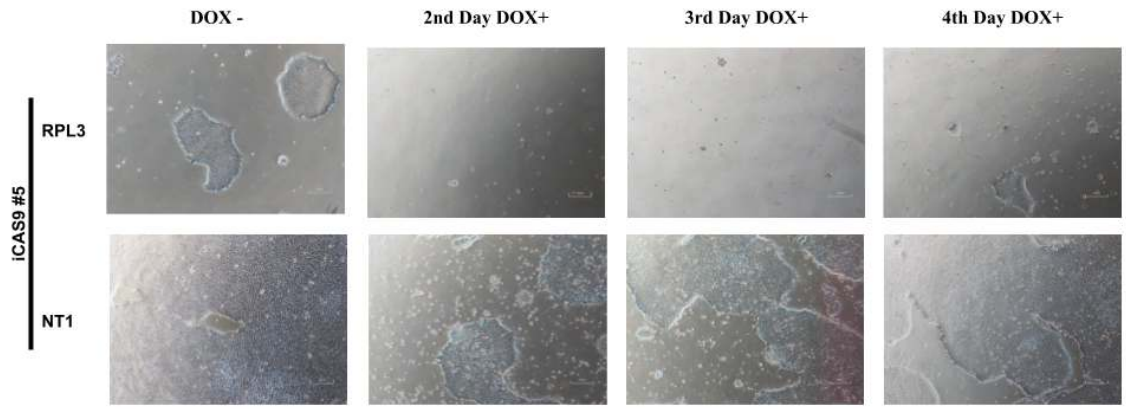

Figure 3.21. Phase-contrast microscopy images showing the effect of doxycycline (DOX) induction on RPL3 knockout (top row) and NT1 control (bottom row) iCas9#5 hiPSC colonies. DOX was added after seeding, on the 2nd, 3rd, and 4th days of culture.

To test whether cell death was caused by stress from low seeding density and DOX induction, we seeded 1×10^5 cells in 12-well plates. Both NT1 control and RPL3 knockout iCas9#5 cell lines are shown in Figure 3.21. The left side shows cultures without DOX, while in the right side, DOX was added on the 2nd, 3rd, and 4th days after seeding.

After DOX addition, some cell death was still observed in NT1 controls. For RPL3 knockouts, the expected result was obtained. Since RPL3 is an essential gene, knockout led to complete cell death after DOX treatment.

Together, these results show that the iCas9-sgRNA platform works as intended in a DOX-dependent manner. Growth with TP53 KO, loss of pluripotency with POU5F1 KO, and lethality with RPL3 KO were observed as gene-specific outcomes. However, optimized seeding density is critical for robust results.

3.5 Testing the Effects of HDAC2, LSD1 and PCGF3 on Naive Conversion

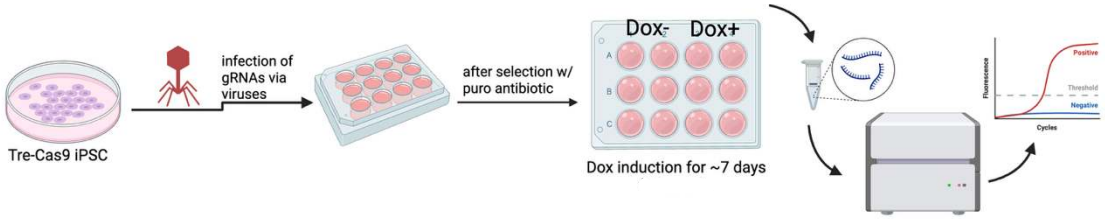

Figure 3.22: Schematic representation of the experimental workflow for generating TRE-Cas9 iPSCs with gRNA integration by viral infection and monitoring doxycycline-induced Cas9 activation in mTeSR with DOX and without DOX conditions.

In pluripotent cell programming, LSD1 and HDAC2 function mainly as epigenetic repressors by contributing to the shutdown of genes linked to pluripotency. As a result, they act as obstacles to naive conversion, and their deletion promotes entry into the naive state (Collier et al., 2022). In contrast, PCGF3, a subunit of the Polycomb complex, was identified in the same study as a factor that supports naive conversion. For this reason, LSD1 and HDAC2 knockouts were employed as positive controls in this thesis, whereas PCGF3 was evaluated separately as a distinct regulator. To this end, Dox-inducible Cas9 Clone 5 cells were transduced with the corresponding gRNAs, and these genes were targeted and functionally assessed during primed condition and naive conversion experiments (Figure 3.22 and 3.26). Knockout experiments were then performed under both primed (mTeSR) (Figure 3.23-3.25) and naive culture conditions (Figure 3.27).

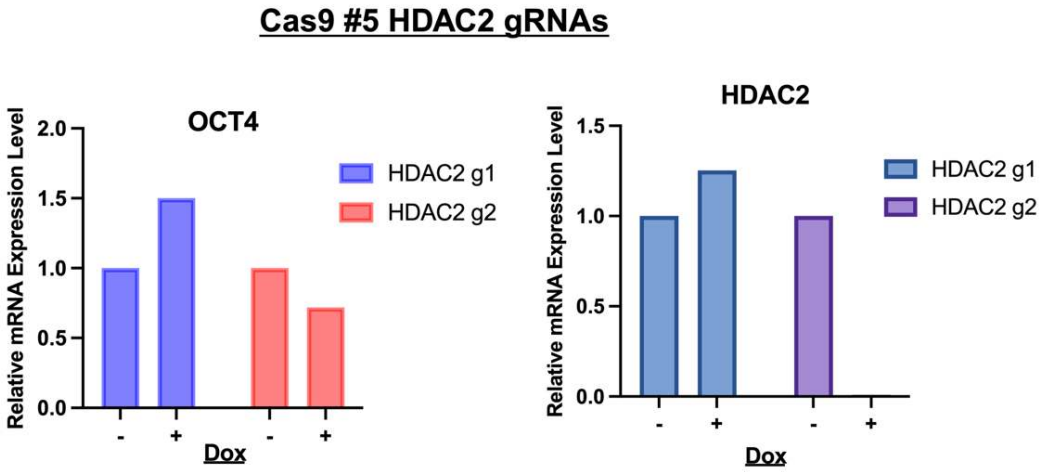

Figure 3.23 Inducible Cas9 activity with HDAC2 gRNAs assessed by qPCR, measuring the expression levels of OCT4 (left) and HDAC2 (right).

Figure 3.23 shows qPCR measurements of OCT4 (left) and HDAC2 (right) in iCas9 #5 cultured in mTeSR under Dox− and Dox+ conditions for 7 days. Expression levels were normalized to the housekeeping gene GAPDH and scaled to the Dox− control. Cells transduced with HDAC2 gRNAs showed a Dox-dependent decrease in the respective transcripts. Specifically, OCT4 expression in HDAC2 gRNA-2 cells was reduced compared to Dox−, as OCT4 was included as a pluripotency marker. HDAC2 expression also showed a marked decrease under Dox+, particularly with HDAC2 gRNA-2 (right). These data are consistent with Cas9 activation upon doxycycline induction and demonstrate target-specific editing in the inducible system. However, knockout efficiency varied between gRNAs targeting the same gene.

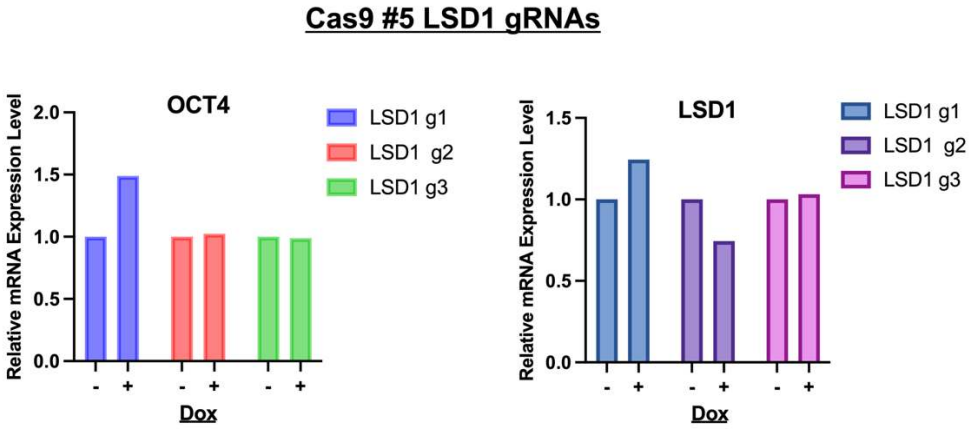

Figure 3.24. Inducible Cas9 activity with LSD1 gRNAs assessed by qPCR, measuring the expression levels of OCT4 and LSD1.

Using the same experimental setup as in Figure 3.23, iCas9 clone 5 cells were transduced with three independent LSD1-targeting gRNAs (gRNA-1/2/3) and cultured with or without doxycycline. qPCR was performed for OCT4 and LSD1 (KDM1A). In contrast to the OCT4/HDAC2 experiments, no Dox-dependent reduction of LSD1 mRNA was observed with any of the guides. It means that expression levels were similar to Dox-. OCT4 levels were also unchanged, especially in LSD1 g2 and g3. These data suggest that Cas9 induction did not produce a clear LSD1 knockout under the tested conditions. Only LSD1 g2 showed a slight decrease below 1. Editing efficiency appears to be gRNA-dependent, and further optimization may be needed.

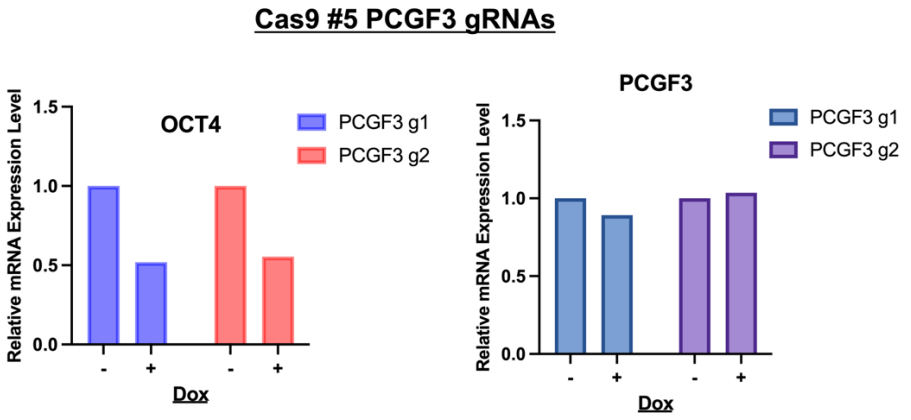

Figure 3.25 Inducible Cas9 activity with PCGF3 gRNAs assessed by qPCR, measuring the expression levels of OCT4 and PCGF3.

iCas9 clone 5 cells were transduced with PCGF3-targeting gRNAs and maintained in primed conditions (mTeSR) for 7 days ± doxycycline. qPCR for PCGF3 and the pluripotency marker OCT4 was performed and expressed relative to Dox−. PCGF3 mRNA did not decrease upon Dox induction with any guide, indicating that a robust PCGF3 knockout was not achieved under these conditions (Figure 3.25). OCT4, however, showed a reduction in the Dox+ samples compared with Dox−. Overall, these data suggest insufficient editing of PCGF3 in this setup; as expected, editing efficiency is gRNA-dependent and may require further optimization.

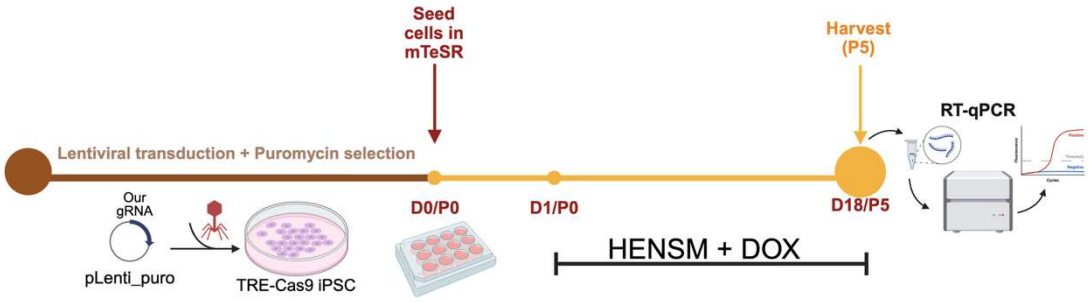

Figure 3.26. Schematic representation of the experimental workflow for generating TRE-Cas9 iPSCs with gRNA integration by viral infection and monitoring doxycycline-induced Cas9 activation in HENSM+Dox condition.

Dox-inducible Cas9 Clone 5 cells were transduced with the corresponding gRNAs, and these genes were targeted and functionally assessed under naive conversion (Figure 3.26). On Day 1 after seeding, HENSM with Dox was added and maintained until Passage

5. The cells were then harvested, and RT-qPCR analysis was performed to evaluate whether knockout of these gRNAs affected naive conversion efficiency, or not.

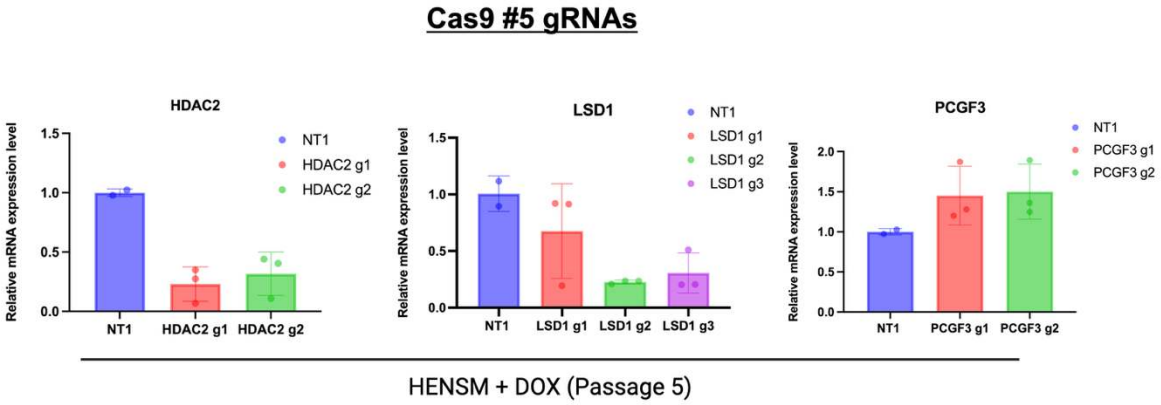

Figure 3.27. Inducible Cas9 Activity Assessed by qPCR Using Gene-Specific gRNAs A.) HDAC2 gRNAs B.) LSD1gRNAs C.) PCGF3 gRNAs under naive conditions.

In figure 3.27, iCas9 cells were maintained in HENSM with doxycycline to passage 5 and transduced with gene-specific gRNAs (HDAC2, LSD1 and PCGF3) or a non-targeting control (NT1). RT-qPCR values were normalized to a housekeeping gene and expressed relative to NT1. Both guides reduced HDAC2 mRNA compared with NT1. Similarly, all guides lowered LSD1 mRNA relative to NT1. In contrast, gRNAs did not decrease PCGF3 mRNA below the NT1 reference. These data indicate Dox-dependent Cas9 activity with effective editing at HDAC2 and LSD1, whereas PCGF3 showed no detectable knockout under these conditions. Editing efficiency is gRNA dependent.

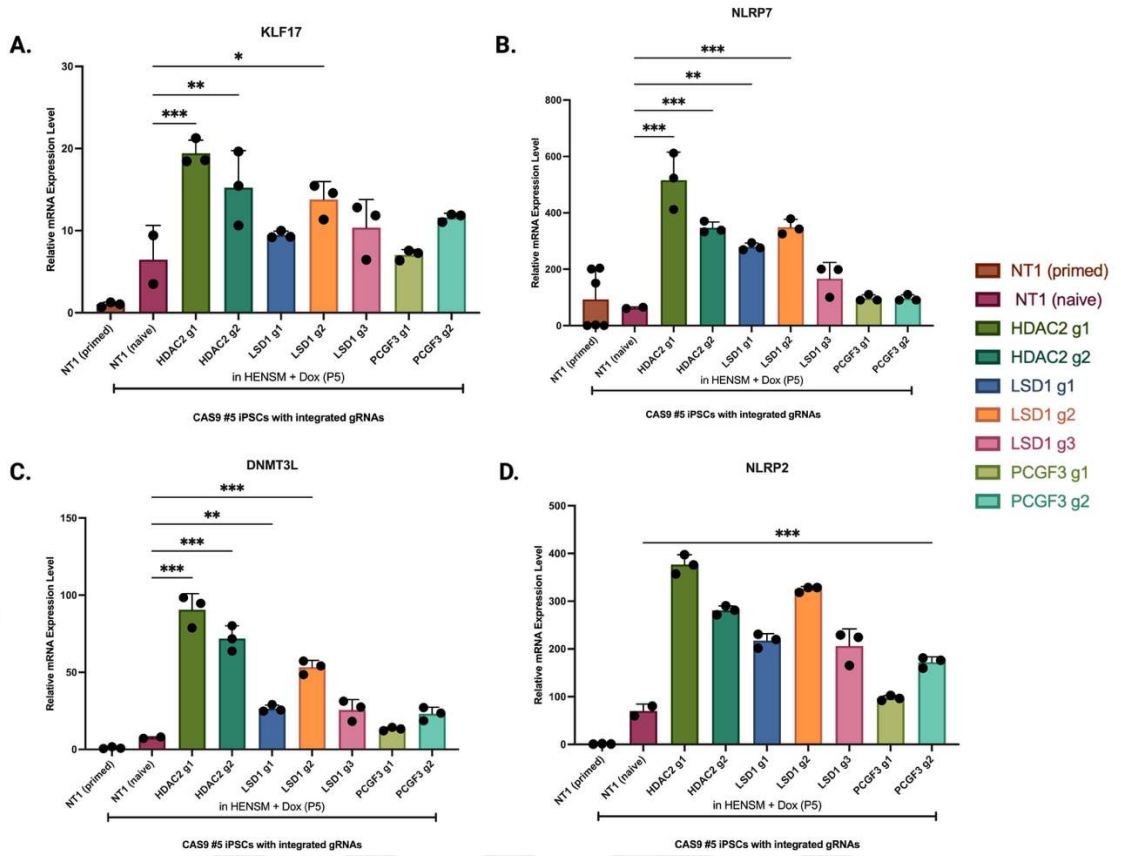

Figure 3.28. Effect of gRNA-mediated knockout of naive-associated genes on specific naive marker A.) KLF17 B.) NLRP7 C.) DNMT3L D.) NLRP2 expression in inducible Cas9 iPSCs under HENSM conditions with Dox at passage 5 (n=3, one-way ANOVA used, only significant comparisons (p or q ≤ 0.05) are indicated)(ns (p > 0.05), *p ≤ 0.05, **p ≤ 0.01, ***p ≤ 0.001).

To evaluate the functional impact of gene knockouts on naive pluripotency, iCas9 iPSCs with integrated gRNAs targeting HDAC2, LSD1 and PCGF3 were analyzed under naive conversion conditions with Dox at passage 5. Statistical analysis was performed using ordinary one-way ANOVA, and significance was determined according to the following thresholds: ns (not significant, p ≥ 0.05), *p ≤ 0.05, **p ≤ 0.01, ***p ≤ 0.001. The expression of multiple naive-associated markers that are KLF17, NLRP2, SUSD2, NLRP7, DNMT2L and TFCP2L1 was quantified and compared to NT1 control (Figure 3.28-3.30). Across all genes and gRNAs, a clear effect was observed with HDAC2 knockouts, where naive markers KLF17, NLRP7, NLRP2, and DNMT3L showed significant changes.

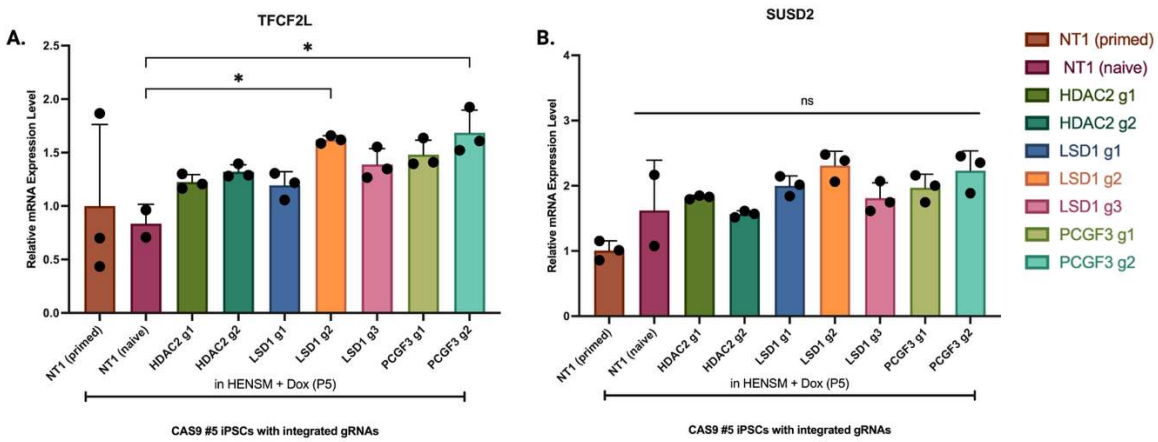

Figure 3.29. Effect of gRNA-mediated knockout of naive-associated genes on naive markers A.) SUSD2 and B.) TFCP2L1 expression in inducible Cas9 iPSCs under HENSM conditions with Dox at passage 5 (n=3, one-way ANOVA used, only significant comparisons (p or q ≤ 0.05) are indicated)(ns (p > 0.05), *p ≤ 0.05, **p ≤ 0.01, ***p ≤ 0.001).

As shown in Figure 3.28 and 3.29, knockout of HDAC2 and LSD1 significantly increased the expression of several naive markers, excluding SUSD2 and TFCP2L1, whereas with the strongest effects observed for NLRP2, NLRP7 and DNMT3L (***p < 0.001). In contrast, PCGF3 knockout did not lead to significant changes in marker expression compared to the NT1 control. Notably, SUSD2 expression remained unaffected across all groups (ns), while TFCP2L1 showed a moderate increase in LSD1 knockout cells (*p < 0.05).

Together, these findings indicate that HDAC2 and LSD1 act as barriers to naive conversion. Also, it was expected that PCGF3 does not exert a major influence under these conditions (Collier et al., 2022).

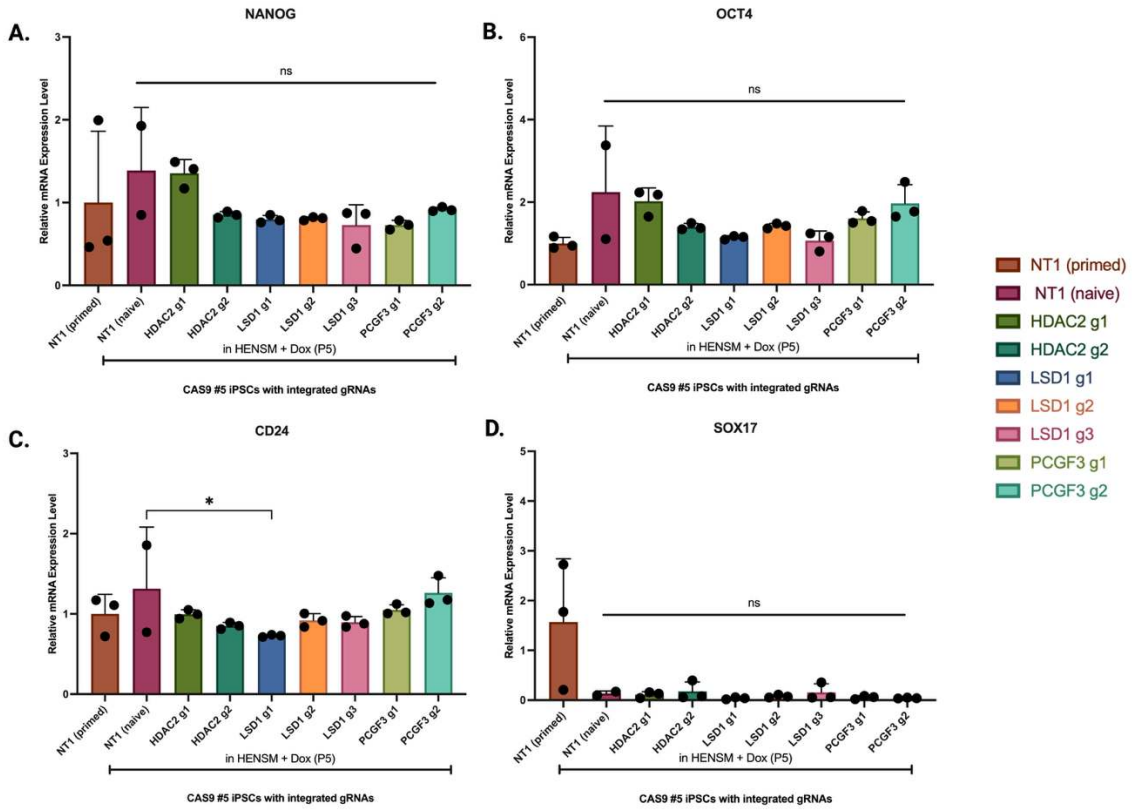

Figure 3.30. Effect of gRNA-mediated knockout of naive-associated genes on primed markers A.) NANOG B.) endogenous OCT4 C.) CD24 D.) SOX17 expression in iCas9 iPSCs under HENSM conditions with Dox at passage 5 (n=3, one-way ANOVA used, only significant comparisons (p or q ≤ 0.05) are indicated)(ns (p > 0.05), *p ≤ 0.05, **p ≤ 0.01, ***p ≤ 0.001).

We analyzed the expression of additional markers, including NANOG, endogenous OCT4, CD24 and SOX17. As shown in Figure 3.30, NANOG expression remained largely unchanged across all groups, indicating that the loss of HDAC2, LSD1, or PCGF3 does not significantly impact this core pluripotency factor. Similarly, OCT4 levels were not altered. The primed-associated marker CD24 was consistently expressed in all conditions without significant differences. Finally, SOX17, a definitive endoderm marker, showed only minimal or no induction, indicating that the cells did not undergo spontaneous endodermal differentiation upon loss of these regulators. Collectively, these findings demonstrate that while HDAC2 and LSD1 knockouts enhanced naive-specific gene expression (as shown in Figure 3.28 and Figure 3.29), they did not perturb core pluripotency maintenance (NANOG and OCT4) or drive endodermal differentiation (SOX17), nor did they significantly alter primed-associated CD24 expression.

Chapter 4:
DISCUSSION

Transition from the primed to the naive state in human induced pluripotent stem cells (hiPSCs) is central to developmental biology, yet it remains technically demanding and mechanistically unresolved. To examine epigenetic barriers during naive conversion under HENSM conditions, we used the complementary WIBR3 ΔPE OCT4-GFP reporter system, which reports activation of the distal OCT4 enhancer in the naive state (Fischer, Khan, & Theunissen, 2021). This reporter helped us to monitor transcriptional and phenotypic changes in real time. Four chromatin-associated regulators that are MENIN, DOT1L, P300/CBP, and BRD9 were perturbed with selective small-molecule inhibitors. Flow cytometry consistently detected increases in GFP signal. The effect was strongest upon inhibition of MENIN or DOT1L.

Treatment with the DOT1L inhibitor EPZ5676 and the Menin-MLL inhibitor VTP50469 consistently improved naive induction. We observed a larger GFP-positive fraction together with strong induction of naive markers (NLRP2, TFCP2L1, KLF17) and a parallel decline in primed/lineage genes. Mechanistically, DOT1L-dependent H3K79 methylation helps stabilize the primed program. Blocking DOT1L reduces gene-body methylation and creates a more permissive chromatin state, in line with prior reports that DOT1L inhibition facilitates conversion to LIF-dependent naive hiPSCs (Onder et al., 2012; Isono et al., 2020). Menin, which recruits MLL1/2 to developmental promoters to deposit H3K4me3, is similarly required to maintain primed transcription, so VTP50469 disrupts this interaction and dampens those transcripts (Krivtsov et al., 2019). Recent chemical screens that rank DOT1L and Menin-MLL inhibitors among the most effective reprogramming accelerants support our data. Overall, these results indicate that DOT1L and MENIN are key epigenetic barriers whose inhibition enables resetting toward an ICM-like naive pluripotent state.

In contrast to DOT1L and Menin, inhibition of p300/CBP or BRD9 produced only marginal effects on naive conversion in our assays, indicating that chromatin regulators contribute unequally to this transition. Because p300/CBP broadly supports enhancer-driven transcription, it is unlikely to be the rate-limiting step for activating the naive network (Martire et al.,2020). Broad inhibition of p300/CBP, such as with CBP30, can suppress primed transcriptional programs (Sevinç et al., 2022). However, it also reduces

activation of naive enhancers. As a result, the overall benefit remains minimal. Although p300/CBP inhibition has been reported to aid reprogramming in some intermediate contexts, we observed no appreciable benefit during direct primed-to-naive resetting of hiPSCs. Likewise, attenuating BRD9 (a core ncBAF subunit) did not improve conversion, consistent with a stage-dependent role in which BRD9 helps stabilize pluripotent circuitry once established. Overall, global p300/CBP-mediated acetylation does not appear to be the principal epigenetic barrier to naive entry, and some acetyltransferase activity is likely required to establish or maintain naive-specific enhancers.

The endogenous KLF17-GFP reporter line generated in our laboratory was functionally characterized in the thesis. Although the proportion of GFP-positive cells was limited, the reporter showed that GFP expression was nearly absent in primed cultures but became detectable under naive conditions. This observation is in line with reports that KLF17 is silent in conventional primed hESCs but reactivated when cells are shifted to naive culture. Immunofluorescence analysis confirmed that GFP signal appeared only after naive induction, while flow cytometry indicated that GFP-positive cells corresponded to the subpopulation acquiring naive features. In addition, KLF17-GFP^{+} cells overlapped with colonies displaying domed morphology and expressing known naive markers. Together, these findings support the role of KLF17 as a reliable naive-specific marker in hPSCs and are consistent with studies showing that KLF17 is enriched in the pre-implantation epiblast but low in other pluripotent states (Lea et al., 2021). The activation timing of KLF17 during reprogramming provides useful information about the sequence of events in naive conversion. In our experiments, GFP fluorescence became visible only after several days in naive conditions, later than the earliest signs of resetting such as the downregulation of primed markers. This indicates that KLF17 induction is a delayed event, marking cells that have progressed further toward the naive state (Messmer et al., 2019). Our results are in line with recent studies showing that KLF17 and other naive-associated genes are upregulated at later stages of induction, rather than at the beginning. Consistently, KLF17-GFP expression remained absent during the early phase and reached maximum levels only at advanced stages, suggesting that KLF17 functions more as a stabilizer of the naive program than as an initial trigger. Supporting this, overexpression of KLF17 in primed hESCs has been reported to promote a naive-like transcriptional profile and to facilitate resetting. However, KLF17 is not strictly essential because of functional redundancy with other KLF factors. In our reporter line, GFP appears relatively late. This means it mainly labels

cells that are already committed to a naive identity. Such timing is useful for isolating stable naive populations but may fail to capture transient intermediate states. To better distinguish early and late events during conversion, several improvements can be considered. One option is to combine the KLF17 reporter with an additional early-stage marker. For example, activation of ALP (ALPG) is detected earlier, around day 6-8 of naive induction. A dual-reporter strategy, such as an ALP-promoter-driven fluorescent protein together with KLF17-GFP, could therefore separate cells entering the naive trajectory from those that are fully converted (Bi et al., 2020). In a similar way, monitoring the loss of primed-specific markers (SSEA4 or ZIC2) by live staining or reporters could reveal the onset of conversion before KLF17 expression is detected. Another improvement would be more frequent sampling and the application of single-cell analyses during reprogramming, which would allow the identification of intermediate states preceding KLF17 activation. Recent single-cell transcriptomic studies of the primed-to-naive transition have identified transient subpopulations and alternative routes (Bi et al., 2022). Applying our reporter line in such analyses could clarify the timing of KLF17 activation relative to other events. In summary, the KLF17-GFP reporter has proven useful for identifying naive hPSCs and validating KLF17 as a naive-specific marker. However, the late activation of KLF17 indicates that additional strategies are needed to capture the earliest steps of resetting. Using KLF17-GFP together with other reporters or with time-based analyses could give a clearer picture of the primed-to-naive transition. In addition, adding molecules such as VPA increasing naive conversion (for short treatments) or inhibitors like EPZ5676 and VTP50469 into HENSM medium may improve conversion efficiency or support the maintenance of the naive state during passages. Under such optimized conditions, the number of GFP-positive cells may increase, allowing easier isolation of naive populations by cell sorting for later experiments.

We generated a doxycycline-inducible Cas9 iPSC line by inserting a tetracycline-regulated Cas9 cassette into the AAVS1 safe harbor locus. Correct integration at AAVS1 was confirmed, and this site is known to support stable transgene expression in hPSCs without affecting endogenous pluripotency genes. Our design, similar to reported iCRISPR/iCas9 systems, placed a TRE-driven Cas9 together with a constitutive rtTA in the PPP1R12C (AAVS1) locus. After targeting, the engineered iPSC line maintained normal pluripotency markers (OCT4, NANOG, SOX2) and a stable karyotype. Upon doxycycline addition, Cas9 expression was strongly induced, as shown by both mRNA

and protein analysis, while uninduced cells displayed minimal basal Cas9. This regulation is important because it avoids constant Cas9 activity, which can lead to DNA damage or stress. Studies have shown that inducible Cas9 from the AAVS1 site gives uniform expression and high editing efficiency (Oceguera-Yanez et al., 2016), without triggering the p53 response seen with constitutive Cas9 (Ihry et al., 2018). In line with this, our iCas9 line showed even Cas9 protein levels across the cells after induction and provided a reliable system for genome editing.

To check the iCas9 iPSC line, we targeted several genes, including essential ones (TP53, RPL3, POU5F1/OCT4) (Ihry, 2019) and naive regulators (HDAC2, LSD1, PCGF3) (Collier et al., 2022). In some cases, the expected knockout phenotypes were not seen. For instance, when 1,000 cells per well were plated in a 12-well dish, all wells still contained viable cells. This suggested that either the editing efficiency was low, or the seeding density was not suitable. In this setup, TGFBR2 served as a positive control for pluripotency, while POU5F1 acted as a negative control (Ihry, 2019). TP53 was used as a positive control for cell viability, and RPL3 as a negative control, since their knockout should produce distinct survival outcomes. Interestingly, when the seeding density was increased to 80,000 cells per well in a 12-well plate, the knockouts produced the expected results Phenotypic outcomes for genes linked to the naive state (HDAC2, LSD1, PCGF3) are more difficult to interpret, since cells can tolerate the loss of these epigenetic regulators. Nevertheless, if editing were efficient, we would expect changes in naive marker expression or proliferation over time. The lack of such changes suggests that Cas9/gRNA activity in these experiments was only partially effective. Editing efficiency can be improved by refining gRNA design and testing. Each gRNA should first be checked for cutting activity, and several gRNAs for the same gene can be applied together. Dox induction also needs adjustment by trying different doses and times to find a balance between strong Cas9 expression and cell health. If induction remains weak, higher rtTA levels could provide support. An additional observation in our inducible Cas9 system was the appearance of dual bands for Cas9 on Western blot following Dox induction. The Western blot showed two closely migrating bands (approximately the size expected for Cas9, ~160 kDa) in induced cells, whereas uninduced cells had no such bands. The exact cause of the double band is not known, but several explanations can be suggested. One is that part of the Cas9 protein may be post-translationally modified (Ergünay et al., 2022). For instance, phosphorylation or sumoylation could slightly change its movement in the gel and produce two forms. As Cas9 is a large protein with

many domains, partial cleavage, such as removal of a small fragment, might also create two close bands. Importantly, this double band did not seem to reduce Cas9 activity, since the cells could still be edited. This pattern more likely reflects biochemical heterogeneity in the Cas9 protein. If needed, mass spectrometry could be used to identify modifications present in the bands. What matters for our experiments is that the induced Cas9 is mostly full-length and active. The second band might also indicate degradation, such as ubiquitinated forms, or partial processing linked to high expression levels. Adjusting the doxycycline dose to avoid overexpression stress may help reduce such effects.

In summary, this thesis demonstrates that DOT1L and MENIN act as major epigenetic barriers in the primed-to-naive transition of human iPSCs. By using the ΔPE OCT4-GFP and KLF17-GFP reporter lines, we showed that treatment with EPZ5676 and VTP50469 enhanced GFP signal, improved naive-like colony morphology, and upregulated naive markers across passages and cell lines. While the ΔPE OCT4-GFP reporter provides a useful readout, its leaky activity limits specificity. To overcome this, the KLF17-GFP reporter line was generated and characterized, offering a more naive-specific readout. With this system, GFP shifts observed by flow cytometry upon EPZ5676 and VTP50469 treatment enabled clearer distinction of naive cells during conversion. This advantage allows sorting and enrichment of cell pools with stronger naive features, providing a practical platform to study naive acquisition. Importantly, this reporter system also facilitates future exploration of additional chromatin regulators and inhibitor effects, broadening opportunities to dissect the molecular control of human naive pluripotency. In addition, a stable doxycycline-inducible AAVS1-Cas9 iPSC line was generated, which enables controlled loss-of-function analyses and effectively links measurement with intervention. This line can be used for large-scale, unbiased CRISPR knockout screens to identify genetic regulators of naive state acquisition. Through such a screen, it will be possible to determine gRNAs that are either depleted or enriched during naive conversion, thereby revealing candidate genes and regulators that directly influence conversion efficiency. These findings provide a practical tool and a straightforward experimental framework for systematically optimizing naive induction. In the future, the approaches and resources established here may also support the production of more reliable naive cell lines for conversion protocols and downstream applications.

BIBLIOGRAPHY

Adewumi, O., Aflatoonian, B., Ahrlund-Richter, L., Amit, M., Andrews, P. W., Beighton, G., ... & Emanuelsson, K. (2007). Characterization of human embryonic stem cell lines by the International Stem Cell Initiative. *Nature Biotechnology*, *25*(7), 803-816. https://doi.org/10.1038/nbt1318

Agarwal, S. K., & Jothi, R. (2012). Genome-Wide Characterization of Menin-Dependent H3K4me3 Reveals a Specific Role for Menin in the Regulation of Genes Implicated in MEN1-Like Tumors. PLoS ONE, 7(5), e37952. https://doi.org/10.1371/journal.pone.0037952

Amit, M., Carpenter, M. K., Inokuma, M. S., Chiu, C. P., Harris, C. P., Waknitz, M. A., & Thomson, J. A. (2000). Clonally derived human embryonic stem cell lines maintain pluripotency and proliferative potential for prolonged periods of culture. *Developmental Biology*, *227*(2), 271-278. https://doi.org/10.1006/dbio.2000.9912

An, C., Feng, G., Zhang, J., Cao, S., Wang, Y., Wang, N., ... & Wang, H. (2020). Overcoming autocrine FGF signaling-induced heterogeneity in naive human ESCs enables modeling of random X chromosome inactivation. *Cell Stem Cell*, *27*(3), 482-497.e4. https://doi.org/10.1016/j.stem.2020.06.002

Avior, Y., Sagi, I., & Benvenisty, N. (2016). Pluripotent stem cells in disease modelling and drug discovery. *Nature Reviews Molecular Cell Biology*, *17*(3), 170-182. https://doi.org/10.1038/nrm.2015.27

Baker, C. L., & Pera, M. F. (2018). Capturing totipotent stem cells. *Cell Stem Cell*, *22*(1), 25-34. https://doi.org/10.1016/j.stem.2017.12.011

Bayerl, J., Ayyash, M., Shani, T., Manor, Y. S., Gafni, O., Massarwa, R., ... Tawil, S. (2021). Principles of signaling pathway modulation for enhancing human naive pluripotency induction. Cell Stem Cell, 28(9), 1549-1565. https://doi.org/10.1016/j.stem.2021.04.001

Bi, Y., Tu, Z., Zhou, J., Zhu, X., Wang, H., Gao, S., & Wang, Y. (2022). Cell fate roadmap of human primed-to-naive transition reveals preimplantation cell lineage signatures. *Nature Communications*, *13*(1). https://doi.org/10.1038/s41467-022-30924-1

Biswas, S., & Rao, C. M. (2018). Epigenetic tools (The Writers, The Readers and The Erasers) and their implications in cancer therapy. *European Journal of Pharmacology*, *837*, 8-24. https://doi.org/10.1016/j.ejphar.2018.08.021

Bock, C., Datlinger, P., Chardon, F., Coelho, M. A., Dong, M. B., Lawson, K. A., ... & Zhuang, X. (2022). High-content CRISPR screening. Nature Reviews Methods Primers, 2(1). https://doi.org/10.1038/s43586-021-00093-4

Bredenkamp, N., Stirparo, G. G., Nichols, J., Smith, A., & Guo, G. (2019). The cell-surface marker Sushi Containing Domain 2 facilitates establishment of human naive pluripotent stem cells. *Stem Cell Reports*, *12*(6), 1212-1222. https://doi.org/10.1016/j.stemcr.2019.03.014

Bredenkamp, N., Yang, J., Clarke, J., Stirparo, G. G., von Meyenn, F., Dietmann, S., ... & Guo, G. (2019). Wnt inhibition facilitates RNA-mediated reprogramming of human somatic cells to naive pluripotency. *Stem Cell Reports*, *13*(6), 1083-1098. https://doi.org/10.1016/j.stemcr.2019.10.009

Brons, I. G., Smithers, L. E., Trotter, M. W., Rugg-Gunn, P., Sun, B., Chuva de Sousa Lopes, S. M., ... & Vallier, L. (2007). Derivation of pluripotent epiblast stem cells from mammalian embryos. *Nature*, *448*(7150), 191-195. https://doi.org/10.1038/nature05950

Chen, H., Aksoy, I., Gonnot, F., Osteil, P., Aubry, M., Hamela, C., ... & De Vos, J. (2015). Reinforcement of STAT3 activity reprogrammes human embryonic stem cells to naive-like pluripotency. *Nature Communications*, *6*(1), 8095. https://doi.org/10.1038/ncomms8095

Choi, H., Joo, J., Hong, Y., Kim, J., Song, H., Lee, J., ... & Do, J. T. (2016). Distinct enhancer activity of Oct4 in naive and primed mouse pluripotency. *Stem Cell Reports*, *7*(5), 911-926. https://doi.org/10.1016/j.stemcr.2016.09.012

Collier, A. J., Panula, S. P., Schell, J. P., Chovanec, P., Reyes, A. P., Petropoulos, S., & Rugg-Gunn, P. J. (2017). Comprehensive cell surface protein profiling identifies specific markers of human naive and primed pluripotent states. *Cell Stem Cell, 20*(6), 874-890. https://doi.org/10.1016/j.stem.2017.02.014

Collier, A. J., & Rugg-Gunn, P. J. (2018). Identifying Human Naive Pluripotent Stem Cells − Evaluating State-Specific Reporter Lines and Cell-Surface Markers. BioEssays, 40(5). https://doi.org/10.1002/bies.201700239

Collier, A. J., Bendall, A., Fabian, C., Malcolm, A. A., Tilgner, K., Semprich, C. I., & Rugg-Gunn, P. J. (2022). Genome-wide screening identifies Polycomb repressive complex 1.3 as an essential regulator of human naive pluripotent cell reprogramming. *Science Advances, 8*(12), eabk0013. https://doi.org/10.1126/sciadv.abk0013

De Los Angeles, A., Ferrari, F., Xi, R., Fujiwara, Y., Benvenisty, N., Deng, H., ... & Daley, G. Q. (2015). Hallmarks of pluripotency. *Nature*, *525*(7570), 469-478. https://doi.org/10.1038/nature15515

De Miguel, M. P., Arnalich Montiel, F., Lopez Iglesias, P., Blazquez Martinez, A., & Nistal, M. (2009). Epiblast-derived stem cells in embryonic and adult tissues. *The International Journal of Developmental Biology*, *53*(8-10), 1529-1540. https://doi.org/10.1387/ijdb.072413md

Desai, N., Rambhia, P., & Gishto, A. (2015). Human embryonic stem cell cultivation: Historical perspective and evolution of xeno-free culture systems. *Reproductive Biology and Endocrinology*, *13*(1), 9. https://doi.org/10.1186/s12958-015-0005-4

Du, P., & Wu, J. (2024). Hallmarks of totipotent and pluripotent stem cell states. *Cell Stem Cell*, *31*(3), 312-333. https://doi.org/10.1016/j.stem.2024.01.009

Duggal, G., Warrier, S., Ghimire, S., Broekaert, D., Van, M., Lierman, S., ... & Heindryckx, B. (2015). Alternative routes to induce naive pluripotency in human embryonic stem cells. *Stem Cells*, *33*(9), 2686-2698. https://doi.org/10.1002/stem.2071

Dunn, S. J., Martello, G., Yordanov, B., Emmott, S., & Smith, A. G. (2014). Defining an essential transcription factor program for naive pluripotency. *Science*, *344*(6188), 1156-1160. https://doi.org/10.1126/science.1248882

Ebrahimi, A., Sevinç, K., Sevinç, G. G., Cribbs, A. P., Philpott, M., Uyulur, F., ... & Önder, T. T. (2019). Bromodomain inhibition of the coactivators CBP/EP300 facilitate cellular reprogramming. Nature Chemical Biology, 15(5), 519-528. https://doi.org/10.1038/s41589-019-0264-z

Eiselleova, L., Peterkova, I., Neradil, J., Slaninova, I., Hampl, A., & Dvorak, P. (2008). Comparative study of mouse and human feeder cells for human embryonic stem cells. *The International Journal of Developmental Biology*, *52*(4), 353-363. https://doi.org/10.1387/ijdb.082590le

Ergünay, T., Ayhan, Ö., Celen, A. B., Georgiadou, P., Pekbilir, E., Abaci, Y. T., … Sahin, U. (2022). Sumoylation of Cas9 at lysine 848 regulates protein stability and DNA binding. Life Science Alliance, 5(4), e202101078. https://doi.org/10.26508/lsa.202101078

Filippakopoulos, P., Picaud, S., Mangos, M., Keates, T., Lambert, J. P., Barsyte-Lovejoy, D., & Knapp, S. (2012). Histone recognition and large-scale structural analysis of the human bromodomain family. *Cell*, *149*(1), 214-231. https://doi.org/10.1016/j.cell.2012.02.013

Fischer, L. A., Khan, S. A., & Theunissen, T. W. (2021). Induction of human naive pluripotency using 5i/L/A medium. In *Methods in molecular biology* (pp. 13-28). https://doi.org/10.1007/978-1-0716-1908-7_2

Gafni, O., Weinberger, L., Mansour, A. A., Manor, Y. S., Chomsky, E., Ben-Yosef, D., ... & Gilad, S. (2013). Derivation of novel human ground state naive pluripotent stem cells. Nature, 504(7479), 282-286. https://doi.org/10.1038/nature12745

Gatchalian, J., Malik, S., Ho, J., Lee, D.-S., Timothy, Shokhirev, M. N., … Hargreaves, D. C. (2018). A non-canonical BRD9-containing BAF chromatin remodeling complex regulates naive pluripotency in mouse embryonic stem cells. Nature Communications, 9(1). https://doi.org/10.1038/s41467-018-07528-9

Graf, T., & Enver, T. (2009). Forcing cells to change lineages. *Nature*, *462*(7273), 587-594. https://doi.org/10.1038/nature08533

Guo, G., von Meyenn, F., Rostovskaya, M., Clarke, J., Dietmann, S., Baker, D., ... & Smith, A. (2017). Epigenetic resetting of human pluripotency. Development, 144(15), 2748-2763. https://doi.org/10.1242/dev.146811

Guo, G., Stirparo, G. G., Strawbridge, S. E., Spindlow, D., Yang, J., Clarke, J., ... Smith, A. (2021). Human naive epiblast cells possess unrestricted lineage potential. Cell Stem Cell, 28(6), 1040-1056.e6. https://doi.org/10.1016/j.stem.2021.02.025

Hanna, J. H., Saha, K., & Jaenisch, R. (2010). Pluripotency and cellular reprogramming: Facts, hypotheses, unresolved issues. *Cell*, *143*(4), 508-525. https://doi.org/10.1016/j.cell.2010.10.008

Henry, M. P., Hawkins, J. R., Boyle, J., & Bridger, J. M. (2019). The genomic health of human pluripotent stem cells: Genomic instability and the consequences on nuclear organization. *Frontiers in Genetics*, *9*. https://doi.org/10.3389/fgene.2018.00623

Hochedlinger, K., & Jaenisch, R. (2015). Induced pluripotency and epigenetic reprogramming. *Cold Spring Harbor Perspectives in Biology*, *7*(12), a019448. https://doi.org/10.1101/cshperspect.a019448

Hotta, A., Cheung, A. Y. L., Farra, N., Vijayaragavan, K., Séguin, C. A., Draper, J. S., ... & Ellis, J. (2009). Isolation of human iPS cells using EOS lentiviral vectors to select for pluripotency. *Nature Methods*, *6*(5), 370-376. https://doi.org/10.1038/nmeth.1325

Ihry, R. J., Salick, M. R., Ho, D. J., Sondey, M., Kommineni, S., Paula, S., … Dolmetsch, R. (2019). Genome-Scale CRISPR Screens Identify Human Pluripotency-Specific Genes. Cell Reports, 27(2), 616-630.e6. https://doi.org/10.1016/j.celrep.2019.03.043

Iltis, A. S., Koster, G., Reeves, E., & Kirstin. (2023). Ethical, legal, regulatory, and policy issues concerning embryoids: A systematic review of the literature. *Stem Cell Research & Therapy*, *14*(1), 221. https://doi.org/10.1186/s13287-023-03448-8

Isono, W., Kawasaki, T., Ichida, J. K., Ayabe, T., Hiraike, O., Umezawa, A., & Akutsu, H. (2020). The combination of dibenzazepine and a DOT1L inhibitor enables a stable maintenance of human naive-state pluripotency in non-hypoxic conditions. *Regenerative Therapy, 15*, 161-168. https://doi.org/10.1016/j.reth.2020.08.001

Karagiannis, P., & Takashima, Y. (2017). Surface markers guide the journey toward naive pluripotency. *Cell Stem Cell*, *20*(6), 737-738. https://doi.org/10.1016/j.stem.2017.05.004

Karasürmeli, N. (2023). Investigating genetic and epigenetic regulators of human naive pluripotent stem cells (Master's thesis). Yükseköğretim Kurulu Ulusal Tez Merkezi. Retrieved from https://tez.yok.gov.tr/

Kagawa, H., Javali, A., Khoei, H. H., Sommer, T. M., Sestini, G., Novatchkova, M., ... & Rivron, N. (2022). Human blastoids model blastocyst development and implantation. *Nature*, *601*(7894), 600-605. https://doi.org/10.1038/s41586-021-04267-8

Koen, Timmers, M., & Brown, M. (2018). Twenty years of menin: emerging opportunities for restoration of transcriptional regulation in MEN1. Endocrine Related Cancer, 24(10), T135-T145. https://doi.org/10.1530/erc-17-0281

Keshet, G., & Benvenisty, N. (2021). Large-scale analysis of imprinting in naive human pluripotent stem cells reveals recurrent aberrations and a potential link to FGF signaling. *Stem Cell Reports*, *16*(10), 2520-2533. https://doi.org/10.1016/j.stemcr.2021.09.002

Kilens, S., Meistermann, D., Moreno, D., Chariau, C., Gaignerie, A., Reignier, A., ... & Le Caignec, C. (2018). Parallel derivation of isogenic human primed and naive induced pluripotent stem cells. *Nature Communications*, *9*(1), 4. https://doi.org/10.1038/s41467-017-02107-w

Kim, H., Wu, J., Ye, S., Tai, C. I., Zhou, X., Yan, H., ... & Ying, Q. L. (2013). Modulation of β-catenin function maintains mouse epiblast stem cell and human embryonic stem cell self-renewal. *Nature Communications*, *4*(1), 2403. https://doi.org/10.1038/ncomms3403

Kondo, Y., Iwao, T., Yoshihashi, S., Mimori, K., Ogihara, R., Nagata, K., ... & Matsunaga, T. (2014). Histone Deacetylase Inhibitor Valproic Acid Promotes the Differentiation of Human Induced Pluripotent Stem Cells into Hepatocyte-Like Cells. PLoS ONE, 9(8), e104010. https://doi.org/10.1371/journal.pone.0104010

Krivtsov, A. V., Evans, K., Gadrey, J. Y., Eschle, B. K., Hatton, C., Uckelmann, H. J., … Lee, H. J. (2019). A Menin-MLL Inhibitor Induces Specific Chromatin Changes and Eradicates Disease in Models of MLL-Rearranged Leukemia. Cancer Cell, 36(6), 660-673.e11. https://doi.org/10.1016/j.ccell.2019.11.001

Kumar, B., Navarro, C., Winblad, N., Schell, J. P., Zhao, C., Weltner, J., … Elsässer, S. J. (2022). Polycomb repressive complex 2 shields naive human pluripotent cells from

trophectoderm differentiation. Nature Cell Biology, 24(6), 845-857. https://doi.org/10.1038/s41556-022-00916-w

Qin, H., Hejna, M., Liu, Y., Percharde, M., Wossidlo, M., Blouin, L., ... & Ramalho-Santos, M. (2016). YAP induces human naive pluripotency. *Cell Reports*, *14*(10), 2301-2312. https://doi.org/10.1016/j.celrep.2016.02.036

Ladewig, J., Koch, P., & Brüstle, O. (2013). Leveling Waddington: The emergence of direct programming and the loss of cell fate hierarchies. *Nature Reviews Molecular Cell Biology*, *14*(4), 225-236. https://doi.org/10.1038/nrm3543

Lai, W. H., Ho, J. C. Y., Lee, Y. K., Ng, K. M., Au, K. W., Chan, Y. C., ... & Siu, C. W. (2010). ROCK inhibition facilitates the generation of human-induced pluripotent stem cells in a defined, feeder-, and serum-free system. *Cellular Reprogramming*, *12*(6), 641-653. https://doi.org/10.1089/cell.2010.0051

Law, J. A., & Jacobsen, S. E. (2010). Establishing, maintaining and modifying DNA methylation patterns in plants and animals. *Nature Reviews Genetics*, *11*(3), 204-220. https://doi.org/10.1038/nrg2719

Lea, R. A., McCarthy, A., Boeing, S., Fallesen, T., Elder, K., Snell, P., ... & Niakan, K. K. (2021). KLF17 promotes human naive pluripotency but is not required for its establishment. *Development*, *148*(22). https://doi.org/10.1242/dev.199378

Legate, K. R., Wickström, S. A., & Fässler, R. (2009). Genetic and cell biological analysis of integrin outside-in signaling. *Genes & Development*, *23*(4), 397-418. https://doi.org/10.1101/gad.1758709

Leung, C. Y., & Zernicka-Goetz, M. (2015). Mapping the journey from totipotency to lineage specification in the mouse embryo. *Current Opinion in Genetics & Development*, *34*, 71-76. https://doi.org/10.1016/j.gde.2015.08.002

Li, R., Liang, J., Ni, S., Zhou, T., Qing, X., Li, H., … Zhang, B. (2010). A Mesenchymal-to-Epithelial Transition Initiates and Is Required for the Nuclear Reprogramming of Mouse Fibroblasts. Cell Stem Cell, 7(1), 51-63. https://doi.org/10.1016/j.stem.2010.04.014

Ludwig, T., & A. Thomson, J. (2007). Defined, Feeder-Independent Medium for Human Embryonic Stem Cell Culture. Current Protocols in Stem Cell Biology. https://doi.org/10.1002/9780470151808.sc01c02s2

Liu, X., Nefzger, C. M., Rossello, F. J., Chen, J., Knaupp, A. S., Firas, J., ... & Laslett, A. L. (2017). Comprehensive characterization of distinct states of human naive pluripotency generated by reprogramming. *Nature Methods*, *14*(11), 1055-1062. https://doi.org/10.1038/nmeth.4436

Lo, B., & Parham, L. (2009). Ethical issues in stem cell research. *Endocrine Reviews*, *30*(3), 204-213. https://doi.org/10.1210/er.2008-0031

Lowell, S., Benchoua, A., Heavey, B., & Smith, A. G. (2006). Notch promotes neural lineage entry by pluripotent embryonic stem cells. *PLoS Biology*, *4*(5), e121. https://doi.org/10.1371/journal.pbio.0040121

Martello, G., Sugimoto, T., Diamanti, E., Joshi, A., Hannah, R., Ohtsuka, S., & Smith, A. (2012). Esrrb is a pivotal target of the Gsk3/Tcf3 axis regulating embryonic stem cell self-renewal. *Cell Stem Cell*, *11*(4), 491-504. https://doi.org/10.1016/j.stem.2012.06.008

Martire, S., Nguyen, J., Sundaresan, A., & Banaszynski, L. A. (2020). Differential contribution of p300 and CBP to regulatory element acetylation in mESCs. BMC Molecular and Cell Biology, 21(1). https://doi.org/10.1186/s12860-020-00296-9

Mashtalir, N., D'Avino, A. R., Michel, B. C., Luo, J., Pan, J., Otto, J. E., ... & Kadoch, C. (2018). Modular organization and assembly of SWI/SNF family chromatin remodeling complexes. Cell, 175(5), 1272-1288.e20. https://doi.org/10.1016/j.cell.2018.09.032

Murry, C. E., & Keller, G. (2008). Differentiation of embryonic stem cells to clinically relevant populations: Lessons from embryonic development. *Cell*, *132*(4), 661-680. https://doi.org/10.1016/j.cell.2008.02.008

Musselman, C. A., Lalonde, M. E., Côté, J., & Kutateladze, T. G. (2012). Perceiving the epigenetic landscape through histone readers. *Nature Structural & Molecular Biology*, *19*(12), 1218-1227. https://doi.org/10.1038/nsmb.2436

Nichols, J., & Smith, A. (2009). Naive and primed pluripotent states. *Cell Stem Cell*, *4*(6), 487-492. https://doi.org/10.1016/j.stem.2009.05.015

Niakan, K. K., Han, J., Pedersen, R. A., Simon, C., & Reijo, R. A. (2012). Human pre-implantation embryo development. *Development*, *139*(5), 829-841. https://doi.org/10.1242/dev.060426

O'Brien, C. M., Chy, H. S., Zhou, Q., Blumenfeld, S., Lambshead, J. W., Liu, X., … Jarde, T. (2017). New Monoclonal Antibodies to Defined Cell Surface Proteins on Human Pluripotent Stem Cells. Stem Cells, 35(3), 626-640. https://doi.org/10.1002/stem.2558

Oceguera-Yanez, F., Kim, S.-I., Matsumoto, T., Tan, G. W., Xiang, L., Hatani, T., & Woltjen, K. (2015). Engineering the AAVS1 locus for consistent and scalable transgene expression in human iPSCs and their differentiated derivatives. *Methods, 101*, 43-55. https://doi.org/10.1016/j.ymeth.2015.12.012

Okubo, T., Rivron, N., Kabata, M., Masaki, H., Kishimoto, K., Semi, K., … Takashima, Y. (2023). Hypoblast from human pluripotent stem cells regulates epiblast development. Nature, 626(7998), 357-366. https://doi.org/10.1038/s41586-023-06871-2

Onder, T. T., Kara, N., Cherry, A., Sinha, A. U., Zhu, N., Bernt, K. M., ... & Daley, G. Q. (2012). Chromatin-modifying enzymes as modulators of reprogramming. *Nature*, *483*(7391), 598-602. https://doi.org/10.1038/nature10953

Pastor, W., Chen, D., Liu, W., Kim, R., Sahakyan, A., Lukianchikov, A., & Clark, A. T. (2016). Naive human pluripotent cells feature a methylation landscape devoid of blastocyst or germline memory. *Cell Stem Cell*, *18*(3), 323-329. https://doi.org/10.1016/j.stem.2016.01.019

Romayor, I., Herrera, L., Burón, M., Martin-Inaraja, M., Prieto, L., Etxaniz, J., ... & Eguizabal, C. (2022). A comparative study of cell culture conditions during conversion from primed to naive human pluripotent stem cells. *Biomedicines*, *10*(6), 1358. https://doi.org/10.3390/biomedicines10061358

Salami, H., Mowal, S. J., Moukhah, R., Hajebrahimi, Z., Hosseini, S. A., & Edalat, H. (2019). Evaluating the differential effects of valproic acid on Wharton's Jelly

mesenchymal stem cells. *Advanced Pharmaceutical Bulletin, 9*(3), 497-504. https://doi.org/10.15171/apb.2019.059

Sevinç, K., Sevinç, G. G., Cavga, A. D., Philpott, M., Kelekçi, S., Can, H., ... & Önder, T. T. (2022). BRD9-containing non-canonical BAF complex maintains somatic cell transcriptome and acts as a barrier to human reprogramming. Stem Cell Reports, 17(12), 2629-2642. https://doi.org/10.1016/j.stemcr.2022.10.005

Shakiba, N., White, C. A., Lipsitz, Y. Y., Yachie-Kinoshita, A., Tonge, P. D., Samer, & Zandstra, P. W. (2015). CD24 tracks divergent pluripotent states in mouse and human cells. *Nature Communications, 6*(1), 1-11. https://doi.org/10.1038/ncomms8329

Shalem, O., Sanjana, N. E., Hartenian, E., Shi, X., Scott, D. A., Mikkelsen, T. S., ... & Zhang, F. (2013). Genome-Scale CRISPR-Cas9 Knockout Screening in Human Cells. Science, 343(6166), 84-87. https://doi.org/10.1126/science.1247005

Steger, D. J., Lefterova, M. I., Ying, L., Stonestrom, A. J., Schupp, M., Zhuo, D., ... & Vakoc, C. R. (2008). DOT1L/KMT4 recruitment and H3K79 methylation are ubiquitously coupled with gene transcription in mammalian cells. *Molecular and Cellular Biology*, *28*(8), 2825-2839. https://doi.org/10.1128/mcb.02076-07

Sun, W. S., Chun, J. L., Do, J. T., Kim, D. H., Ahn, J. S., Kim, M. K., ... & Lee, J. W. (2016). Construction of a dual-fluorescence reporter system to monitor the dynamic progression of pluripotent cell differentiation. *Stem Cells International*, *2016*, 1390284. https://doi.org/10.1155/2016/1390284

Tadros, W., & Lipshitz, H. D. (2009). The maternal-to-zygotic transition: A play in two acts. *Development*, *136*(18), 3033-3042. https://doi.org/10.1242/dev.033183

Takahashi, K., & Yamanaka, S. (2006). Induction of pluripotent stem cells from mouse embryonic and adult fibroblast cultures by defined factors. *Cell*, *126*(4), 663-676. https://doi.org/10.1016/j.cell.2006.07.024

Takahashi, K., Tanabe, K., Ohnuki, M., Narita, M., Ichisaka, T., Tomoda, K., & Yamanaka, S. (2007). Induction of pluripotent stem cells from adult human fibroblasts by defined factors. *Cell*, *131*(5), 861-872. https://doi.org/10.1016/j.cell.2007.11.019

Takashima, Y., Guo, G., Loos, R., Nichols, J., Ficz, G., Krueger, F., ... & Smith, A. (2014). Resetting transcription factor control circuitry toward ground-state pluripotency in human. *Cell*, *158*(6), 1254-1269. https://doi.org/10.1016/j.cell.2014.08.029

Tesar, P. J., Chenoweth, J. G., Brook, F. A., Davies, T. J., Evans, E. P., Mack, D. L., Gardner, R. L., & McKay, R. D. (2007). New cell lines from mouse epiblast share defining features with human embryonic stem cells. *Nature*, *448*(7150), 196-199. https://doi.org/10.1038/nature05972

Theunissen, T. W., Powell, B. E., Wang, H., Mitalipova, M., Faddah, D. A., Reddy, J., ... & Gray, N. (2014). Systematic identification of culture conditions for induction and maintenance of naive human pluripotency. *Cell Stem Cell*, *15*(4), 471-487. https://doi.org/10.1016/j.stem.2014.07.002

Theunissen, T. W., Friedli, M., He, Y., Planet, E., O'Neil, R. C., Markoulaki, S., ... & Trono, D. (2016). Molecular criteria for defining the naive human pluripotent state. *Cell Stem Cell*, *19*(4), 502-515. https://doi.org/10.1016/j.stem.2016.06.011

Thomson, J. A., Itskovitz-Eldor, J., Shapiro, S. S., Waknitz, M. A., Swiergiel, J. J., Marshall, V. S., & Jones, J. M. (1998). Embryonic stem cell lines derived from human blastocysts. *Science*, *282*(5391), 1145-1147. https://doi.org/10.1126/science.282.5391.1145

Trusler, O., Huang, Z., Goodwin, J., & Laslett, A. L. (2018). Cell surface markers for the identification and study of human naive pluripotent stem cells. *Stem Cell Research*, *26*, 36-43. https://doi.org/10.1016/j.scr.2017.11.017

Vallier, L., Mendjan, S., Brown, S., Chng, Z., Teo, A., Smithers, L. E., & Pedersen, R. A. (2009). Activin/Nodal signalling maintains pluripotency by controlling Nanog expression. *Development*, *136*(8), 1339-1349. https://doi.org/10.1242/dev.033951

Waddington, C.H. (1957). The Strategy of the Genes (1st ed.). Routledge. https://doi.org/10.4324/9781315765471

Wang, S. H., Hao, J., Zhang, C., Duan, F. F., Chiu, Y. T., Shi, M., ... & Wang, Y. (2022). KLF17 promotes human naive pluripotency through repressing MAPK3 and ZIC2. *Science China Life Sciences*, *65*(10), 1985-1997. https://doi.org/10.1007/s11427-021-2076-x

Wang, Y., Zhao, C., Hou, Z., Yang, Y., Bi, Y., Wang, H., ... & Gao, S. (2018). Unique molecular events during reprogramming of human somatic cells to induced pluripotent stem cells (iPSCs) at naive state. *eLife*, *7*, e29518. https://doi.org/10.7554/elife.29518

Wang, H., & Helin, K. (2025). Roles of H3K4 methylation in biology and disease. Trends in Cell Biology, 35(2), 115-128. https://doi.org/10.1016/j.tcb.2024.06.001

Ware, C. B., Nelson, A. M., Mecham, B., Hesson, J., Zhou, W., Jonlin, E. C., ... & Ruohola-Baker, H. (2014). Derivation of naive human embryonic stem cells. *Proceedings of the National Academy of Sciences*, *111*(12), 4484-4489. https://doi.org/10.1073/pnas.1319738111

Ware, C. B. (2017). Concise review: Lessons from naive human pluripotent cells. *Stem Cells*, *35*(1), 35-41. https://doi.org/10.1002/stem.2507

Ware, C. B., Jonlin, E. C., Anderson, D. J., Cavanaugh, C., Hesson, J., Sidhu, S., ... & Mathieu, J. (2023). Derivation of naive human embryonic stem cells using a CHK1 inhibitor. *Stem Cell Reviews and Reports*, *19*(8), 2980-2990. https://doi.org/10.1007/s12015-023-10613-2

Watanabe, A., Yamada, Y., & Yamanaka, S. (2013). Epigenetic regulation in pluripotent stem cells: A key to breaking the epigenetic barrier. *Philosophical Transactions of the Royal Society B: Biological Sciences*, *368*(1609), 20120292. https://doi.org/10.1098/rstb.2012.0292

Weinberger, L., Ayyash, M., Novershtern, N., & Hanna, J. H. (2016). Dynamic stem cell states: Naive to primed pluripotency in rodents and humans. Nature Reviews Molecular Cell Biology, 17(3), 155-169. https://doi.org/10.1038/nrm.2015.28

Wille, C. K., & Sridharan, R. (2022). DOT1L inhibition enhances pluripotency beyond acquisition of epithelial identity and without immediate suppression of the somatic transcriptome. Stem Cell Reports, 17(2), 384-396. https://doi.org/10.1016/j.stemcr.2021.12.004

Witte, S., Bradley, A., Enright, A. J., & Muljo, S. A. (2015). High-density P300 enhancers control cell state transitions. BMC Genomics, 16(1). https://doi.org/10.1186/s12864-015-1905-6

Wood, K., Tellier, M., & Murphy, S. (2018). DOT1L and H3K79 Methylation in Transcription and Genomic Stability. Biomolecules, 8(1), 11-11. https://doi.org/10.3390/biom8010011

Wong, C. C., Loewke, K. E., Bossert, N. L., Behr, B., De Jonge, C. J., Baer, T. M., & Pera, R. A. R. (2010). Non-invasive imaging of human embryos before embryonic genome activation predicts development to the blastocyst stage. *Nature Biotechnology*, *28*(10), 1115-1121. https://doi.org/10.1038/nbt.1686

Wu, J., & Belmonte, J. C. I. (2015). Dynamic pluripotent stem cell states and their applications. *Cell Stem Cell*, *17*(5), 509-525. https://doi.org/10.1016/j.stem.2015.10.009

Wu, Y., Zhong, A., Evangelisti, A., Sidharta, M., Huangfu, D., Studer, L., & Zhou, T. (2025). Leveraging CRISPR activation for rapid assessment of gene editing products in human pluripotent stem cells. Stem Cell Reports, 20(6), 102499. https://doi.org/10.1016/j.stemcr.2025.102499

Xu, C., Inokuma, M. S., Denham, J., Golds, K., Kundu, P., Gold, J. D., & Carpenter, M. K. (2001). Feeder-free growth of undifferentiated human embryonic stem cells. *Nature Biotechnology*, *19*(10), 971-974. https://doi.org/10.1038/nbt1001-971

Xu, H., & Liang, H. (2022). The regulation of totipotency transcription: Perspective from in vitro and in vivo totipotency. *Frontiers in Cell and Developmental Biology*, *10*, 1024093. https://doi.org/10.3389/fcell.2022.1024093

Xiao, J., Mai, D. H., & Xie, L. (2016). Resetting human naive pluripotency. *Genetics & Epigenetics*, *8*, GEG.S38093. https://doi.org/10.4137/geg.s38093

Yagi, Y., Fushida, S., Harada, S., Kinoshita, J., Makino, I., Oyama, K., … Hirakawa, K. (2010). Effects of valproic acid on the cell cycle and apoptosis through acetylation of histone and tubulin in a scirrhous gastric cancer cell line. Journal of Experimental & Clinical Cancer Research, 29(1). https://doi.org/10.1186/1756-9966-29-149

Ying, Q. L., Wray, J., Nichols, J., Batlle-Morera, L., Doble, B., Woodgett, J., & Smith, A. (2008). The ground state of embryonic stem cell self-renewal. *Nature*, *453*(7194), 519-523. https://doi.org/10.1038/nature06968

Yu, S., Zhou, C., He, J., Yao, Z., Huang, X., Rong, B., … Zhang, M. (2022). BMP4 drives primed to naive transition through PGC-like state. Nature Communications, 13(1). https://doi.org/10.1038/s41467-022-30325-4

Zhou, W., Choi, M., Margineantu, D., Margaretha, L., Hesson, J., Cavanaugh, C., ... & Ruohola-Baker, H. (2012). HIF1α induced switch from bivalent to exclusively glycolytic metabolism during ESC-to-EpiSC/hESC transition. *The EMBO Journal*, *31*(9), 2103-2116. https://doi.org/10.1038/emboj.2012.71

Zimmerlin, L., Park, T. S., Huo, J. S., Verma, K., Pather, S. R., Talbot, C. C., & Zambidis, E. T. (2016). Tankyrase inhibition promotes a stable human naive pluripotent state with improved functionality. *Development*, *143*(23), 4368-4380. https://doi.org/10.1242/dev.138982

Appendix A: Validation and Characterization of KLF17 Reporter Cell Line

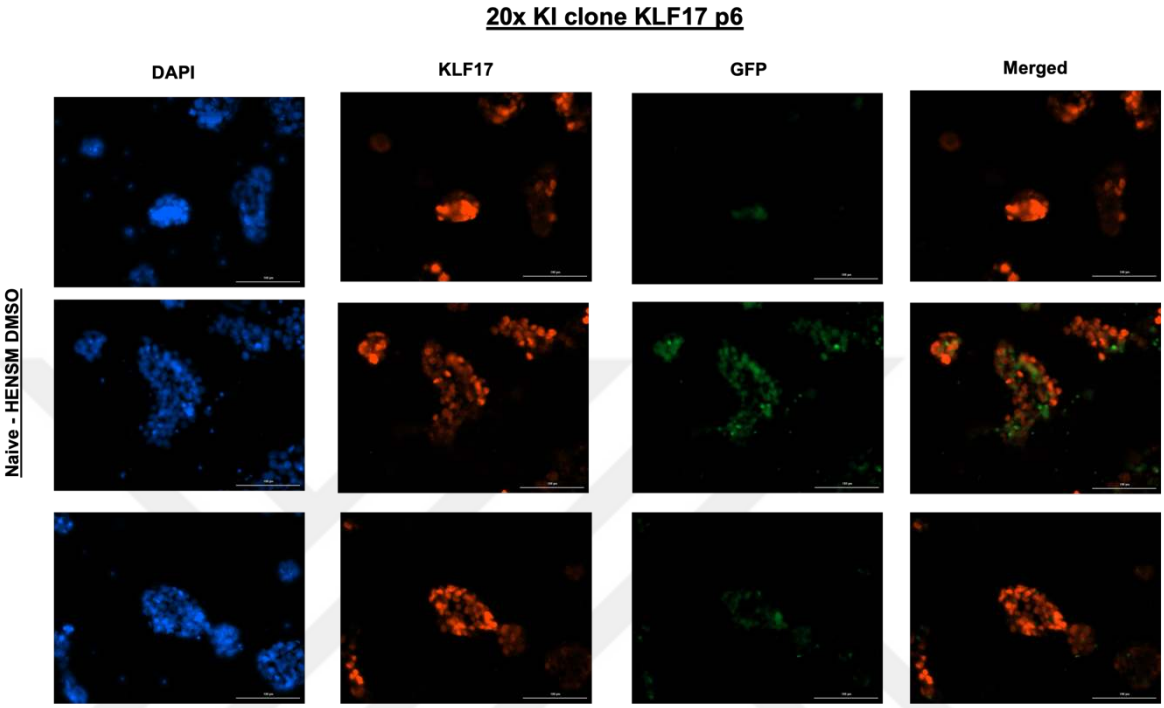

Appendix A.1. Representative immunofluorescence images of KI KLF17 c10. KLF17 staining (red) is shown after naive conversion with HENSM at passage 6 (left) and in primed state with mTSER (right), acquired with the Cytation cell imaging reader at 10× magnification. Nuclei were counterstained with DAPI (blue).

Additional immunofluorescence images were captured from different angles at 20x magnification, showing KLF17 antibody staining in the KLF17 reporter cell line. The observed antibody signal overlapped with GFP fluorescence, confirming reporter activity (Appendix A.1).